ANKARA YILDIRIM BEYAZIT UNIVERSITY

GRADUATE SCHOOL OF NATURAL AND APPLIED SCIENCES

PERFORMANCE EVALUATION OF PHOTOVOLTAIC PANEL TECHNOLOGIES USING A DESIGNED MULTI-PHOTOVOLTAIC PANEL POWER MEASUREMENT SYSTEM

Ph. D. Thesis

Mehmet KARABULUT

Department of Electrical and Electronics Engineering

SEPTEMBER, 2020

ANKARA

PERFORMANCE EVALUATION OF PHOTOVOLTAIC PANEL TECHNOLOGIES USING A DESIGNED MULTI-PHOTOVOLTAIC PANEL POWER MEASUREMENT SYSTEM

A Thesis Submitted to

The Graduate School of Natural and Applied Sciences of

Ankara Yıldırım Beyazıt University

In Partial Fulfillment of the Requirements for the Degree of PhD

in Electrical and Computer Engineering,

Department of Electrical and Electronics Engineering

by

Mehmet KARABULUT

SEPTEMBER, 2020

ANKARA

PHD THESIS EXAMINATION RESULT FORM

We have read the thesis entitled **"Performance Evaluation of Photovoltaic Panel Technologies Using a Designed Multi-Photovoltaic Panel Power Measurement System"** completed by **Mehmet Karabulut** under the supervision of **Assoc. Prof. Dr. Sinan KIVRAK** and we certify that in our opinion it is fully adequate, in scope and quality, as a thesis for the degree of PhD.

Assoc. Prof. Dr. Sinan KIVRAK

(Supervisor)

Prof. Dr. Kamil Çağatay BAYINDIR

(Jury Member)

Prof. Dr. Şerafettin EREL

(Jury Member)

Prof. Dr. Yüksel OĞUZ

(Jury Member)

Assoc. Prof. Dr. Mehmet DEMİRTAŞ

(Jury Member)

Prof. Dr. Ergün ERASLAN

Director

Graduate School of Natural and Applied Sciences

I hereby declare that, in this thesis which has been prepared in accordance with the Thesis Writing Manual of Graduate School of Natural and Applied Sciences,

- All data, information, and documents are obtained in the framework of academic and ethical rules,
- All information, documents, and assessments are presented in accordance with scientific ethics and morals,
- All the materials that have been utilized are fully cited and referenced,
- No change has been made on the utilized materials,
- All the works presented are original,

and in any contrary case of above statements, I accept to renounce all my legal rights.

Date: 21.09.2020

Signature:

Name & Surname: Mehmet KARABULUT

ACKNOWLEDGMENTS

First of all, I would like to thank Assoc. Prof. Dr. Sinan KIVRAK for his support and motivation during my PhD study. Besides, I would like to sincerely thank my co-supervisor Asst. Prof. Dr. Hüseyin KUSETOĞULLARI for his generous support during the thesis period. Their valuable advice guided my research and other critical stages, including the preparation of this thesis. In addition to my precious professors, I would like to thank Kemal YAYLA for his support during the thesis period. Also, I would like to thank my dear family for their support.

2020, 21 September **Mehmet KARABULUT**

PERFORMANCE EVALUATION OF PHOTOVOLTAIC PANEL TECHNOLOGIES USING A DESIGNED MULTI-PHOTOVOLTAIC PANEL POWER MEASUREMENT SYSTEM

ABSTRACT

This thesis presents a new multi-Photovoltaic Panel Measurement and Analysis System (PPMAS) developed to measure atmospheric parameters and generated power of photovoltaic (PV) panels. The designed system presented with an experimental study evaluates the performance of four new and four old PV panel technologies, which are based on PolyCrystalline (Poly), MonoCrystalline (Mono), Copper Indium Selenide (CIS), and Cadmium Telluride (CdTe) in real-time, under same atmospheric conditions. The PPMAS system is installed in Yildirim Beyazit University, Ankara Province, in Turkey. The designed PPMAS consists of three different sub-systems which are 1) Photovoltaic Panel Measurement sub-system (PPMS), 2) Meteorology measurement sub-system (MMS), and 3) Data acquisition sub-system (DAS). PPMS is used to measure the power generation for PV panels. MMS involves different sensors, and it is designed to determine atmospheric conditions, including wind speed, wind direction, outdoor temperature, humidity, ambient light, and panel temperatures. The measured values by PPMS and MMS are stored in a database using the DAS sub-system. In order to improve the measurement accuracy, PPMS and MMS are calibrated. This study also focuses on outdoor testing performances of four new and four old PV panels. Average monthly panel efficiencies are estimated as 8.46, 8.11, 5.65, and 3.88 in percentage, for new Mono, new Poly, new CIS, and new CdTe PV panels, respectively. Moreover, the average monthly panel efficiencies of old panels are calculated as 8.22, 7.85, 5.35, and 3.63 in percentage, in the same order. Test results obtained from the experimental system are also statistically examined and discussed to analyze the performance of PV panels in terms of monthly panel efficiencies.

Keywords: Photovoltaic panel, pv panel measurement system, meteorology measurement system, polycrystalline (poly), monocrystalline (mono), copper indium selenide (cis), cadmium telluride (cdte)

TASARLANAN ÇOKLU FOTOVOLTAİK PANEL GÜÇ ÖLÇÜM SİSTEMİ KULLANILARAK FOTOVOLTAİK PANEL TEKNOLOJİLERİNİN PERFORMANSLARININ DEĞERLENDİRİLMESİ

ÖZ

Bu tez çalışması, atmosferik parametrelerin ve fotovoltaik (PV) panellerin üretilen gücünün ölçümü için geliştirilmiş yeni birçoklu Fotovoltaik Panel Ölçüm ve Analiz Sistemini (PPMAS) sunmaktadır. Deneysel bir çalışma ile birlikte sunulan bu tasarlanan sistem, PolyCrystalline (Poly), MonoCrystalline (Mono), Copper Indium Selenide (CIS) ve Cadmium Telluride (CdTe) temelli dört yeni ve dört eski PV panel teknolojisinin performansını gerçek-zamanlı olarak aynı atmosferik koşullar altında değerlendirmektedir. PPMAS sistemi Türkiye'de Ankara ili Yıldırım Beyazıt Üniversitesi'ne kurulmuştur. Tasarlanan PPMAS, 1) Fotovoltaik panel ölçüm alt-sistemi (PPMS), 2) Meteoroloji ölçüm alt-sistemi (MMS) ve 3) Veri toplama alt-sistemi (DAS) olmak üzere üç farklı alt sistemden oluşmaktadır. PPMS, PV paneller için güç üretimini ölçmek için kullanılır. MMS, farklı sensör türlerini içerir ve rüzgar hızı, rüzgar yönü, dış ortam sıcaklığı, nem, ortam ışığı ve panel sıcaklıkları dahil olmak üzere atmosferik koşulları belirlemek için tasarlanmıştır. PPMS ve MMS ile ölçülen değerler, DAS alt sistemi kullanılarak bir veri tabanında saklanır. Ölçüm doğruluğunu iyileştirmek için PPMS ve MMS kalibre edilmiştir. Bu çalışma aynı zamanda dört yeni ve dört eski PV panelin dış mekan performans testlerine odaklanmaktadır. Ortalama aylık panel verimliliği Mono-yeni, Poly-yeni, CIS-yeni ve CdTe-yeni PV paneller için sırasıyla yüzde 8.46, 8.11, 5.65 ve 3.88 olarak hesaplanmıştır. Ayrıca eski panellerin aylık ortalama panel verimleri aynı sırayla yüzde 8.22, 7.85, 5.35 ve 3.63 olarak hesaplanmıştır. Deneysel sistemden elde edilen test sonuçları, istatistiksel olarak incelenmiş ve PV panellerin performansını, aylık panel verimlilikleri açısından, analiz etmek için tartışılmıştır.

Anahtar Kelimeler: Fotovoltaik panel, pv panel ölçüm sistemi, meteoroloji ölçüm sistemi, polycrystalline (poly), monocrystalline (mono), copper indium selenide (cis), cadmium telluride (cdte)

CONTENTS

PHD. THESIS EXAMINATION RESULT FORM ii
ACKNOWLEDGMENTS iv
ABSTRACT v
ÖZ vi
CONTENTS vii
NOMENCLATURE ix
LIST OF TABLES xii
LIST OF FIGURES xiii
CHAPTER 1 - INTRODUCTION 1
1.1 Photovoltaics 2
1.1.1 Equivalent Circuit of a PV Cell 4
1.1.2 I-V Characterization of Photovoltaic Cell 6
1.2 Photovoltaic Panel Technologies 8
1.2.1 The First-Generation: Crystalline Silicon PV Panel 8
1.2.1.1 Mono-Crystalline PV Panel 9
1.2.1.2 Poly-Crystalline PV Panel 9
1.2.2 The Second Generation: Thin Film PV Panels 10
1.2.2.1 Cadmium Telluride PV Panel 10
1.2.2.2 Copper Indium Gallium Selenide PV Panel 11
1.2.2.3 Amorphous Silicon PV Panel 12
1.2.3 The Third Generation: Organic PV Panels 12
1.3 Review of Related Works and Thesis Study 13
CHAPTER 2 - MICROCONTROLLER DIGITAL INTERFACING 16
2.1 Parallel Interface 17
2.2 Serial Interface 18
2.2.1 One Wire Interface 18
2.2.2 RS232 / RS422 Interface 19
2.2.3 I2C Interface 20
2.2.4 SPI Interface 20
2.2.5 Ethernet 21
2.3 On/Off Control 21
CHAPTER 3 - METHODOLGY 22
3.1 Designed Multi-Photovoltaic Panel Measurement and Analysis System 23
3.1.1 Photovoltaic Panel Measurement Sub-system (PPMS) 26
3.1.1.1 Algorithm of PPMS Sub-system 30
3.1.1.2 PIC18F4520 Microcontroller in PPMS 31
3.1.1.3 Voltage Measurement of PV Panels 32
3.1.1.4 Current Measurement of PV Panels 33
3.1.1.5 MOSFET as an Electronic Load and I-V Characterization of a PV Panel ... 34
3.1.1.6 DAC Circuit to Drive MOSFET 36
3.1.1.7 Relay Driving Circuit and PV Panel Selection 36
3.1.1.8 One-cycle Operation of PPMS Sub-system 37
3.1.2 Meteorology Measurement Sub-system (MMS) 38
3.1.2.1 Algorithm of MMS Sub-system 41
3.1.2.2 PIC16F886 Microcontroller in MMS Sub-system 42

3.1.2.3 Wind Speed Sensor 42
3.1.2.4 Wind Direction Sensor 43
3.1.2.5 Ambient Temperature and Humidity Sensor 45
3.1.2.6 PV Panel Temperature Measurement Sensor 46
3.1.2.7 Ambient Light Sensor 47
3.1.3 Data Acquisition Sub-system (DAS) 48
3.1.3.1 DAS Computer 48
3.1.3.2 DAS Sub-system Computer Serial Interface 49
3.1.3.3 Algorithm of DAS Software Application 50
3.1.3.4 Data Monitoring and Recording 50
3.1.4 Power Supply of the System 55
3.1.4.1 DC-DC Converter 56
CHAPTER 4 - EXPERIMENTAL RESULTS & DISCUSSION 58
4.1 Verification of Designed PPMAS System 58
4.1.1 Calibration of MMS 58
4.1.2 Calibration of PPMS 59
4.2 PV Panels 59
4.3 Climate Data in Ankara Province 60
4.4 Solar Radiation 60
4.5 Effect of Atmospheric Variations on PV Panel Temperatures 61
4.6 Daily Investigation of PPMAS 63
4.7 Performance Assessment of Different PV Panels for Power Generation 70
4.8 Statistical Analysis of Data 77
4.8.1 Performance Analysis of PV Panels and Photovoltaic Panel Measurement System using Non-Parametric Tests 77
4.9 Global Relevance of the Research Results 80
CHAPTER 5 - CONCLUSIONS AND FUTURE WORK 82
REFERENCES 86
CURRICULUM VITAE 99

NOMENCLATURE

Acronyms

°C	Centigrade
A	Ampere
AC	Alternative Current
ADC	Analog Digital Converter
ASCII	American Standard Code for Information Interchange
C#	C-Sharp
C	Capacitance
CdTe	Cadmium Telluride
CIGS	Copper Indium Gallium (di)Selenide
DAS	Data Acquisition Sub-system
DC	Direct Current
FF	Fill Factor
G	Solar Irradiance
I2C	Inter-Integrated Circuit
IC	Integrated Circuit
ID	Identification Number
Imp	Current at Maximum Power Point
Isc	Short Circuit Current
Kb/s	Kilobit/Second
kHz	Kilohertz
kV	Kilovolt
m	Meter
m/s	meter/second

Mbit	Mega bit
MHz	Megahertz
MMS	Meteorology Measurement Sub-system
MOSFET	Metal Oxide Semiconductor Field Effect Transistor
mV	Millivolt
mΩ	Milliohm
PC	Personal Computer
PCB	Printed Circuit Board
Pmax	Maximum Power
PV	Photovoltaic
PPMAS	Photovoltaic Panel Measurement and Analysis System
PPMS	Photovoltaic Panel Measurement Sub-system
PWM	Pulse Width Modulation
R	Resistor
RH	Relative Humidity
SPI	Serial Peripheral Interface
TCP / IP	Transmission Control Protocol/ Internet Protocol
TTL	Transistor-Transistor Logic
UART	Universal Asynchronous Receiver Transmitter
USART	Universal Synchronous/Asynchronous Receiver Transmitter
USB	Universal Serial Bus
V	Voltage
Vmp	Voltage at Maximum Power Point
Voc	Open Circuit Voltage
W	Watt

Wh	Watt-Hour
η	Efficiency

LIST OF TABLES

Table 1.1 Relay configuration for pv panel selection 28

Table 3.1 Wind direction and corresponding angles 45

Table 3.2 Specifications of DAS computer 48

Table 4.1 Climate data for Ankara province (Turkey) between the years of 1927 and 2019 60

Table 4.2 Characteristics of new and old pv panel technologies used in the study .. 62

Table 4.3 Monthly average of humidity between December 2019 and May 2020 in Ankara. 76

Table 4.4 Average rankings of eight pv panels using the non-parametric statistical procedure, statistics and p-values. 77

Table 4.5 Adjusted *p*-values for Friedman (Mono-new is the control pv panel). 78

Table 4.6 Adjusted *p*-values for Friedman Aligned (Mono-new is the control pv panel). 79

Table 4.7 Adjusted *p*-values for Quade (Mono-new is the control pv panel). 79

Table 4.8 Adjusted *p*-values for tests for multiple comparisons among all pv panels.. 80

Table 4.9 Global relevance of the research results. 81

LIST OF FIGURES

Figure 1.1 Photovoltaic effect 3
Figure 1.2 PV cell and pv panel 4
Figure 1.3 PV cell equivalent circuit 5
Figure 1.4 I-V and P-V curve of a pv cell 6
Figure 1.5 Mono-Crystalline pv cell structure 9
Figure 1.6 Poly-Crystalline pv cell structure in thin film form 10
Figure 1.7 Cadmium telluride pv cell structure 11
Figure 1.8 Copper indium gallium selenide pv cell structure 11
Figure 1.9 Amorphous silicon pv cell structure 12
Figure 2.1 Microcontroller digital interfacing techniques 17
Figure 2.2 Parallel interface 17
Figure 2.3 Serial interface 18
Figure 2.4 One-Wire interface 19
Figure 2.5 RS232 interface 19
Figure 2.6 I2C interface 20
Figure 2.7 SPI interface 21
Figure 3.1 PPMAS block diagram 23
Figure 3.2 PPMAS junction box 24
Figure 3.3 Location of Ankara, Turkey. 25
Figure 3.4 PPMAS system, pv panels and wind measurement mast. 25
Figure 3.5 Photovoltaic panel measurement sub-system (PPMS) 28
Figure 3.6 IXFH60N65X2 mosfet and pv panel measurement circuit 29
Figure 3.7 a) PPMS sub-system pcb, b) 3D view of PPMS sub-system pcb 30
Figure 3.8 PPMS algorithm 31
Figure 3.9 PIC18F4520 microcontroller 32
Figure 3.10 Microcontroller and voltage divider interfacing 32
Figure 3.11 Voltage divider circuit used in PPMS 33
Figure 3.12 ACS-712 33
Figure 3.13 Microcontroller and ACS-712 interfacing 34
Figure 3.14 Safe operating area of IXFH60N65X2 mosfet 35
Figure 3.15 12-Bit DAC circuit 36
Figure 3.16 PV panel selection and relay circuit 37

Figure 3.17 Meteorology measurement system (MMS) 39
Figure 3.18 a) MMS pcb and b) 3D view of MMS pcb.. 40
Figure 3.19 MMS sub-system algorithm 41
Figure 3.20 PIC16F886 microcontroller.. 42
Figure 3.21 Wind speed sensor 43
Figure 3.22 Microcontroller and wind speed sensor interfacing............................... 43
Figure 3.23 Wind direction sensor 44
Figure 3.24 Microcontroller and wind direction sensor interfacing 44
Figure 3.25 DHT22 temperature & humidity sensor 45
Figure 3.26 Microcontroller and DHT22 interfacing.. 46
Figure 3.27 DS18B20 pv panel temperature sensor.. 46
Figure 3.28 Microcontroller and DS18B20 interfacing 47
Figure 3.29 Max44009 ambient light sensor 47
Figure 3.30 Microcontroller and Max44009 interfacing... 47
Figure 3.31 View of DAS sub-system computer 49
Figure 3.32 HW-417 serial to usb converter 49
Figure 3.33 DAS sub-system algorithm.. 50
Figure 3.34 Data fields 51
Figure 3.35 An example C# code block view in designed software interface 52
Figure 3.36 Serial port configuration of the interface in C# 53
Figure 3.37 Database connection and string operations... 53
Figure 3.38 Designed software interface in C# for DAS sub-system computer 54
Figure 3.39 View of data monitoring interface in DAS computer............................ 54
Figure 3.40 System power supply 55
Figure 3.41 Batteries and charge controller in the power supply 56
Figure 3.42 DC-DC converter pcb a) front-side b) back-side................................... 56
Figure 4.1 Weekly average results of solar radiation between December 2019 - May 2020 in Ankara 61
Figure 4.2 Weekly average ambient temperature, panel temperature, and wind speed between December 2019 and May 2020 in Ankara 62
Figure 4.3 Illimunation of the Sun in 12.01.2020 63
Figure 4.4 Single day pv measurements a) mono-new b) mono-old 64
Figure 4.5 Single day pv measurements a) poly-new b) poly-old 65
Figure 4.6 Single day pv measurements a) CIS-new b) CIS-old 66

Figure 4.7 Single day pv measurements a) CdTe-new b) CdTe-old 67

Figure 4.8 Instant power generation of pv panels a) new pv panels with solar radiation b) old pv panels with solar radiation 68

Figure 4.9 Single day generated total powers of pv panels.. 69

Figure 4.10 Ambient temperature and humidity measurements on 12.01.2020 69

Figure 4.11 Weekly average power generated by new and old pv panels, (a), (b) December and January, (c), (d) February and March, (e), (f), April and May. 73

Figure 4.12 Monthly panel efficiency of (a) four new pv panels, (b) four old pv panels. 75

CHAPTER 1

INTRODUCTION

Increasing energy demand and decreasing fossil-based energy sources accelerate the trend towards renewable energy worldwide. As reported by the International Energy Agency (IEA), total renewable energy-based potential in the world is expected to grow by 50 % that corresponds to approximately 1220 Gigawatts of increase between 2019 and 2024 [1]. It is estimated that about 25 % and 57 % of the renewable energy will be generated using wind tribunes and solar panels, respectively [1]. Hence, the trend and popularity of renewable energy are growing rapidly. Note that this thesis focuses on analyzing various types of photovoltaic (PV) panel technologies that are connected to the proposed measurement system and examining the power generation performance of these technologies under varying daily weather parameters.

PV energy is one of the most important renewable energy sources with widespread electricity generation in different places, such as solar farms and rooftops [2]. With the growth of renewable energy generation, it is essential to provide a trade-off between the payback period of renewable energy investment and PV panels' lifetime. According to the PV panel technologies, the payback period of investment is variable because the power generation performance of PV panels is affected by two main factors: 1) panel efficiency and 2) varying weather conditions. The PV panel characteristic parameters must be verified for effective power generation by considering these two main factors. To achieve the best characteristic parameters of PV panels, manufacturers work on developing the PV panels and evaluate the peak power of them within the scope of Standard Test Conditions (STC) that are defined with 1) 25°C PV cell temperature, 2) 1000 W/m² irradiance and 3) 1.5 air mass (AM1.5) [3]. However, it is highly likely that generated power of manufactured PV panels in the STC environment is different than the outdoor environment. The actual power generation of the evaluated PV panels can be achieved in the STC environment, but it cannot be obtained under real case conditions [4]. This difference may cause power loss in energy generation daily, weekly, monthly, and yearly due to the varying meteorological conditions in different locations. Different materials have been used to produce and develop different types of PV panels to decrease power loss and increase PV panel efficiency.

For instance, conventional crystalline silicon PV cells have doped junctions such as "emitters" or "back surface fields" [5]. Amorphous silicon PV cells are mostly made by chemically vaporizing a thin silicone coat, placing on a surface such as plastic, metal, or glass [6]. Namely, Cadmium Telluride PV cells are formed by Cadmium Telluride and Cadmium Sulphide p-n junction materials on a glass substrate [7]. Copper, Gallium, Indium, and Selenide materials are deposited on a substrate layer by a sequence of chemical processes to form Copper Indium Diselenide PV cells [8]. PolyCrystalline, MonoCrystalline, Thin Film produced by CIS material and Thin Film manufactured by CdTe material are widely used for renewable energy generation since these technologies provide several advantages in terms of price, energy efficiency, and lifetime [9, 10].

Silicon is a leading material used in MonoCrystalline, PolyCrystalline, and Thin Film modules, which corresponds to more than 90% of the annual solar cell production [11]. In MonoCrystalline silicon cells, each solar cell is made from a single source of silicon. Monocrystalline silicon cells are produced by cutting 300 µm thick cylindrical bars of Monocrystalline silicon in special ovens [12]. On the other hand, Polycrystalline silicon cells are made by combining melted pure silicone blocks. [12]. Thin Film cells are made from photovoltaic material placed between thin layers, such as glass, plastic, or metal [13]. Different types of thin-film panels are made by other materials such as CIS, CdTe, and Amorphous-Si photovoltaic materials. CIS based Thin Film cells consist of layers of ZnO, CdS, CIS, and Mo, which are organized on a glass, metal, or polymer substrate, whereas CdTe-based Thin Film modules are formed from transparent conductive oxide (TCO) layers such as SnO2 or Cd2SnO4 [13].

1.1 Photovoltaics

Photovoltaics absorb photons radiated from the sun to generate electricity in dc (direct current) by photovoltaic effect [14]. The first contact with the photovoltaic effect was made by the French physicist Alexandre-Edmond Becquerel. In other words, the photovoltaic effect was discovered by him in 1839, when he observed electricity generation during an experiment involving electrodes in an electrolyte solution exposed to light [15]. Subsequently, it took 115 years to build the first few watts of solar cells, and in the following 50 years, the worldwide electricity generation capacity reached 3 GW [16]. Photovoltaics has continued to spread rapidly in recent years with technology developments and the decrease in production costs. The generation capacity became 300 GW in 2016 and is expected to reach TW of capacity soon [16].

The concept of the photovoltaic effect in a PV cell is shown in Figure 1.1, where photons from sunlight hit the semiconductor material in the PV cell, causing electrons to move. This mobility in the PV cell forms a potential difference, which is the basis of electricity generation.

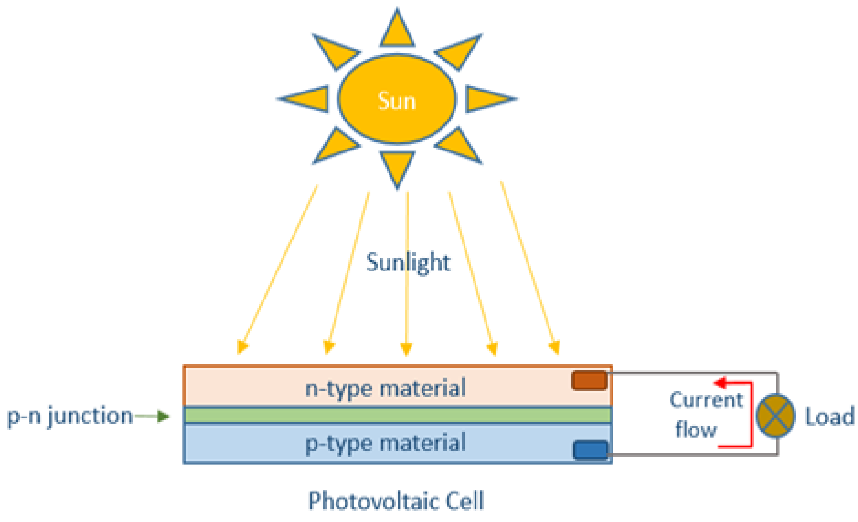

Figure 1.1 Photovoltaic effect

A PV cell's voltage output is less than one volt concerning the light source's intensity, which is not sufficient for most of the electrical applications [17, 18]. Hence, to form a PV module that generates the necessary power, PV cells are linked in series and parallel on a plastic or glass sheet (Figure 1.2). In other words, the serial connection of the PV cells in a PV module (usually called a PV panel) increases the voltage, and the parallel connection increases the current. For example, a brand of a commercially available PV panel can have 300 W production power with 72 PV cells. The higher number of PV cells does not always mean that the PV panel has higher power. In another example, a different brand PV panel can have 320 W output power with 60 PV cells. This difference is also related to factors such as efficiency and quality of the PV cell.

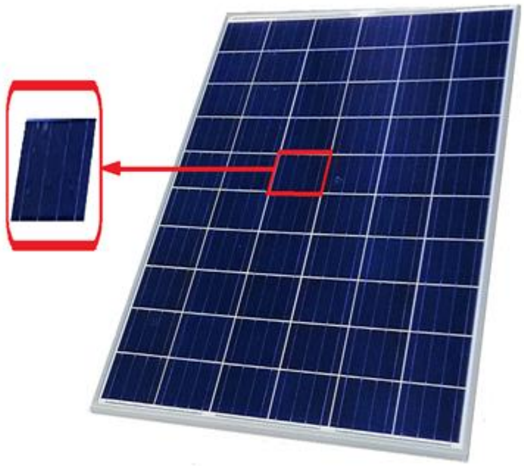

Figure 1.2 PV cell and pv panel

1.1.1 Equivalent Circuit of a PV Cell

Photovoltaic panels are made by serial and parallel connections of many PV cells. Therefore, to understand a PV cell's electronic profile, an equivalent model is examined in Figure 1.3. A PV cell has a p-n junction, which is very similar to a semiconductor diode [19]. Because of this similarity, in the equivalent circuit, the Photovoltaic cell is modeled as a current source, the diode in parallel, and a shunt resistor. The current "*I*" generated current by PV cell can be expressed in the equation (1) below.

$$I = I_{light} - I_{diode} - I_{shunt} \tag{1}$$

where;

I = Output current of the PV cell (A)

I_{light} = Generated current by the light source (A)

I_{diode} = Diode current (A)

I_{shunt} = Current drops on shunt resistor (A).

The Shockley diode equation is used to calculate the current (I_{diode}) passing through the diode [19, 20, 21].

$$I_{diode}=I_0\ [exp\ [\frac{qVj}{nkT}]\ -\ 1] \tag{2}$$

In Equation (2);

I_0 = reverse saturation current (A)

V_j = voltage across the diode (V)

q = elementary charge

n = ideality factor for diode

k = Boltzmann's constant

T = absolute temperature

Ohm's law is applied, to obtain I_{shunt},

$$I_{shunt} = \frac{Vj}{Rshunt} \tag{3}$$

Where, R_{shunt} is shunt resistor (Ω)

Substituting equation (2) and (3) into equation (1);

$$I=I_{light}-[I_0\ [exp\ [\frac{qVj}{nkT}]\ -\ 1]]-[\frac{Vj}{Rshunt}] \tag{4}$$

Equation (4) is the I-V characteristic equation of the circuit model in Figure 1.3, which relates the parameters of an ideal PV panel with its output current and voltage [19, 20, 21].

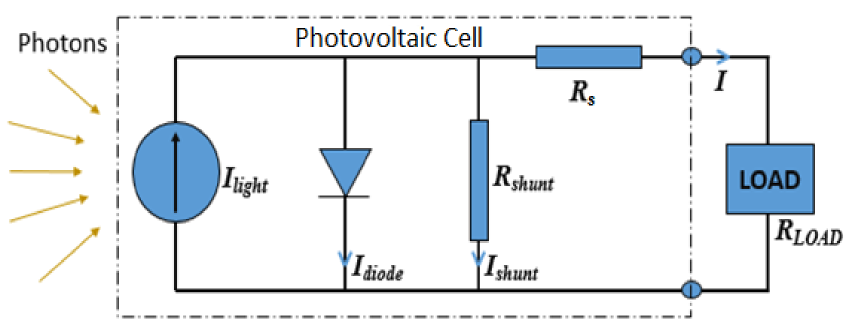

Figure 1.3 PV cell equivalent circuit

1.1.2 I-V Characterization of Photovoltaic Cell

One of the fundamental properties of a PV cell is the I-V curve (Figure 1.4). In other words, the I-V curve represents the actual performance of a PV cell in terms of I-V characteristics in ambient conditions.

Generally, I-V characteristics are specified in a PV cell datasheet created by performing the measurements under STC (Standard Test Conditions). Here, two critical factors that directly affect the I-V characteristic are considered as temperature and radiation. Therefore, an I-V curve obtained under STC is valid only for a single temperature and irradiance value. Also, I-V characteristics are valid under an ideal condition where the PV cell's entire surface is uniformly illuminated.

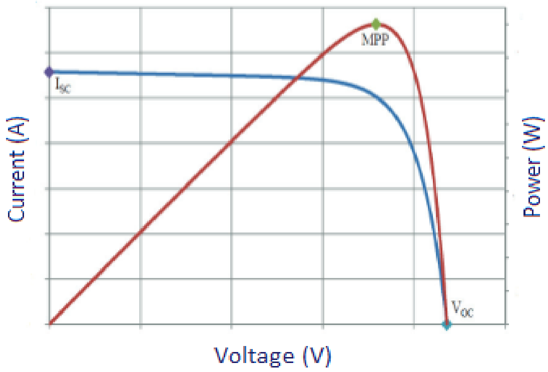

Figure 1.4 I-V and P-V curve of a pv cell [22]

The real I-V curve of a PV panel can be obtained under outdoor conditions. In this thesis, the I-V characteristic measurements of PV panels are carried out instantaneously under outdoor conditions; other necessary calculations such as power measurement and efficiency are made according to this systematic.

The characteristic parameters used in the performance evaluation of a PV panel can be listed as follows:

P_{max}: Maximum power

V_{mp}: Voltage at the maximum power point

I_{mp}: Current at the maximum power point

V_{oc}: Open circuit voltage

I_{sc}: Short circuit current

FF: Fill Factor

η: Efficiency

The current-voltage (I-V) characteristic of a PV panel represents all possible operating points. There is a unique point on the graph where the PV cell's power reaches its maximum value. This maximum value is known as Maximum Power Point (MPP), which is symbolized as P_{max}.

$$P_{max} = V_{mp} * \ I_{mp} \tag{5}$$

Also, there are two components, current, and voltage, that make up the MPP point. The relation of P_{max}, V_{mp}, and I_{mp} are shown in Eq (5). Here, the current component is defined as I_{mp} (current at maximum power), and the voltage component is defined as V_{mp} (current at maximum power).

Open Circuit Voltage - V_{oc} is the voltage between the PV panel's positive and negative terminals when no load is connected, or current is not drawn from the source. V_{oc} is the greatest voltage value that a PV panel can generate, which is greater than V_{mp}.

Short Circuit Current - I_{sc} is the highest current value that a PV panel can generate greater than I_{mp}. Namely, the current that flows where positive and negative terminals of the PV panel is short circuit.

Another critical parameter of the I-V characteristic is the Fill Factor (*FF*), which is an indicator to evaluate the PV panel's quality. Equation (6) shows the relationship between *FF* and other characteristic parameters. In other words, *FF* represents the ratio of maximum power to ideal power. Here, ideal power is a product of V_{oc} and I_{sc}. *FF* and temperature of the PV panel are inversely proportional; when the PV panel temperature increases, the *FF* ratio decreases [23]. Also, *FF* should be higher than 0.7 for an efficient PV panel [24].

$$FF = \frac{P_{max}}{P_{ideal}} = \frac{V_{mp} * I_{mp}}{V_{oc} * I_{sc}} \tag{6}$$

One of the performance measurement criteria is the efficiency of the PV panel. PV panel efficiency is a metric that expresses the rate of solar energy converted to electrical energy through a PV panel. In other words, PV panel efficiency; refers to the proportion of generated power to input power in percentage (%). Here, input power is a product of solar radiation value by the PV panel surface area. Efficiency is written in Equation (7)

$$\eta = \left(\frac{P}{Area_{pv} . H}\right). 100 \tag{7}$$

Some critical factors affect the PV panel efficiency. This factors can be listed as panel technology, temperature, solar radiation, dust, and atmospheric conditions such as humidity, rain, and snow.

1.2 Photovoltaic Panel Technologies

PV panel technologies, which are widely used today, can be classified into three generations, according to their materials and technologies used. Although the first and the second generation photovoltaic panel technologies are commercially available in the market, the third generation, organic photovoltaic technologies, is still in the research phase.

1.2.1 The First-Generation: Crystalline Silicon PV Panel

Crystalline Silicon PV panels are the most widely used PV panel technology among commercially produced PV panels [25]. It consists of cells made of crystallized silicon. This panel technology is divided into two categories. These are Mono-Crystalline and Poly-Crystalline PV panel technologies. Mono-Crystalline PV panel technology has slightly higher conversion efficiency than Poly-Crystalline PV technology [26]. Both PV technologies provide efficiency, approximately ranging from 10% to 20%. Additionally, Crystalline silicon panels have a lifespan of about 25 years.

1.2.1.1 Mono-Crystalline PV Panel

This PV panel type, also known as a single crystalline, is a widely used PV panel type today with higher efficiency. Mono-Crystalline PV technology is produced by the Czochralski method [27]. According to the technique, Mono-Crystalline PV cells are made based on a unique design, where silicon wafers cut 0.3mm thick from a single crystal block of very high purity molten silicon [26]. Then, it is converted into a cell form. As a result of the Czochralski process, most of the initial silicon remains waste. Considering the waste part, it causes an increase in the cost of a Mono-Crystalline PV panel. In Figure 1.5, the Mono-Crystalline PV cell can be seen.

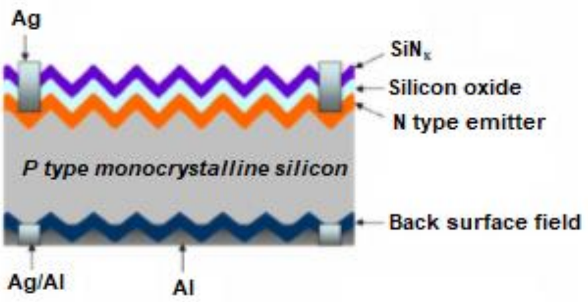

Figure 1.5 Mono-crystalline pv cell structure [28]

1.2.1.2 Poly-Crystalline PV Panel

It is also called multi-crystalline PV panel and another widely used cell type today. Figure 1.6 shows the structure of Poly-crystalline silicon cell in thin-film form. Polycrystalline silicon cells are made by cutting silicon ingots that are re-crystallized after melting [29]. The ingots, which are cut into very thin wafers, are then combined to form a cell. Production costs are also lower as the manufacturing process is more straightforward than the Mono-Crystalline cell [30]. Also, the efficiency of the Poly-Crystalline PV cell is lower [31].

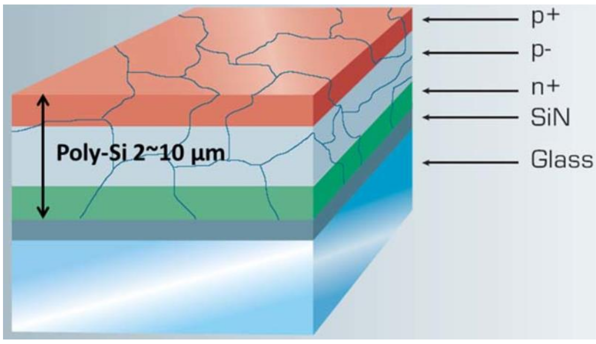

Figure 1.6 Poly-crystalline pv cell structure in thin-film form [32]

1.2.2 The Second Generation: Thin Film PV Panels

Thin-film PV panels are made by placing semiconductor films on a substrate layer such as plastic or glass, by a chemical process. Compared to Crystalline Silicon wafers, they have a very thin structure. Even though they absorb the light easier than crystalline silicon cells, their energy conversion efficiency is low (5-7%) [33]. Thin-film panels are produced in three different technologies: Amorphous Silicon (a-Si), Copper Indium Selenide (CIS / CIGS), and Cadmium Telluride (CdTe).

1.2.2.1 Cadmium Telluride PV Panel

CdTe PV panel is based on a semiconductor created by combining Cadmium (Cd) and Tellurium (Te) elements (Figure 1.7). Mainly, it consists of n-doped Cadmium Sulfide and p-doped Cadmium Telluride junctions [34]. Here, the n-doped surface is known as the window layer, and the p-doped surface is known as the absorber layer. A transparent front contact such as glass or plastic covers the Cadmium Sulphide surface, and the Cadmium Telluride side is in contact with a rear substrate. The p-n junction layer of CdTe PV is much thinner than typical crystalline silicon. They are low cost, in terms of production.

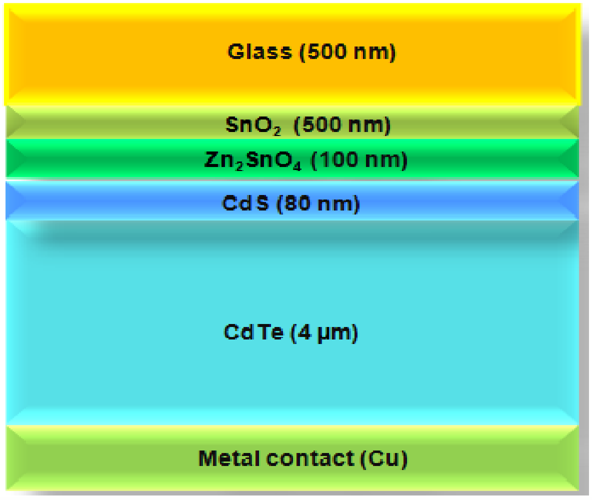

Figure 1.7 Cadmium telluride pv cell structure [35]

1.2.2.2 Copper Indium Gallium Selenide PV Panel

Copper Indium Gallium Selenide abbreviated as CIGS and can be defined as a semiconductor made by depositing a very thin layer of Copper, Indium, Gallium, and Selenium materials with a chemical process (Figure 1.8). This very thin compound layer deposited by chemical processes is spread between two glass or plastic surfaces, and the potential difference can be observed with the electrodes placed in the panel.

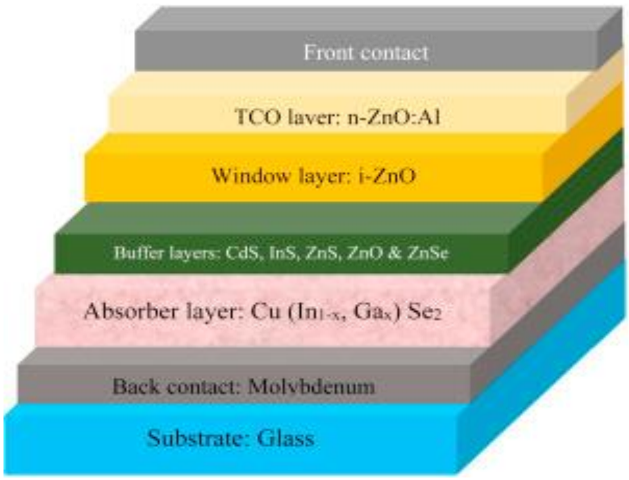

Figure 1.8 Copper indium gallium selenide pv cell structure [36]

1.2.2.3 Amorphous Silicon PV Panel

Amorphous silicon is a thin-film semiconductor that has a non-crystalline atomic form [37]. The structure of the Amorphous silicon PV cell can be seen in Figure 1.9. Amorphous silicon PV panels are also made using silicon as Crystalline PV panels but in a different technique. Unlike Crystalline PV panels, Amorphous PV panels are made by placing non-cristal forms of silicon on plastic, glass, or metallic surfaces (Figure 1.9). Amorphous silicon PV panels are lower efficiency, comparing with other PV technologies.

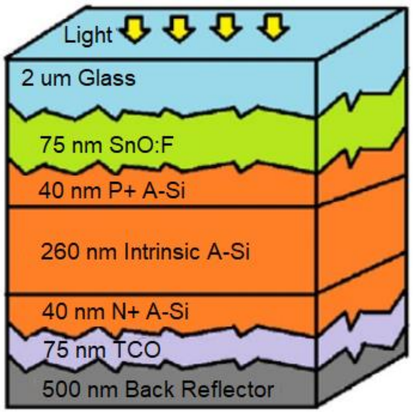

Figure 1.9 Amorphous silicon pv cell structure [38]

1.2.3 The Third Generation: Organic PV Panels

The third generation of PV technology is organic PV cells, where solar energy is absorbed by the organic layer of the cell and transformed into electrical energy. Most organic PV cells consist of a novel nonfullerene or fullerene-derivative acceptor and a polymeric donor deposited by solution processing under inert conditions [39]. When the polymer layer of the cell starts to absorb the light from the sun, the migration of electrons (in the acceptor side) towards one electrode and holes (in the donor side) towards the other electrode begins [40]. Thus, the potential difference required for the generation of current and voltage is obtained.

1.3 Review of Related Works and Thesis Study

The electricity generation performance of PV panels may differ according to the locations. For instance, MonoCrystalline and PolyCrystalline PV panels have been installed to generate electricity in Bursa, Turkey [41]. The results are obtained with one week experiment, and they show that the MonoCrystalline PV panel generates slightly more electricity than PolyCrystalline.

In [42], MonoCrystalline (2.35 kW), PolyCrystalline (2.64 kW), and Amorphous Silicon (2.40 kW) PV panels are analyzed in 2014, in Duzce (Turkey). The efficiency and generated power of PV panels are compared yearly. Solar radiation, ambient temperature, PV panel temperature, and wind measurements are recorded during the test study. Many other works have been conducted to evaluate the performance of various PV panels in different locations such as Slovenia [43], Norway [44], Ireland [45], Morocco [46], Brazil [47], Nigeria [48], Jordan [49], Algeria [50] and Croatia [51]. To the best of our knowledge, this is the first work that assesses the outdoor performance of four different types of new and old PV panels. In order to achieve this, PV panels are installed in Ankara, Turkey, and it is crucial to select the most efficient PV panel technology to generate electricity efficiently in this location.

There must be a measurement system to measure weather conditions and PV panels' power generation capacity. In order to measure the generated power of PV panels, various types of measurement systems have been designed and applied. For instance, Rezk et al. [52] have developed a measurement system based on a DAQ card (NI_USB-6009). In work, a charge controller with a battery unit is used as a load, and a multi-crystalline silicon PV panel is used for test activities.

Machacek et al. [53] have implemented a measuring unit (NI_PCI−6023E) and computer-based data acquisition model. A 100W PV Panel is used to perform its current, voltage, and power measurements. Solar radiation, PV panel temperature, and ambient temperature measurements are also measured.

Hammoumi et al. [54] have performed a test study where a PV panel is connected to a variable load and takes the measurements using current and voltage sensors connected to the system.

Demirtas et al. [13] have demonstrated long term performance measurements of CIS and CdTe PV panels. In this work, measurement data includes direct current (DC) and alternating current (AC), voltage, power, and efficiency.

Munoz-Garcia et al. [55] have performed a study to obtain I-V curves of CIS, a-Si, and CdTe PV panel technologies using an electronic load, both indoor and outdoor conditions at STC. Digital thermometer and pyranometer are used to record external conditions. The indoor and outdoor performance of this measurement system has been investigated.

Polverini et al. [56] have realized an experimental indoor study under STC to test 70 pcs of polycrystalline silicon PV panel that is remained about 20 years outdoor.

In order to determine the characterization of a PV panel, different load techniques are applied. Kivrak et al. [57] have designed a system to obtain the measurements of four same types of PV panels using MOSFET electronic load based on a 4-channel measurement Printed Circuit Board (PCB) and tested outdoor.

Brito et al. [58] designed a measurement setup to characterize a 48W PV panel using capacitive loads. In the study, current and voltage measurements were made with the measurement setup created. I-V and P-V curves were performed with the measurement data collected in outdoor conditions, and the curves were displayed in the interface. Also, the effect of outdoor conditions on the PV panel efficiencies was examined.

Van Dyk et al. [59] performed an I-V curve study for PV panels using an array of parallel resistors as a loading technique under outdoor conditions. Switches activate an array of resistors on the experimental platform.

Enrique et al. [60] have simulated a system in PSpice to evaluate the I-V characteristic of the PV panel by using the DC-DC converter load technique.

The aforementioned measurement systems have several drawbacks and limitations such as 1) lack of availability of weather measurement sensors, 2) lack of capability of measuring generated power of many PV panels, 3) lack of accurately measuring power generation under varying weather conditions, 4) lack of sensitivity of measured power, 5) using costly products and circuit boards.

To address the limitations and drawbacks of the other measurement systems, in this study, the multi-Photovoltaic Panel Measurement and Analysis System (PPMAS) is designed to measure the different types of PV panels installed in Ankara, Turkey. Note that the data is collected for six months from the first of December 2019 until the end of May 2020. The overall system consists of three sub-systems which are 1) PV panel measurement sub-system (PPMS), 2) meteorology measurement sub-system (MMS), 3) data acquisition sub-system (DAS). In the PPMS, the P_{max} (maximum Power) parameter of the PV panel is measured. Besides of this, other essential parameters of the PV panels are estimated using the measured P_{max}. Moreover, maximum power point (MPP) measurement technique is applied in this sub-system to measure the P_{max} accurately. The second sub-system includes different sensors that measure wind speed, wind direction, outdoor temperature, humidity, ambient light, and panel temperatures. In the last sub-system, the measured parameters are stored in a database and displayed on a computer. The overall system is performed with four new and four old PV panel technologies based on PolyCrystalline, MonoCrystalline, Copper Indium Selenide (CIS), Cadmium Telluride (CdTe). Thus, the performance of the power generation of new and old PV panels is experimentally and statistically investigated for the best PV panel evaluation and selection under varying weather conditions in Ankara, Turkey. The main objectives and contributions of this study are as follows:

1) Multi-Photovoltaic Panel Measurement and Analysis System (PPMAS) is designed,
2) The performance of new and old PV panel technologies are assessed and analyzed,
3) Atmospheric measurement sub-system is designed,
4) Eight PV panel technologies are examined for the location of Ankara Province, Turkey.

CHAPTER 2

MICROCONTROLLER DIGITAL INTERFACING

Most electronic devices used today have a microcontroller. They are embedded in these electronic devices to perform data processing tasks such as reading, transferring, controlling, and commanding defined for them. Microcontrollers are computers with small dimensions, very low cost, and high performance. With these features, portable and compact electronic devices can be designed.

Many types of microcontrollers are produced by their manufacturers according to their features, power consumption, and cost to fulfill many tasks from simple operations to complex operations. They are advantageous in interacting with other devices such as computers, sensors, displays, keypads, and motors. Microcontrollers can use various interface methods to interact with the devices mentioned according to their features. The basis of the interface for electronic devices is data transmission, in which the data is transferred from one electronic device to another or multiple electronic devices in analog or digital form. Simply, electronic devices talk to each other or their components through data transmission.

Microcontroller based electronics are stand-alone designs that perform the tasks defined for them. These electronics must use the same communication protocol to share data. Many communication protocols have been created to provide this data exchange, namely interfacing.

In Figure 2.1, techniques popularly used for digital interfacing the microcontrollers are classified. Two primary methods stand out here. These methods are serial and parallel communications. In serial data communication, bits are sent sequentially over one channel, while in parallel data communication, bits are transmitted simultaneously through multiple channels.

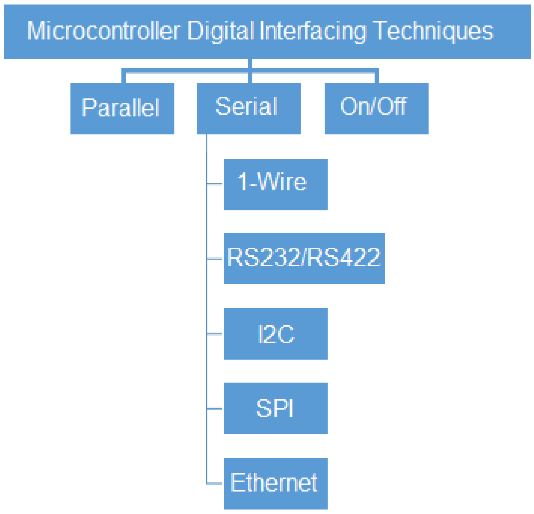

Figure 2.1 Microcontroller digital interfacing techniques

2.1 Parallel Interface

Parallel data transmission is a communication technique used to transmit multiple data over multiple channels simultaneously [61]. Parallel transmission is preferred when 1) data need to be sent quickly, 2) sending large amounts of data. Video streaming can be given as an example of parallel transmission. Here, the data must be received quickly because the data transmission is time-sensitive, and the video stream should be done without any pauses. Parallel communication is essential for applications that require the fast transmission of large amounts of data.

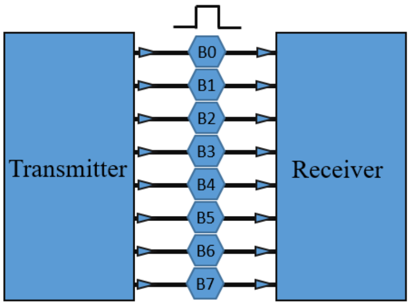

Figure 2.2 Parallel interface

In parallel transmission, data is sent as a group (Figure 2.2), so it is faster than serial communication. It is not suitable for long-distance data transmission. Another disadvantage is that a large number of microcontroller pins are required to enable parallel data transmission. Display units such as LCD, Oled, TFT are other examples of using parallel interfaces.

2.2 Serial Interface

Although Parallel Transmission is a fast and easy to implement communication technique, it requires a slightly large number of input/output lines. When considering a limited number of I/O pins on a microcontroller, serial communication is usually preferred according to the application type. In serial communication, data is transmitted sequentially based on bits [61]. The serial transmission technique is shown in Figure 2.3.

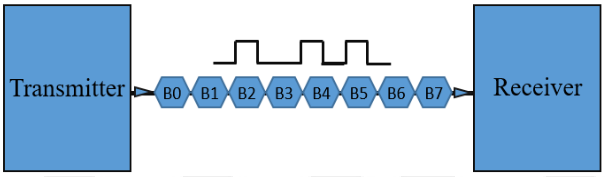

Figure 2.3 Serial interface

In microcontroller-based embedded systems, serial transmission can be performed via different interface methods. Some of these methods are commonly used interfaces such as RS-232, RS-485, SPI, 1-Wire, I2C.

2.2.1 One Wire Interface

It can be communicated with more than one device over a single channel in the one-wire interface (Figure 2.4). It reduces the number of channels required for communication. The one-wire interface consists of master and slave devices, where the master device initiates communication with one or more than one slave device [62]. If there is only one slave device on the line, data can be exchanged directly with this device. If there is more than one slave device, the identification code of these devices must be known. The identification code is the identification information of the device. In one-wire communication, the slave device's identification code to be communicated with is reported to the one-wire line. The slave device, whose identification code is reported, is activated, and data transmission is performed. After the data transmission is complete, the slave devices continue to listen on the one-wire line for the identification code to execute new tasks. In this way, one-wire communication is provided. One of the most famous examples of one wire application is the DS18B20 temperature sensor [63].

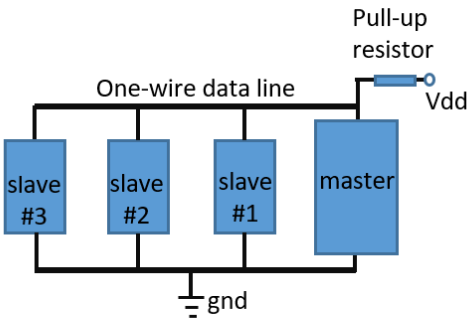

Figure 2.4 One-Wire interface

2.2.2 RS232 / RS422 Interface

RS232 is a popular communication standard used for short-distance data transfer among computers and microcontroller-based devices [64]. RS232 interface can be seen in Figure 2.5. RS232 is a primary interface that can be converted to many interfaces such as RS422, RS485, USB, and Ethernet. In order to provide RS232 communication, it is sufficient to connect TX, RX, and GND pins on both device sides. That is, the ground pin is common, the TX pin of the first device is connected to the RX pin of the second device, the RX pin of the first device is connected to the TX pin of the second device.

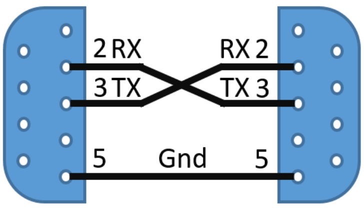

Figure 2.5 RS232 interface

RS-422 is a standard technique for serial data transmission similar to the RS-232 interface [65]. RS-422 provides data transfer with twisted pair and increases the resistance against line noise due to this feature. Thus, data transfer can be achieved over distances, such as 1200 meters. The data transfer rate can go up to 10 Mbits / sec.

2.2.3 I2C Interface

The I2C interface is the abbreviation for Inter-Integrated Circuit [66]. It is a synchronous serial communication interface that works with SDA, SCL, VCC, and GND connections [67]. In order to realize communication, one master and at least one slave device must be connected on the line. The task of the master device is to control communication. Multiple devices on the line can communicate through the I2C interface. The master device decides which device will activate and transfer data. The master device manages this by sending the address information of the slave device to the line. Slave devices control whether the address information on the line belongs to them or not.

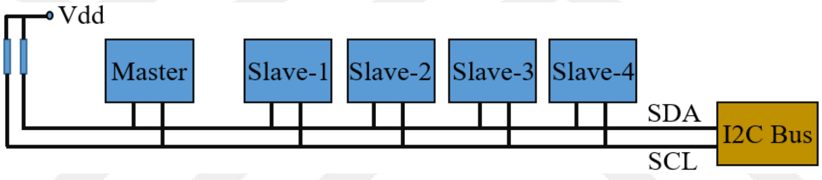

Figure 2.6 I2C interface

In the I2C interface (Figure 2.6), the SDA line is used for data transmission, and the SCL line is used for the clock signal transmission. SCL line provides communication synchronization between devices, while the SDA line provides bidirectional data communication.

2.2.4 SPI Interface

SPI is the abbreviation of Serial Peripheral Interface [68], which is usually an interface used to communicate with peripheral devices such as microcontrollers and sensors (Figure 2.7). There is a separate line to enable synchronization, where the clock signal is sent. The master device selects the device that it wants to communicate with over the SS (Slave Select) pin. In SPI, individual lines are required for clock and data transmission. There are six signal pins VCC, Ground, MISO, MOSI, SCK, and SS to provide data transmission [69]. SPI can also transmit data at speeds like 10Mbps. Theoretically, a master SPI device can be connected to multiple slave SPI devices for data transmission.

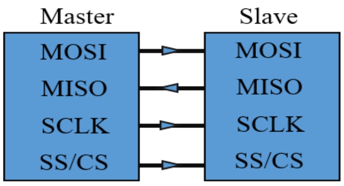

Figure 2.7 SPI interface

2.2.5 Ethernet

Communication interfaces such as RS232, RS422, RS485 are mostly used in embedded electronic devices with microcontrollers. The weak points of these interfaces can be considered as short distance, low transmission rate. Here the advantages of the Ethernet interface become clear. For example, it is possible to transfer data over very long distances with ethernet by using devices such as hubs and switches at speeds such as 100Mbit / s [70]. It is resistant to signal noises that may come from outside. Due to this feature, it is widely used in industrial automation.

2.3 On/Off Control

The most basic and the simplest interface where a microcontroller interacts with the external environment is On / Off control. On / Off control is used in many applications [71-75]. This interaction is realized with the microcontroller's I / O pins. Microcontrollers have multiple I / O pins that allow them to provide more than one On / Off control. With multiple On / Off controls, the microcontroller can perform various tasks simultaneously.

CHAPTER 3

METHODOLOGY

Renewable energy maintains its importance globally as an alternative due to reasons such as the decrease in energy resources and the need for cheap and clean energy. Besides, the demand for cheap and clean energy increases the tendency towards renewable energy sources. Therefore, renewable energy is a crucial issue in daily life. Renewable energy sources meet 14% of the world's energy demand, which are solar, wind, hydroelectric, biomass, marine, and geothermal energies [76]. In terms of renewable energy sources, PV energy is one of the most important renewable energy sources with widespread electricity generation [2].

Today, compared to other renewable energy sources, it is observed that photovoltaic panels are frequently preferred in solar farms and on the rooftops, due to their easy installation, modular and extendable structure. Considering the implementations of PV panels such as rooftops, solar farms, the highest electricity generation, and the shortest payback period of investment can be achieved by selecting feasible PV panel technology before installation. The selection of the feasible PV panel can be achieved by measuring PV panel technology's performance to be used in the location under outdoor conditions.

Photovoltaic panel performance measurement systems are essential in evaluating the real efficiency and performance of PV panels. The usage of PV technologies is increasing day by day with solar farms, and rooftops and studies in this field are still ongoing. Therefore, many studies are performed on the performance measurement systems of photovoltaic panels in the literature. In these studies, the performance of PV panels has been evaluated by applying different measurement systems or techniques. The most important technique is based on the evaluation of the maximum power point.

For these reasons, this thesis is conducted on the PV panel performance evaluation according to the maximum power point method. In the thesis study, a unique multi-

PV panel measurement system is developed by measuring PV panels' maximum power point under outdoor conditions with the MOSFET electronic load technique.

In this part of the thesis, the working principles of the developed measurement system are discussed. Besides, the 6-month measurement work carried out with the developed system is explained in detail.

3.1 Designed Multi-Photovoltaic Panel Measurement and Analysis System

The performance of PV panels is measured and analyzed for many reasons. Researchers, designers, and investors consider these performance metrics and analyses. PV panel measurement techniques and performance analysis studies are examined in the literature. Considering the limitations and drawbacks of the studies reviewed in the literature, a measurement and analysis system has been developed. In this section, the designed measurement and analysis system is discussed, namely Photovoltaic Panel Measurement and Analysis System (PPMAS).

A block diagram of designed PPMAS is shown in Figure 3.1. The PPMAS includes three major sub-systems [77];

-Photovoltaic Panel Measurement Sub-system (PPMS),

-Meteorology Measurement Sub-system (MMS),

-Data Acquisition Sub-system (DAS).

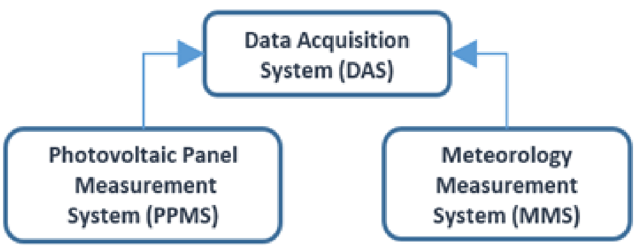

Figure 3.1 PPMAS block diagram

Photovoltaic Panel Measurement Sub-system (PPMS) is a measurement system where PV panels are connected to determine the electrical characteristics such as P_{max}, V_{mp}, I_{mp}, V_{oc}, and I_{sc}.

Meteorology Measurement Sub-system (MMS) is a measurement system where meteorology sensors measure atmospheric conditions such as ambient light, ambient temperature, humidity, wind speed, and wind directions. Additionally, there is a temperature sensor for each PV panel.

Data Acquisition Sub-system (DAS) is a computer-based platform where monitoring and data-storage facilities of PPMS and MMS are performed.

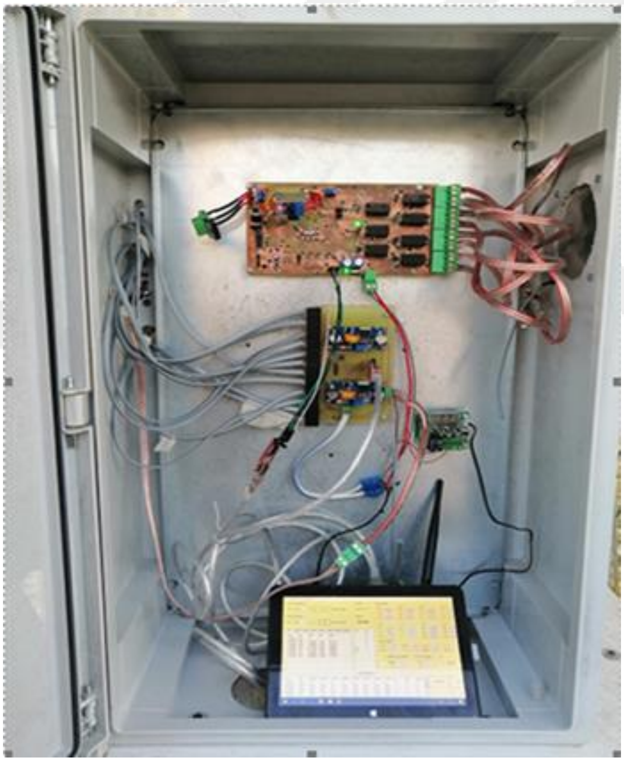

Figure 3.2 PPMAS junction box

The junction box in Figure 3.2 contains the DAS sub-system computer, MMS sub-system PCB, and PPMS sub-system PCB. The PPMAS is a system to evaluate power generation capacities of up to eight PV panels in the outdoor environment in Ankara, Turkey (Figure 3.3). The overall system, including eight PV panels and PPMAS, is shown in Figure 3.4.

Figure 3.3 Location of Ankara, Turkey.

Figure 3.4 PPMAS system, pv panels, and wind measurement mast.

3.1.1 Photovoltaic Panel Measurement Sub-system (PPMS)

The maximum power point must be continuously observed to determining the highest power generated by a PV panel. The maximum power point (MPP) varies depending on panel temperature, humidity, wind, solar radiation, and load. Many software and hardware-based algorithms can be applied for MPP detection. Results obtained without MPP detection cannot reflect the actual performance data related to the PV panel. The PPMS sub-system's purpose is to perform MPP detection of multiple PV panels quickly and accurately [77].

This sub-system is used to obtain P_{max} (maximum power) value of each PV panel in every 1000 milliseconds using MOSFET electronic load. The P_{max} is an important parameter because it is used to evaluate the performances of used PV panels. Moreover, this parameter has also been used in many studies to assess the performance of PV panels [4, 13, 41, 42, 43, 47, 50, 78]. Other essential parameters of PV panels, which are V_{mp} (voltage at maximum power), I_{mp} (current at maximum power), Isc (short circuit current), and V_{oc} (open circuit voltage) are needed to be obtained or estimated. In order to evaluate these parameters, the measured P_{max} is used in equations (6) and (8) where FF is Fill Factor. After modification of the equation (6), the maximum power P_{max} is estimated using the new equation as follows:

$$FF \, . V_{oc} \, . I_{sc} = V_{mp} \, . I_{mp} = P_{max} \tag{8}$$

Note that, in the system, it is crucial to accurately obtain the P_{max} because it is used to estimate the other parameters of PV panels, such as efficiency. It is possible to achieve this by increasing the sensitivity of the PPMS sub-system. The maximum power point (MPP) technique is applied in order to improve the sensitivity [55, 57]. Furthermore, the PPMS sub-system can measure P_{max} of up to eight PV panels and estimate other parameters separately.

A PV panel's efficiency is evaluated by the ratio of energy generated by the PV panel to solar radiation reflected in its surface area [78]. The efficiency is a useful metric that enables a comparison of PV panels, which have different nominal power outputs with different surface areas. The efficiency of a PV panel is expressed in percentage. The equation (9) is used to estimate the efficiency of the PV panels:

$$\eta_{daily} = \left(\frac{P_{daily}}{PV_{area} \cdot H_{daily}}\right).100 \quad (9)$$

Where η_{daily} represents the average daily PV panel efficiency in percentage (%), P_{daily} is the daily average power output in *Watt*, H_{daily} is the amount of daily solar radiation in $Watt/m^2$, *and* PV_{area} symbolizes the surface area of PV panel (m^2). Monthly average PV panel efficiency can be described in the equation (10) as follows, where t is the number of days in a month:

$$\eta_{monthly} = \left(\frac{\sum_{i=1}^{t} P_{(daily)\,i}}{PV_{area} \cdot \sum_{i=1}^{t} H_{(daily)i}}\right).100 \quad (10)$$

The PPMS consists of five main blocks which are 1) power supply block, 2) PPMS PCB block, 3) Relay & Switching block, 4) Measurement Block, and 5) Data transmitting block (Figure 3.5). The power supply block contains a DC-DC converter connected to the input of the PPMS as a power supply. PPMS PCB block (Figure 3.7 (a) and (b)) is the interface of the microcontroller with Relay & Switching Block, Measurement Block, and Data Transmitting Block.

PPMS has PV panel connection pins and one UART headers for Data Transmitting Block interfacing. In this block, the microcontroller manages PPMS measurement activities. Relay & Switching Block contains seven relays used to switch the PV panels. These relays are activated one by one using the microcontroller with a logical configuration. Table 2.1 shows the logical configuration to activate a PV panel by the microcontroller in the PPMS sub-system.

For example, R-4, R-6, and R-7 relays are switched ON (1), and other relays are switched OFF (0) by a microcontroller to activate the PV-8 panel.

Measurement Block is used to measure the PV panels' generated power using MOSFET electronic load (Figure 3.6). ACS-712/30A is connected serially to the drain leg of the MOSFET to measure the current. R_6 & RV_2 voltage dividers are connected parallel to the MOSFET drain and source legs to measure the voltage. Voltage (Vsense) and current (Isense) measurement pins are connected to analog inputs of the Microcontroller (Figure 3.6). The data transmitting block is used for communication purposes between PPMS and DAS computer reliably.

Table 2.1 Relay configuration for pv panel selection

	R-1	R-2	R-3	R-4	R-5	R-6	R-7
PV-1	0	0	0	0	0	0	0
PV-2	1	0	0	0	0	0	0
PV-3	0	0	0	0	1	0	0
PV-4	0	1	0	0	1	0	0
PV-5	0	0	0	0	0	0	1
PV-6	0	0	1	0	0	0	1
PV-7	0	0	0	0	0	1	1
PV-8	0	0	0	1	0	1	1

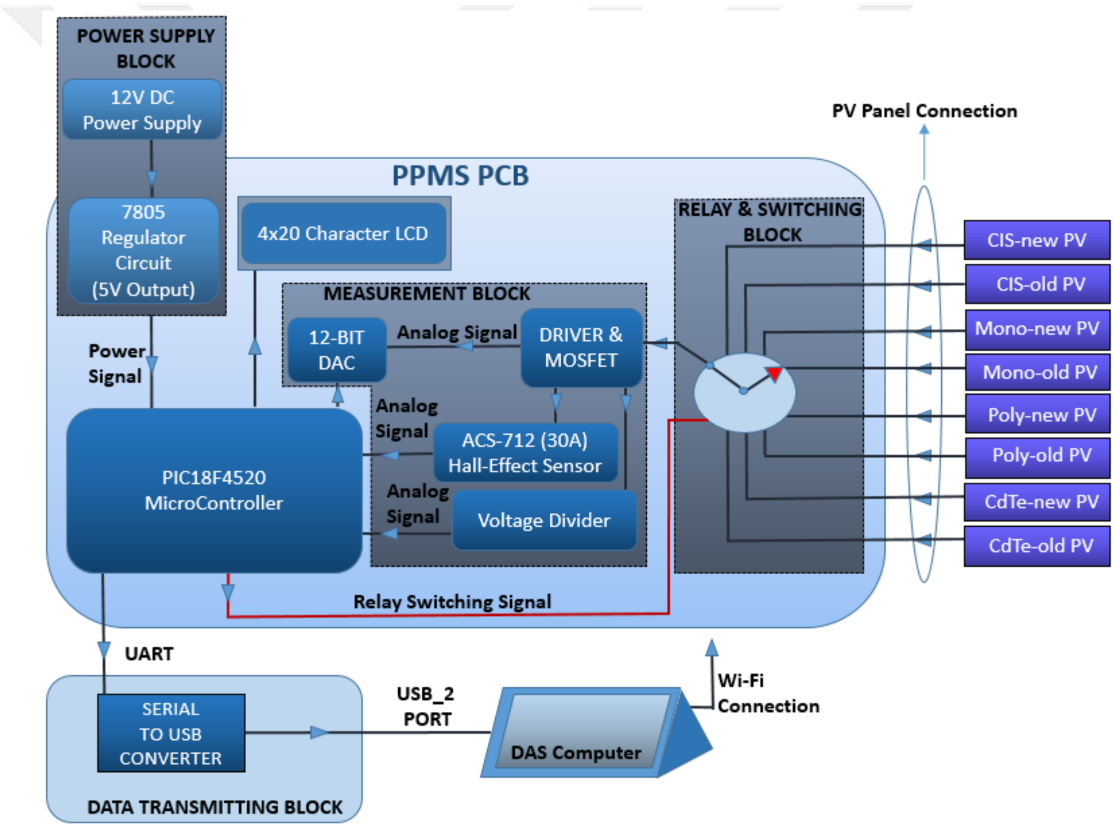

Figure 3.5 Photovoltaic panel measurement sub-system (PPMS)

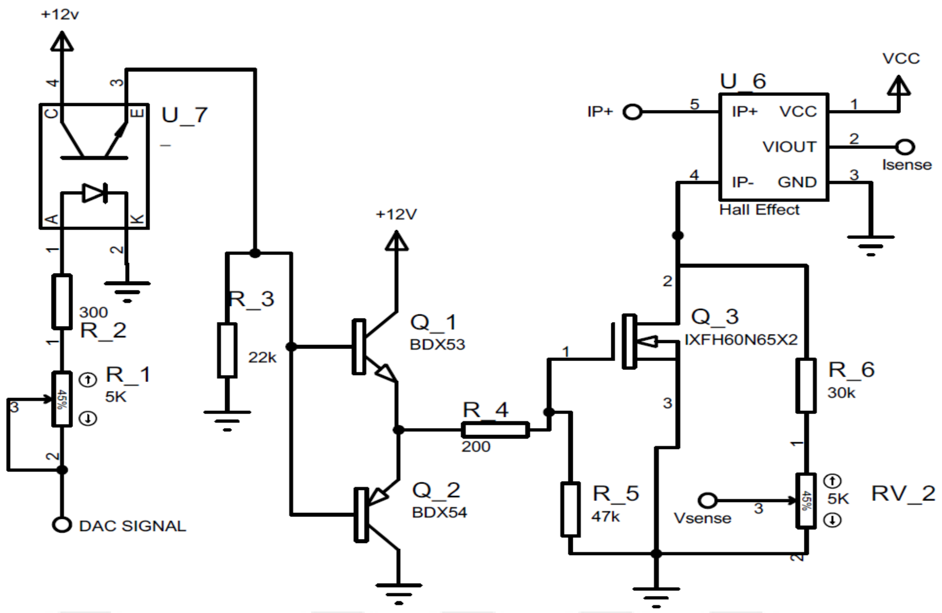

Figure 3.6 IXFH60N65X2 mosfet and pv panel measurement circuit

The PPMS sub-system microcontroller is connected to the seven relays, and each relay is connected to a different PV panel, as shown in Figure 3.5. The purpose of using the microcontroller is to switch each relay to activate the corresponding PV panel in every 1000 milliseconds, sequentially. Thus, the generated power of the activated PV panel is measured using MOSFET. For instance, as depicted in Figure 3.5, the microcontroller activates the fourth relay connected to the 140W Mono-Crystalline PV panel, and MOSFET is used to measure the generated power P_{max}. After 1000 milliseconds, the fifth relay is switched by the microcontroller to measure the 150W Poly-Crystalline PV panel's generated power, and other PV panel measurements are made respectively. The measured and estimated PV panel data parameters are transmitted to the DAS sub-system using serial communication continuously.

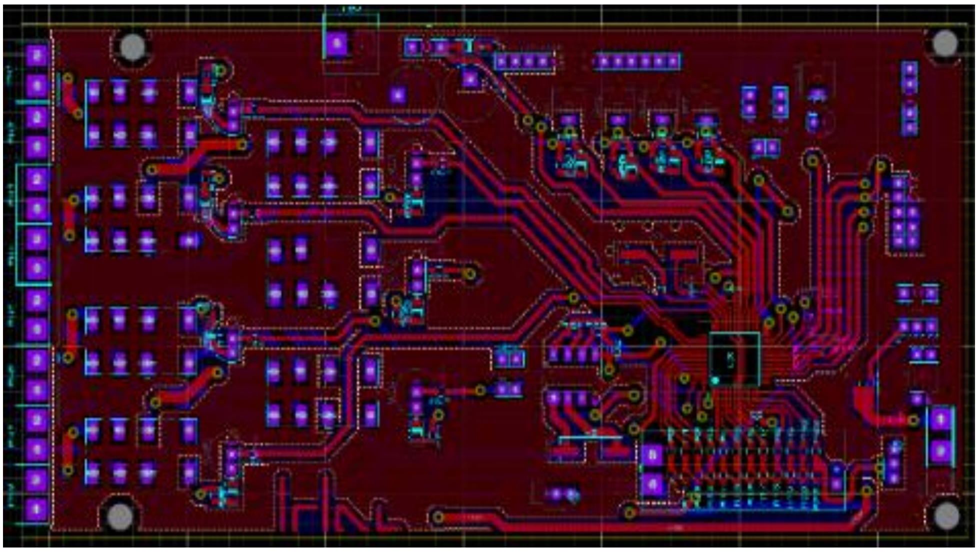

(a)

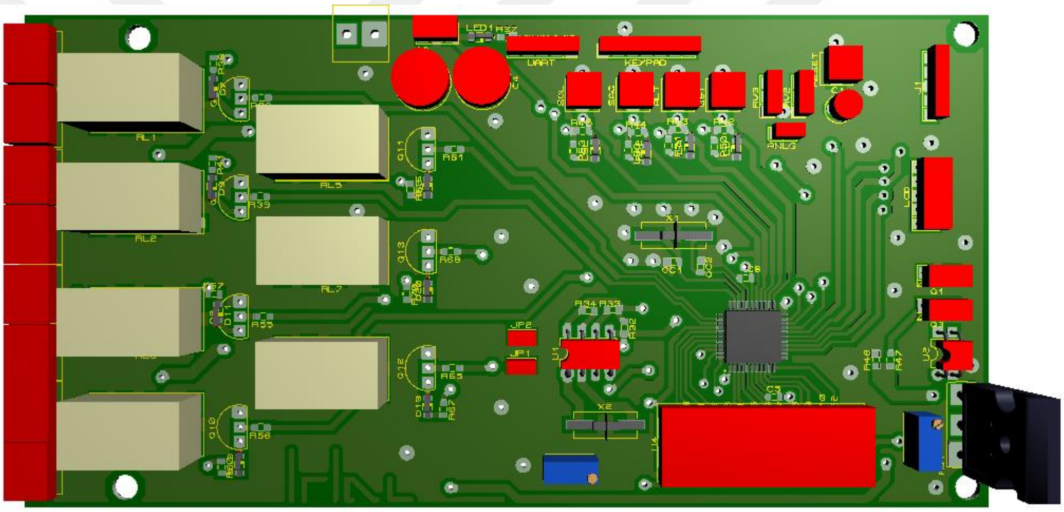

(b)

Figure 3.7 a) PPMS sub-system pcb, b) 3D view of PPMS sub-system pcb

3.1.1.1 Algorithm of PPMS Sub-system

In the PPMS algorithm shown in Figure 3.8, initial adjustments are made for the PPMS microcontroller and parameters. UART-based serial communication is started after initial settings are made. Relays are configured by the microcontroller to select the PV panel to evaluate P_{max} and its Current and Voltage components. MOSFET electronic load is used as a variable resistor by the microcontroller. Zero resistance to infinity resistance is applied to selected PV panel terminals, where the power is evaluated in each step. In other words, the PPMS sub-system microcontroller quickly scans the resistor values of MOSFET to determine the maximum power point from short circuit to open circuit. After determining P_{max}, V_{mp}, and I_{mp}, the PPMS sub-system microcontroller sends the measurements to the DAS sub-system computer via UART for monitoring and database recording purposes. DAS sub-system gets the measurement data in reserved areas in the interface program and saves it in the database.

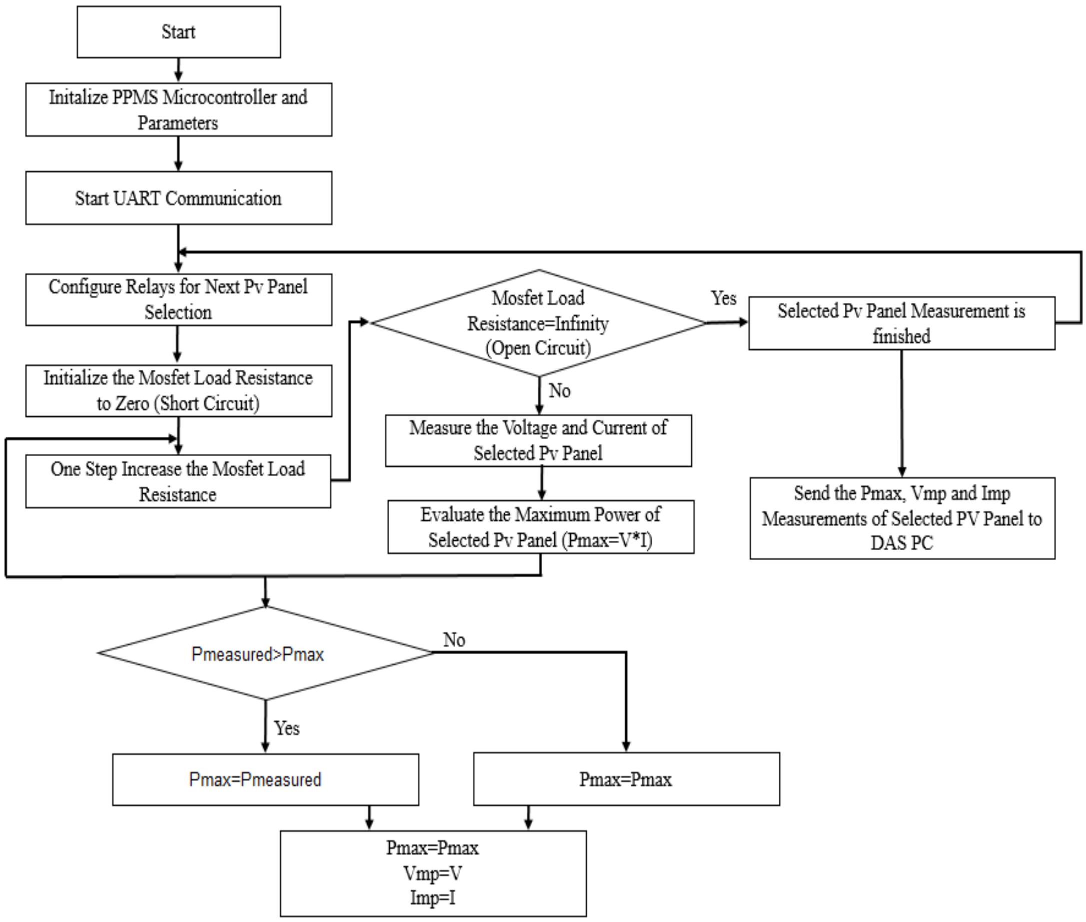

Figure 3.8 PPMS algorithm

3.1.1.2 PIC18F4520 Microcontroller in PPMS

The microcontroller used in the PPMS sub-system is PIC18F4520 and shown in Figure 3.9. The microcontroller is manufactured by Microchip company. CMOS flash-based 8-bit architecture of the microcontroller is embedded into 44 pin package, and some other specifications of PIC18F4520 are; 13-channels A/D converter, a USART, 256 bytes of EEPROM memory, a EUSART, 36 I/O, Dual Analog comparators, 1 x 8-bit timers, 3 x 16-bit timers and 4.2V - 5.5V operating voltage range [79].

Figure 3.9 PIC18F4520 microcontroller

3.1.1.3 Voltage Measurement of PV Panels

Voltage measurement for PV panels in the PPMS sub-system is made with the voltage divider shown in Figure 3.11, which is a well-known technique to measure voltage. The voltage divider is also a simple and essential circuit in electronics. It is used to reduce the high voltage level to the required lower level from a common voltage source (Figure 3.10). Also, the current through the resistors will be the same, since they are connected in series. Two resistors are used in serial to make the voltage divider circuit. Equation (11) is used to evaluate the voltage divider.

$$V2 = V\frac{R2}{R1+R2} \tag{11}$$

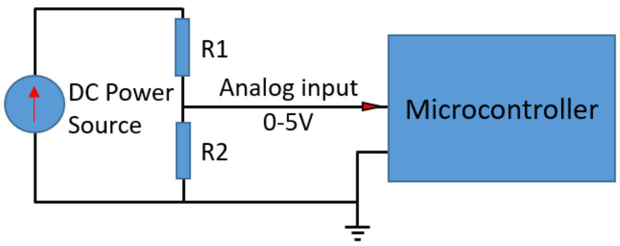

Figure 3.10 Microcontroller and voltage divider interfacing

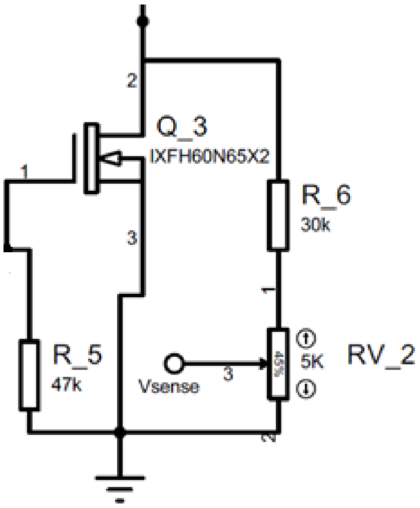

Figure 3.11 Voltage divider circuit used in PPMS

Another example of the voltage divider is the potentiometer, as in Figure 3.11, which is typical in daily life. The potentiometer is a resistor with three terminals. Working principle; The two ends are connected to the fixed terminal, and the third terminal changes the output voltage because it is variable. In other words, the potentiometer is a variable voltage divider that sets the output voltage to the desired level.

3.1.1.4 Current Measurement of PV Panels

ACS-712/30A is used in the PPMS sub-system to measure the current of PV panels. A version of ACS-712 can be seen in Figure 3.12. It works according to the hall effect principle and can measure current up to 30 A. The ACS-712 current sensor works according to the Hall Effect principle. A copper strip connects the IP+ and IP– pins internally, which creates a magnetic field detected by the Hall Effect sensor, depending on the amount of current flowing through it. This magnetic field is converted into an analog voltage by the Hall Effect sensor.

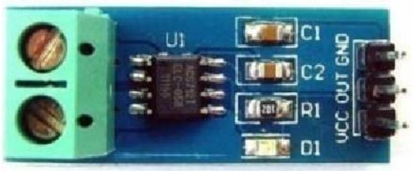

Figure 3.12 ACS-712 [80]

The ACS712 / 30A can measure with an accuracy of 66 mV, representing the analog output voltage generated for each ampere. This analog voltage value is read from the microcontroller's adc input and the current value is calculated by making the necessary calculations. The interface of ACS-712 with microcontroller is shown in Figure 3.13.

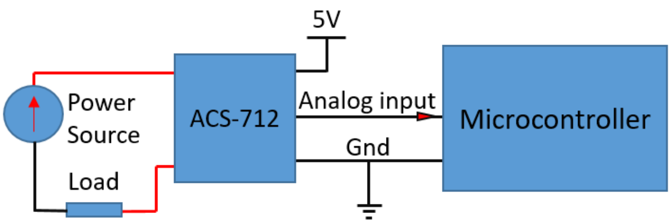

Figure 3.13 Microcontroller and ACS-712 interfacing

The current sensor has a measurement capacity of up to 30A. There is a 2.5V voltage offset value for positive and negative directional current measurements. When the output voltage is 2.5V, generated by the sensor, the measured current is "0A". If the generated voltage is below 2.5V, the current direction is evaluated as negative, and if the generated voltage is above 2.5V, the direction of the current is evaluated as positive.

3.1.1.5 MOSFET as an Electronic Load and I-V Characterization of a PV Panel

One of the most significant parameters of a PV panel is the I-V curve, which includes PV panel performance metrics such as efficiency - η, open-circuit voltage - V_{oc}, short circuit current - I_{sc}, maximum power - P_{max}, the voltage at maximum power point - V_{mp}, current at maximum power point - I_{mp} [24]. The PV panel's current must be controlled from the zero current point to the short circuit point to perform the I-V curve [81]. MOSFET can be used as an electronic load in the designed PPMS sub-system, to control the current and obtain the I-V curve of a PV panel.

Drain-source pins of a MOSFET may behave as a variable resistor when there is a voltage difference on gate-source pins, such that; when gate-source voltage difference is high, drain-source behave as low resistance (can be assumed short circuit), when gate-source voltage difference is low, drain-source behave as high resistance (can be assumed open circuit) [82]. By utilizing this feature of MOSFET, PV panel I-V characteristics can be extracted.

Figure 3.14 shows the SOA graph of IXFH60N65X2 MOSFET, used in the PPMS sub-system. Note that SOA defines the current and voltage conditions in which a MOSFET can operate without any risk of damage. Exceeding the limits of current and voltage values in the SOA graph, even for a moment, may cause permanent damage or breakdown of the MOSFET. For example, by observing the SOA graph of IXFH60N65X2 MOSFET, drain-source pins can allow the current flow as little as one millisecond, approximately 100V 40A. In the designed PPMS sub-system PCB, SOA has been taken into account such that, microcontroller quickly drives the gate pin to manipulate PV panel generated power in the drain pin fastly.

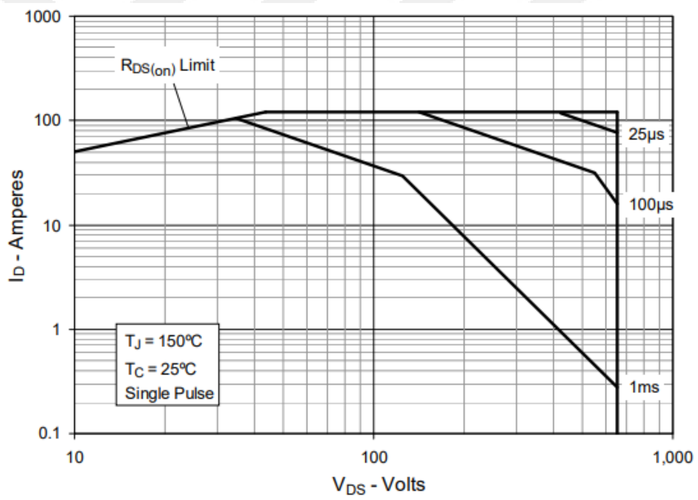

Figure 3.14 Safe operating area of IXFH60N65X2 mosfet [83]

In the thesis study, the microcontroller drives the MOSFET to evaluate all current and voltage values of a PV panel from short circuit to open circuit point in a measurement period (1000 milliseconds). During one measurement period, the PPMS microcontroller observes the highest power point to record in Watts, called P_{max}. After finding P_{max}, its components are recorded as I_{mp} and V_{mp} [77].

3.1.1.6 DAC Circuit to Drive MOSFET

Figure 3.15 depicts the DAC circuit used in the PPMS sub-system PCB. Twelve digital inputs are connected to the 18F4520 microcontroller. The microcontroller drives these digital inputs to build an analog signal. Resistors are connected to the 2R-R ladder combination. It is essential to select the resistors as close as possible to this ratio to generate a precise analog signal. Otherwise, the difference may cause errors in the applied circuit. Small differences due to tolerance of resistors are expected not to cause errors. In PPMS sub-system PCB, the resistors are selected as 660ohm and 330ohm to perform 2R-R configuration. At the RV1 pin, the analog signal is generated as a product.

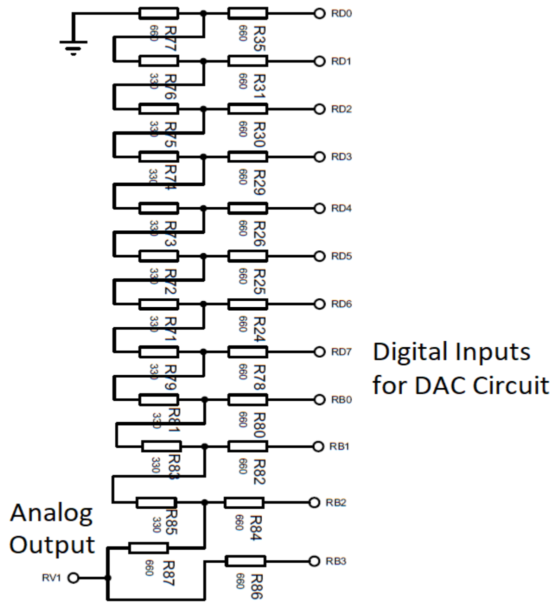

Figure 3.15 12-Bit DAC circuit

3.1.1.7 Relay Driving Circuit and PV Panel Selection

Figure 3.16 is a part of the relay switching circuit in the PPMS sub-system PCB. The drawing has three critical units, which are PV panel connection, relay control, and measurement block connection pin. There is a connection point named RE2, which comes from the 18F4520 microcontroller's digital output. The primary function of RE2 is to provide an On/Off signal to drive the Q5 transistor.

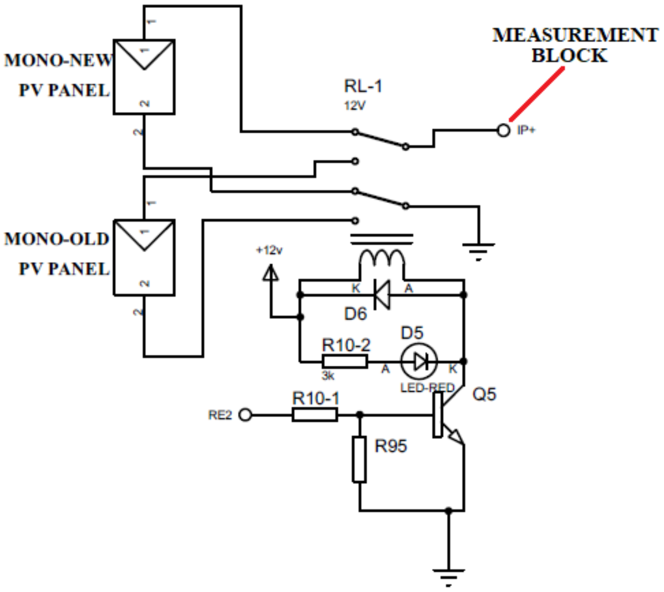

Figure 3.16 PV panel selection and relay circuit

When RE2 is On, the Collector-Emitter of the Q5 transistor switches on, and the RL-1 relay is energized. The position of RL-1 relay changes and Mono-old PV panel selection takes place. In other words, Mono-old PV panel terminals are connected to the IP+ and ground line for I-V characteristic measurement. At the end of 1000ms, the RL-1 relay changes with the Off command sent by the microprocessor to RE2, and the related relays are activated for the measurement of the next PV panel. The PV panel selection algorithm described here is performed in the same way for all PV panels.

3.1.1.8 One-cycle Operation of PPMS Sub-system

The measurement circuit of PPMS is depicted in Figure 3.6. As shown in Figure 3.5, the microcontroller in the PPMS selects the related relay combinations to activate the Mono-old PV panel connection to the Hall-Effect sensor and then to Drain of MOSFET to measure current pass in it when the switching signal comes to the Gate of MOSFET by the 12-bit DAC signal [77]. DAC signal is generated through the R-2R ladder circuit from the digital outputs of the Microcontroller. DAC signal enters to opto-isolator to switch 12V to the totem-pole circuit. The Totem-pole circuit is used to drive MOSFET in the linear region. R_1 potentiometer is an adjustable resistor to adjust the threshold level in terms of voltage for the opto-isolator. At the same time, PV panel (Mono-old PV) connection comes to (IP+) pin of Hall-Effect sensor (ACS-712/30A) serially, which is used to measure the current of (Mono-old PV) PV panel. (IP-) pin of Hall-Effect sensor goes to MOSFET's drain pin so that current flows to drain to the source by using MOSFET as electronic load. The Isense output pin of the Hall-Effect sensor goes to the microcontroller's analog input to measure the current of the PV panel (Mono-old PV). Also, the Vsense pin goes to another analog input channel of the microcontroller to measure the voltage of the PV panel (Mono-old PV), where R_6 and RV_2 are used as a voltage divider. The RV_2 potentiometer manages measurement calibration.

The microcontroller measures and stores the generated power of the PV panel (Mono-old PV) with respect to voltage and current measurements ($P_{max} = V_{mp} * I_{mp}$), continuously during the measurement cycle, which is 1000 milliseconds. The microcontroller assigns the highest power value as P_{max}, among the stored power values. The microcontroller determines the current and voltage values that form the P_{max}, as I_{mp} and V_{mp}, respectively. After P_{max} evaluation of PV panel (Mono-old PV), measurements are completed for one cycle. All other PV panels (CIS-new, CIS-old, Mono-new, Poly-new, Poly-old, CdTe-new, and CdTe-old) connections are switched to the MOSFET in a sequence with respect to a switching strategy to obtain V_{mp}, I_{mp}, and P_{max} of each PV panel in the same manner.

3.1.2 Meteorology Measurement Sub-system (MMS)

When measuring PV panels' power, it is necessary to determine under which weather conditions they reach the maximum power point. It is essential to measure and record the meteorological parameters simultaneously with PV panel measurements to obtain accurate results for the analysis. This approach can determine which PV panel generates more efficient power under the same weather conditions. Meteorology stations used in the analysis of PV panels consist of a wide variety of software and hardware units. Looking at the meteorology systems used in the literature, most of them consist of high-cost measurement sensors. The MMS sub-system aims to produce a low-cost, precise, and accurate measurement system to be used to analyze PV panels [77].

The primary purpose of using the MMS sub-system is to measure the meteorological parameters, which are ambient temperature, humidity, ambient light, wind speed, wind direction, and PV panel temperatures. These parameters are crucial because PV panels' power generation performance depends on these parameters [4, 84, 85].

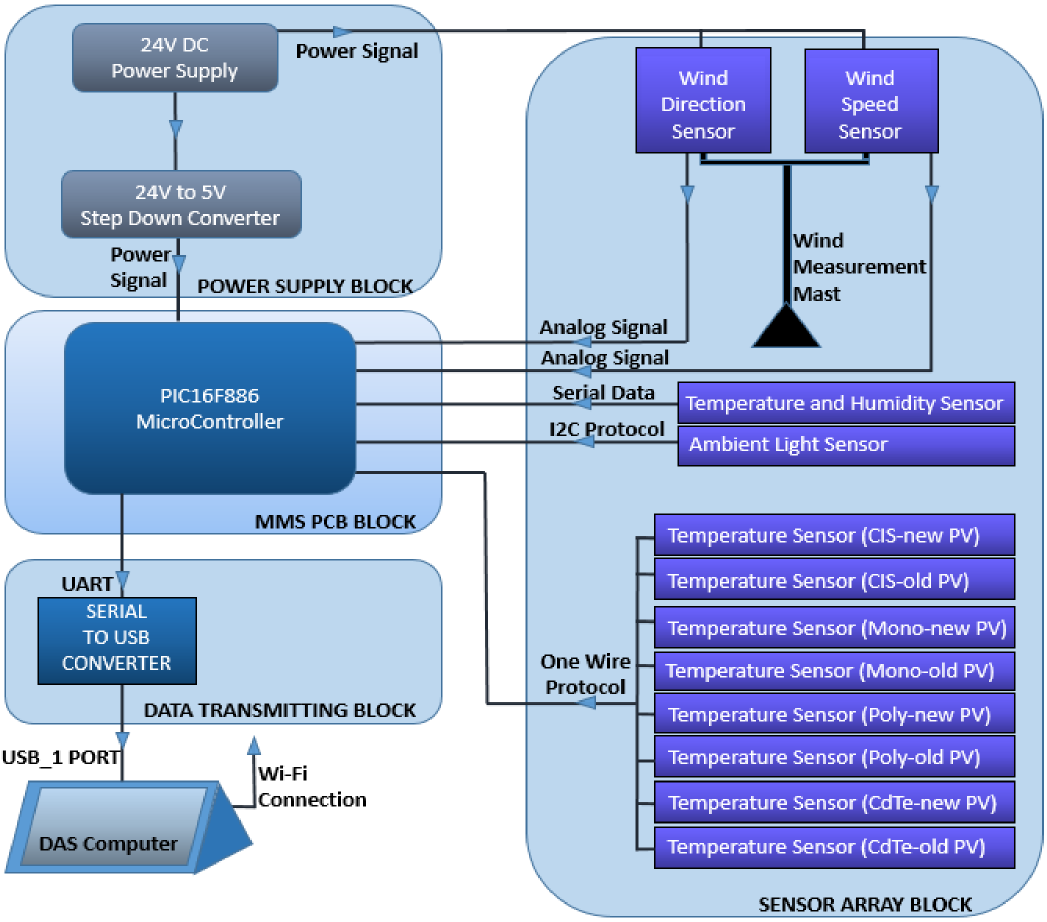

Figure 3.17 Meteorology measurement system (MMS)

In this sub-system, the parameters are measured at each second from 5:00 am until 9:00 pm. The MMS consists of four main blocks, to achieve these measurements, as shown in Figure 3.17. In the MMS PCB block, a microcontroller is employed to measure the meteorological parameters and interconnected with the power supply block, sensor array block, and data transmitting block. For instance, the pin connections between the MMS PCB block and power supply block are illustrated in Figure 3.18 (a) and (b). In the sensor array block, twelve meteorological sensors have been used to measure and understand atmospheric conditions and PV panels' temperature. These sensors are the DHT-22 temperature & humidity sensor, Max44009 ambient light sensor, wind speed & direction sensors, and eight pieces of DS18B20 PV panel temperature sensor. These sensors and the microcontroller are explained in more detail in the following subheadings.

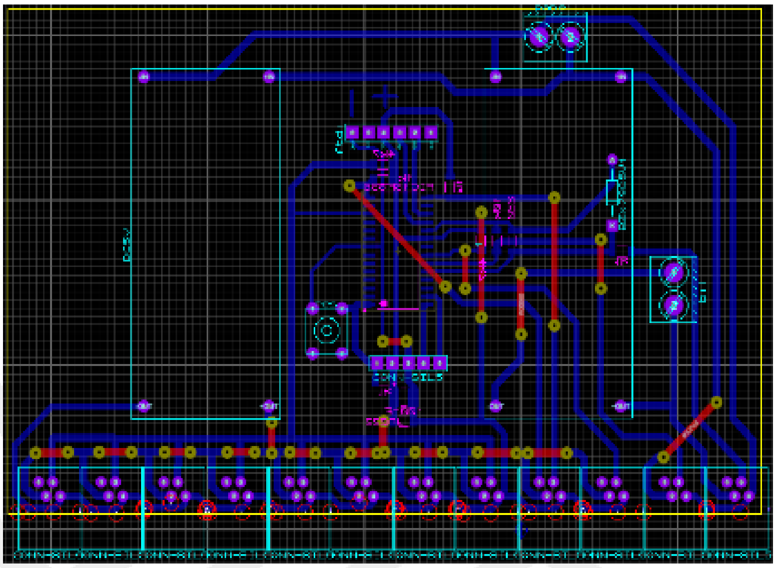

(a)

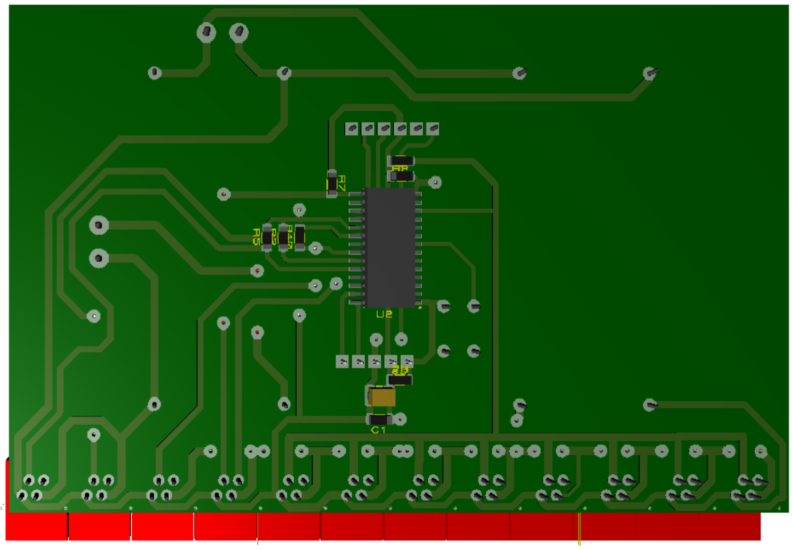

(b)

Figure 3.18 a) MMS pcb and b) 3D view of MMS pcb

The power supply block is used to energize the MMS PCB block and sensor array block. Thus, the components in these blocks can work without any electrical problems.

In this sub-system, data transmitting block is used to transmit the measured meteorological data via a connected cable to a data acquisition sub-system (DAS) computer for storing data. Finally, the DAS sub-system computer's recorded data is transmitted to the personal computer for analyzing purposes when the user requests this data from the DAS sub-system computer.

3.1.2.1 Algorithm of MMS Sub-system

In the algorithm shown in Figure 3.19, initial adjustments are made for the MMS microcontroller and the sensors. UART-based serial communication is started after initial settings are made.

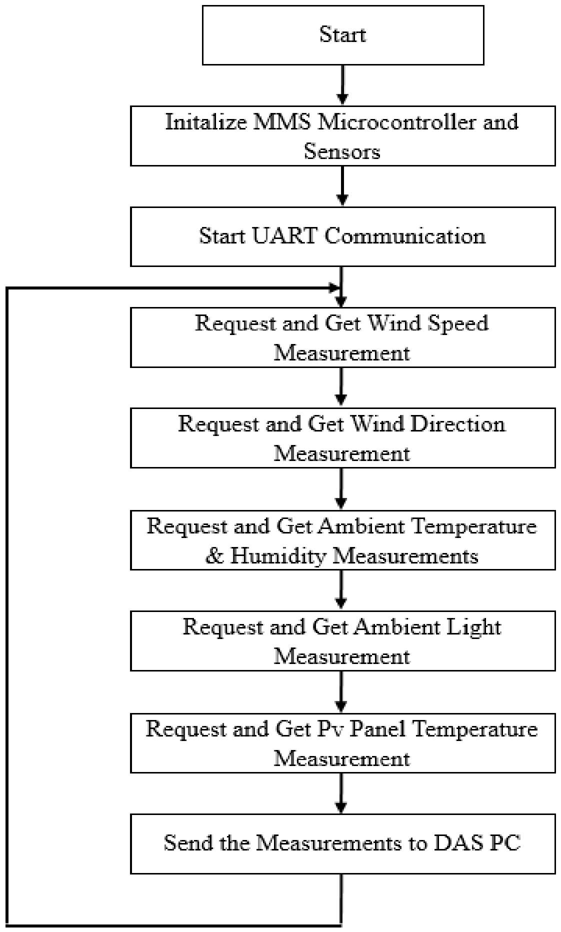

Figure 3.19 MMS sub-system algorithm

The MMS microcontroller queries the wind speed, wind direction, ambient temperature & humidity, ambient light, and PV panel temperatures, respectively, and sends them to the DAS sub-system computer over the UART. DAS sub-system places the measurement data in reserved areas in the interface program and saves this data in the database.

3.1.2.2 PIC16F886 Microcontroller in MMS Sub-system

The microcontroller used in the MMS sub-system is PIC16F886 and shown in Figure 3.20. The microcontroller is manufactured by Microchip company. CMOS flash-based 8-bit architecture of the microcontroller is embedded into the 28 pin package [86]. Some other specifications of PIC16F886 are an 11-channels A/D converter with 10-bit resolutions, a serial port, 256 bytes of EEPROM memory, an Enhanced Universal Asynchronous Receiver Transmitter (EUSART), 24 programmable I/O pins, 2 Analog comparators, 2 x 8-bit timers, and operating voltage interval is 2V - 5.5V [86].

Figure 3.20 PIC16F886 microcontroller

3.1.2.3 Wind Speed Sensor

It is used to measure the speed of the wind in the MMS sub-system (Figure 3.21). The sensor generates an analog signal output according to the speed of the wind. This generated analog signal is measured by the microcontroller, which is located in the MMS sub-system PCB.

The commonly used anemometer sensor rotates in a vertical axis with three cups to measure wind speed. These cups are placed at an angle of 120 degrees. Wind creates an equal amount of force on the cups and rotates in a proportional and balanced manner. In other words, the anemometer's rotation speed changes proportionally according to the speed of the wind.

Figure 3.21 Wind speed sensor

The interface diagram of the sensor and microcontroller is shown in Figure 3.22. The sensor has three wire connections where an analog signal pin for measurement data, (+) and (-) for 12V supply voltage.

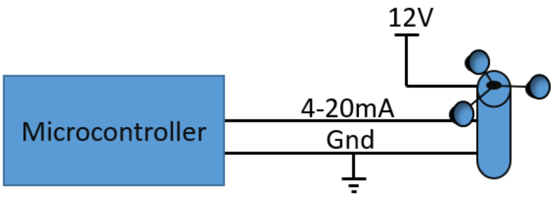

Figure 3.22 Microcontroller and wind speed sensor interfacing

Wind speed measurement limitation of the sensor is in the range of 0.4 m/s and 32 m/s. The sensor operates with a 12V supply voltage. The sensor's output is an analog signal in the range of 0-5V, which corresponds to the measurement value. This analog signal is received through the ADC input of the microcontroller and then evaluated.

3.1.2.4 Wind Direction Sensor

The wind direction sensor seen in Figure 3.23 is used to define the wind direction in the MMS sub-system. When the sensor is energized by 12 V supply voltage, it generates an analog signal output in the range of 4-20 mA depending on the wind's direction. The ADC pin of the microcontroller takes the generated signal. The analog signal evaluated by the microcontroller is classified to correspond to the direction of the wind between 0-360 °. The interfacing of the sensor can be seen in Figure 3.24.

Figure 3.23 Wind direction sensor

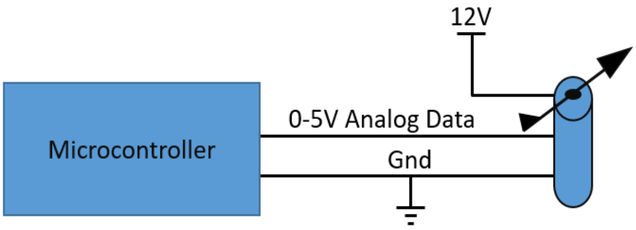

Figure 3.24 Microcontroller and wind direction sensor interfacing

Eight wind directions and angles can be seen in Table 3.1. For example, the direction of the North is 0°/360°, the South is 180°, the North-East is 45°, and the South-West is 225°.

The evaluation of wind directions seen in Table 3.1 is performed using the microcontroller of MMS sub-system PCB with respect to the analog signal generated from the wind direction sensor's output.

It is also possible to evaluate the intermediate directions such as South-SouthEast (SSE) to 157.5°, North-NorthWest (NNW) to 337.5°.

Table 3.1 Wind direction and corresponding angles

Direction of Wind	Acronym	Degree
North	N	0/360
South	S	180
East	E	90
West	W	270
North-East	NE	45
North-West	NW	315
South-East	SE	135
South-West	SW	225

3.1.2.5 Ambient Temperature and Humidity Sensor

DHT-22 sensor is used, measuring the temperature and humidity of the air. (Figure 3.25). The sensor block has a thermistor to measure the temperature and a capacitive sensor to measure the humidity. These two sensors are integrated with an 8-bits microcontroller in the sensor block [87].

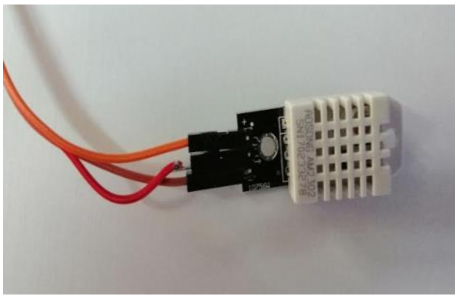

Figure 3.25 DHT22 temperature & humidity sensor

The temperature and humidity sensor has three active pin connections. These are VDD, Ground, and Data pins, respectively. After receiving the start signal from microcontroller it sends the measurements from the data pin, where measurement ranges are between -40 and 80 C for temperature and between 0 and 100% RH for humidity [87]. Simply, the interfacing diagram for microcontroller and DHT-22 sensor can be seen in Figure 3.26.

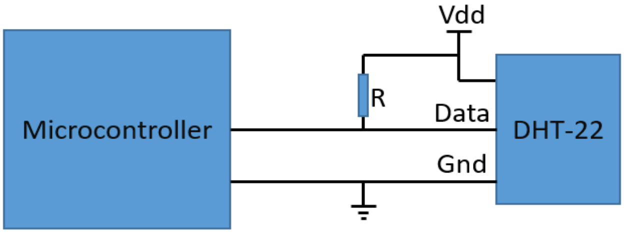

Figure 3.26 Microcontroller and DHT22 interfacing

3.1.2.6 PV Panel Temperature Measurement Sensor

Solar panel temperatures are measured with eight numbers of temperature sensors namely DS18B20. The sensors are mounted backside of the PV panels and wired to MMS sub-system PCB. DS18B20 sensor can be seen in Figure 3.27.

Figure 3.27 DS18B20 pv panel temperature sensor

DS18B20 measurement data is collected serially with the "One-Wire" technique and transferred to the microcontroller. Each sensor transmits measured temperature data with its address information to the microcontroller of MMS PCB. Sensor pinout and interfacing with a microcontroller can be seen in Figure 3.28.

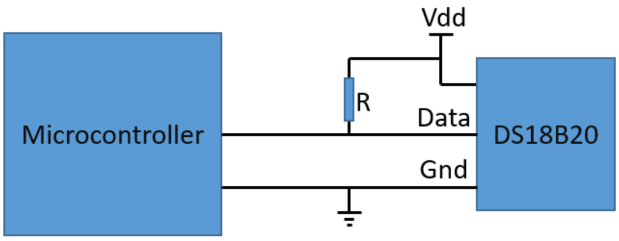

Figure 3.28 Microcontroller and DS18B20 interfacing

The DS18B20 temperature sensor has three pins, namely VDD, Ground, and DQ [88]. DS18B20 has up to 12-bits of measurement precision and 64-bits of unique ID for addressing [88]. Each sensor sends the measurement data with its unique ID to the microcontroller of the MMS sub-system PCB.

3.1.2.7 Ambient Light Sensor

The Max44009 sensor is used to measure the illumination of the sun (Figure 3.29). The Max44009 is set to a tilt angle of 30° to observe the Sun's illumination on the PV panels, which is the same slope of PV panels. Sensor pinout and interfacing with a microcontroller can be seen in Figure 3.30.

Figure 3.29 Max44009 ambient light sensor

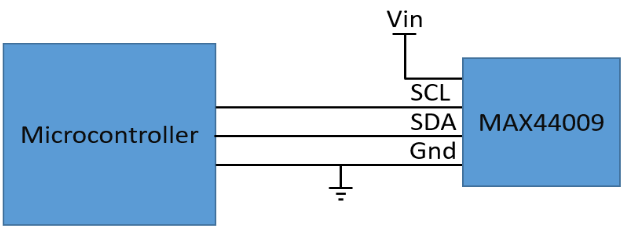

Figure 3.30 Microcontroller and max44009 interfacing

3.1.3 Data Acquisition Sub-system (DAS)

The last sub-system of the PPMAS system is DAS, which manages real-time data monitoring and data storage activities. To achieve this, both measured and estimated parameters in the PPMS sub-system and the MMS sub-system are sent to the DAS sub-system computer via connected communication cables [77]. In the last sub-system, the parameters which are measured in the other sub-systems are stored in a database in the DAS sub-system computer (Figure 3.31), and the recorded data can be transmitted remotely to a personal computer for analyzing and data displaying purposes continuously if a user requests data from DAS sub-system. Note that, DAS sub-system computer can store and monitor all the parameters of all PV panels connected to the PPMS sub-system and the meteorological parameter measurements obtained in the MMS sub-system. Besides, the DAS sub-system has a storage capacity to record 50 years of measurement data in continuous operation.

3.1.3.1 DAS Computer

The DAS subsystem has a Hometech brand computer (Figure 3.31). Features of the computer were obtained by visual inspection on it and presented (in Table 3.2). It has a Quad-Core microprocessor, HDMI, SD card reader, Wifi, 7” touch screen with 1280x800 resolution, Bluetooth, and four USB ports.

Table 3.2 Specfication of DAS computer

Operating System:	Windows 10
CPU:	INTEL (Cherry Trail Z8300)
Core:	Quad
Screen:	7"
Panel:	IPS Panel
Resolution:	1280 x 800
RAM:	2 GB
Memory:	32 GB
Bluetooth:	Yes
HDMI:	Yes
USB:	4 x USB
SD Card:	Yes

Figure 3.31 View of DAS sub-system computer

3.1.3.2 DAS Sub-system Computer Serial Interface

HW-417 is a board with a USB-serial converter integrated on it (Figure 3.32). There are RX, TX, CTS, DTR, VCC, and GND pins on the converter board. There is an FT232RL integrated on the board. The jumper on it, it can be used with 3.3V and 5V cards. It has a mini USB B type connector.

a)

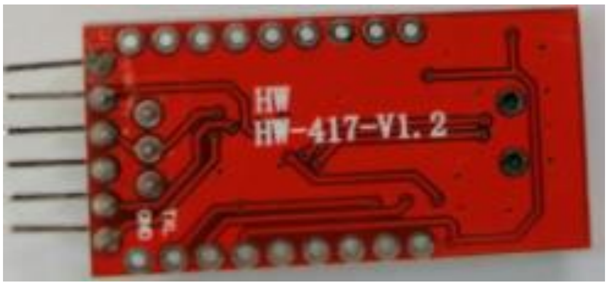

b)

Figure 3.32 HW-417 serial to usb converter

3.1.3.3 Algorithm of DAS Software Application

Figure 3.33 shows the DAS sub-system algorithm. The Visual C# compiler implements the algorithm. The algorithm starts with initialization. It begins with the initialization of data field parameters, UART-1 and UART-2 ports. After the initialization process, The data coming from MMS and PPMS are monitored in real-time on reserved textboxes. The data also recorded to the database of the DAS sub-system computer continuously.

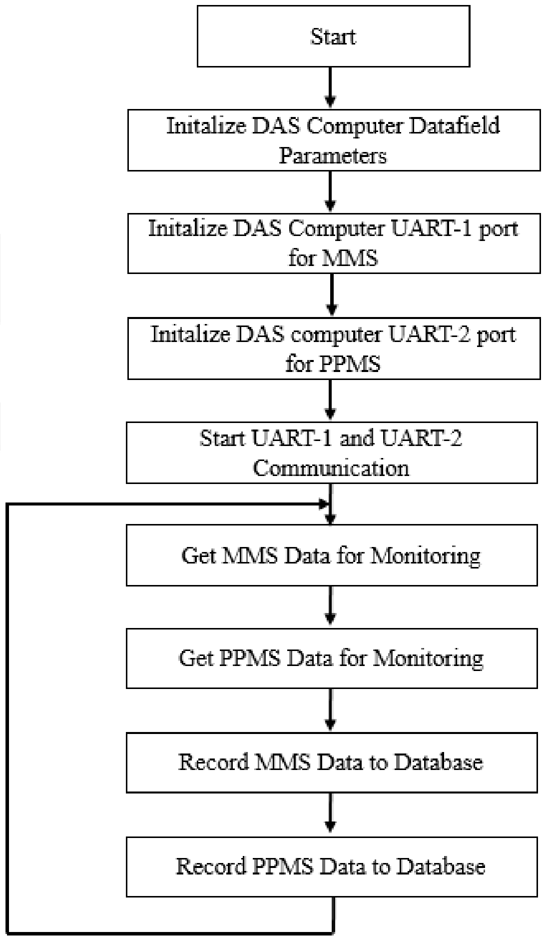

Figure 3.33 DAS sub-system algorithm

3.1.3.4 Data Monitoring and Recording

The MMS and PPMS sub-systems have two main tasks: to perform measurements and transmit measurements to the DAS sub-system. Communication between the PPMS sub-system and the MMS sub-system with the DAS sub-system is provided over

UART. The data is received from the USB ports of the DAS sub-system computer via USB/Serial adapter. Received data is placed in the reserved data fields in an organized manner in the DAS sub-system. These data are processed both for viewing on the DAS sub-system computer and for recording in the database. Data fields sent by MMS and PPMS sub-systems and processed on the DAS computer are shown in Figure 3.34.

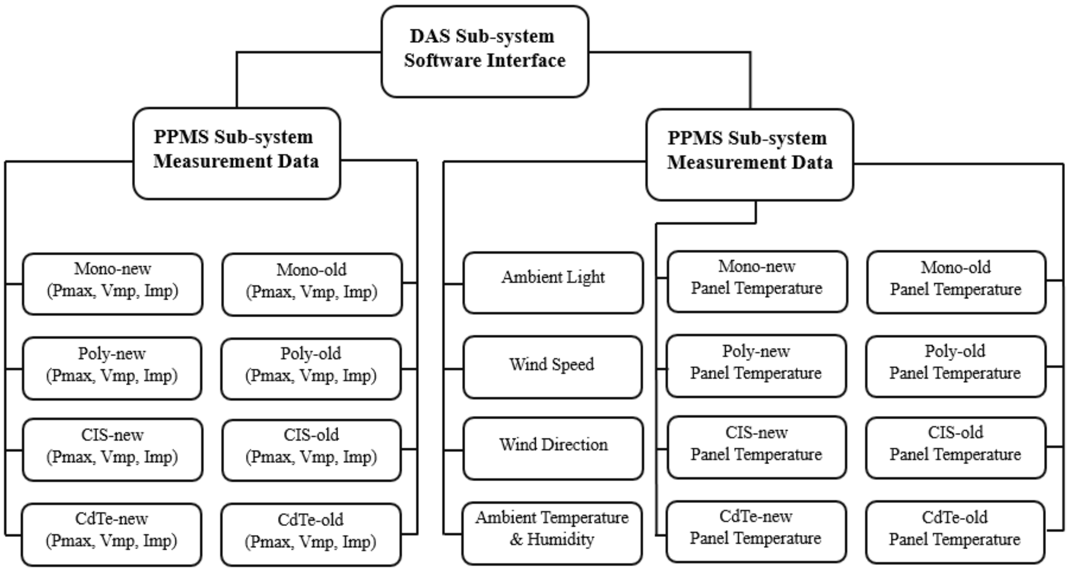

Figure 3.34 Data fields

An interface program is designed in the DAS sub-system computer to visualize and to record the measurements. The interface program used in the DAS sub-system computer is coded with the Visual C#. It is a modern object-oriented programming language and developed by Microsoft. It is an easy language for users with C-based coding knowledge. General features of Visual C# language are the following:

- Simple and general-purpose programming language

- Easy to use modern language

- Object-oriented

- Structured programming language

- Ability to compile on various computer platforms and including many more features.

Due to these benefits, it has been preferred for coding the DAS interface application. Many lines of code are written in C# to organize the measurement data. Some screenshots and code examples are provided for better understanding. For example, C# coding of the interface application can be seen in Figure 3.35. The Graphical User Interface (GUI) of the software application can be seen in Figure 3.38, which is a carefully designed software interface for the user to best track the data.

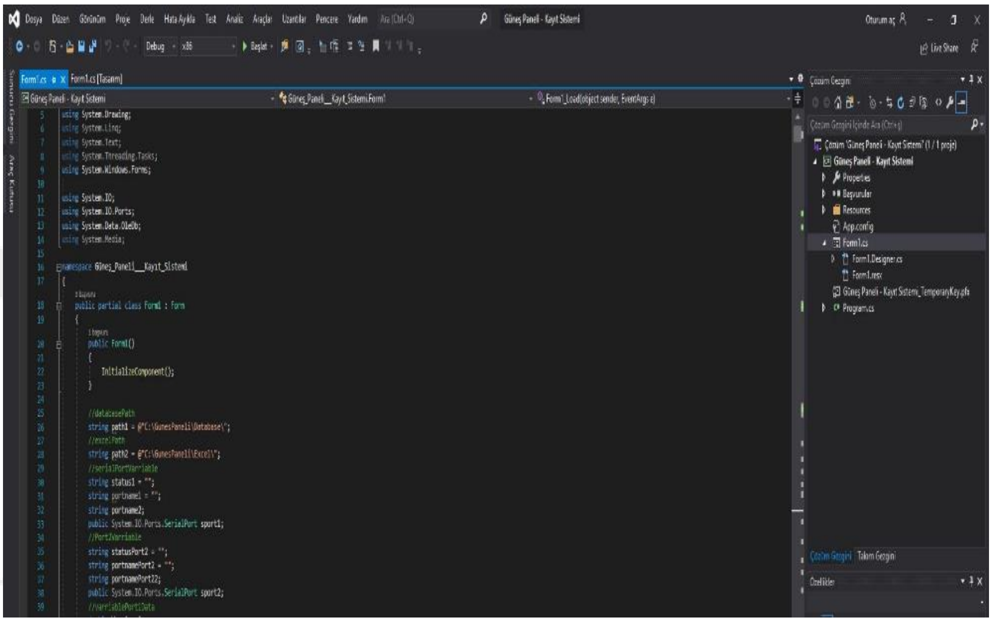

Figure 3.35 An example C# code block view in designed software interface

In Figure 3.36, serial port configuration initialization can be seen in C#. DAS sub-system computer has four USB ports. Two USB ports are configured as a serial port to read the data from PPMS and MMS sub-systems. Both of the serial ports are configured 9600 baud rate with “8-N-1” settings.

In order to prevent the failure in serial port connection, the Try-Catch block is applied to C# coding in Figure 3.36. If any failure occurs in the serial port connection during the run-time, the interface gives a warning to the user.

```csharp
void ConnectPort1()
{
    try
    {
        String port = comboBox1.Text;
        int baudrate = 9600;
        Parity parity = (Parity)Enum.Parse(typeof(Parity), "None");
        int databits = 8;
        StopBits stopbits = (StopBits)Enum.Parse(typeof(StopBits), "One");
        serialport_connect(port, baudrate, parity, databits, stopbits);
        button2.Enabled = true;
        button1.Enabled = false;
    }
    catch (Exception ex)
    {
        MessageBox.Show("Port Dolu", "Hata");

    }
}
```

Figure 3.36 Serial port configuration of the interface in c#

Figure 3.37 depicts the C# coding example for database connection, data field assignment, and string operations.

```csharp
void DatabaseYaz(string date, string time,
                 string vmax11, string ımax11, string pmax11,
                 string vmax22, string ımax22, string pmax22,
                 string vmax33, string ımax33, string pmax33,
                 string vmax44, string ımax44, string pmax44,
                 string vmax55, string ımax55, string pmax55,
                 string vmax66, string ımax66, string pmax66,
                 string vmax77, string ımax77, string pmax77,
                 string vmax88, string ımax88, string pmax88,
                 string ds1, string ds2, string ds3, string ds4, string ds5, string ds6, string ds7, string ds8,
                 string dht1,string dhh1,string lux1, string yon1, string hiz1)

{
    string file = path1 + "\\" + "Database.mdb";
    try
    {
        string vtyolu = @"Provider=Microsoft.Jet.OLEDB.4.0;Data Source=" + file + ";Persist Security Info=True";
        OleDbConnection baglanti = new OleDbConnection(vtyolu);
        baglanti.Open();

        string ekle = "insert into DataLog(Tarih,Saat,Vmax1,Imax1,Pmax1,Vmax2,Imax2,Pmax2,"
                                        + "Vmax3,Imax3,Pmax3,Vmax4,Imax4,Pmax4,"
                                        + "Vmax5,Imax5,Pmax5,Vmax6,Imax6,Pmax6,"
                                        + "Vmax7,Imax7,Pmax7,Vmax8,Imax8,Pmax8,"
                                        + "DST1,DST2,DST3,DST4,DST5,DST6,DST7,DST8,"
                                        + "DHT,DHH,LUX,YON,HIZ) values (@tarih, @saat, @vm11, @ım11, @pm11, @vm22, @ım22, @pm22,"
                                        + "@vm33, @ım33, @pm33, @vm44, @ım44, @pm44, @vm55, @ım55, @pm55, @vm66, @ım66, @pm66, "
                                        + "@vm77, @ım77, @pm77, @vm88, @ım88, @pm88,"
                                        + "@ds11, @ds22, @ds33, @ds44, @ds55, @ds66, @ds77, @ds88, @dht11, @dhh11, @lux11, @yon11, @hiz11)";
        OleDbCommand komut = new OleDbCommand(ekle, baglanti);

        komut.Parameters.AddWithValue("@tarih", DateTime.Parse(date.ToString()));
        komut.Parameters.AddWithValue("@saat", time);
        komut.Parameters.AddWithValue("@vm11", vmax11);
        komut.Parameters.AddWithValue("@ım11", ımax11);
        komut.Parameters.AddWithValue("@pm11", pmax11);
        komut.Parameters.AddWithValue("@vm22", vmax22);
        komut.Parameters.AddWithValue("@ım22", ımax22);
        komut.Parameters.AddWithValue("@pm22", pmax22);
        komut.Parameters.AddWithValue("@vm33", vmax33);
        komut.Parameters.AddWithValue("@ım33", ımax33);
        komut.Parameters.AddWithValue("@pm33", vmax33);
        komut.Parameters.AddWithValue("@vm44", vmax44);
        komut.Parameters.AddWithValue("@ım44", ımax44);
```

Figure 3.37 Database connection and string operations

In GUI, seen in Figure 3.38, two different sections can be seen, where one is real-time measurements, and the other is historical measurements. It can be seen the boxes on the right top side of the interface, which is reserved for measurements of V_{mp}, I_{mp}, and P_{max} of each PV panel. The Left and the bottom side of the interface covers the PV panel's historical data and meteorological measurements.

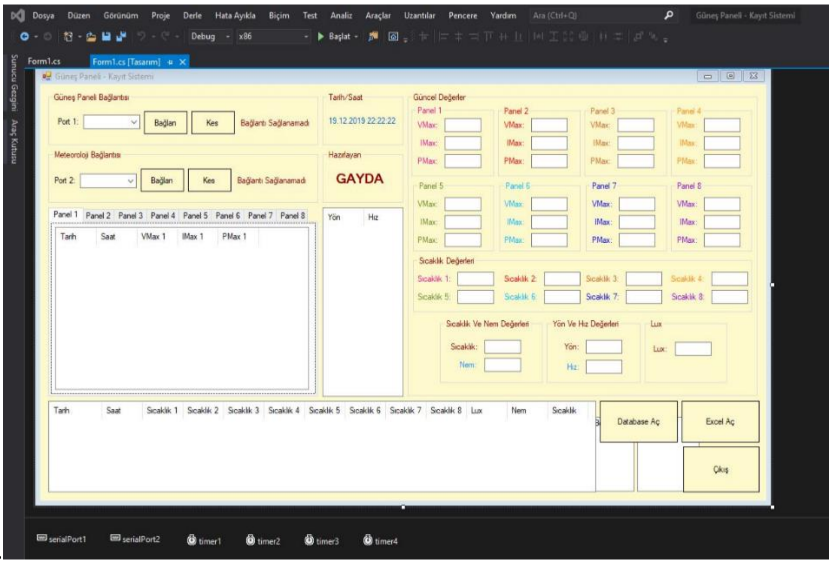

Figure 3.38 Designed software interface in C# for DAS sub-system computer

The screenshot of the interface application, while collecting the data and the relevant explanations are in Figure 3.39. The tasks performed in the interface are as follows: 1) Real-Time measurement display, 2) Historical measurement display, 3) Serial port selection, port opening, and closing, 4) Database record viewing.

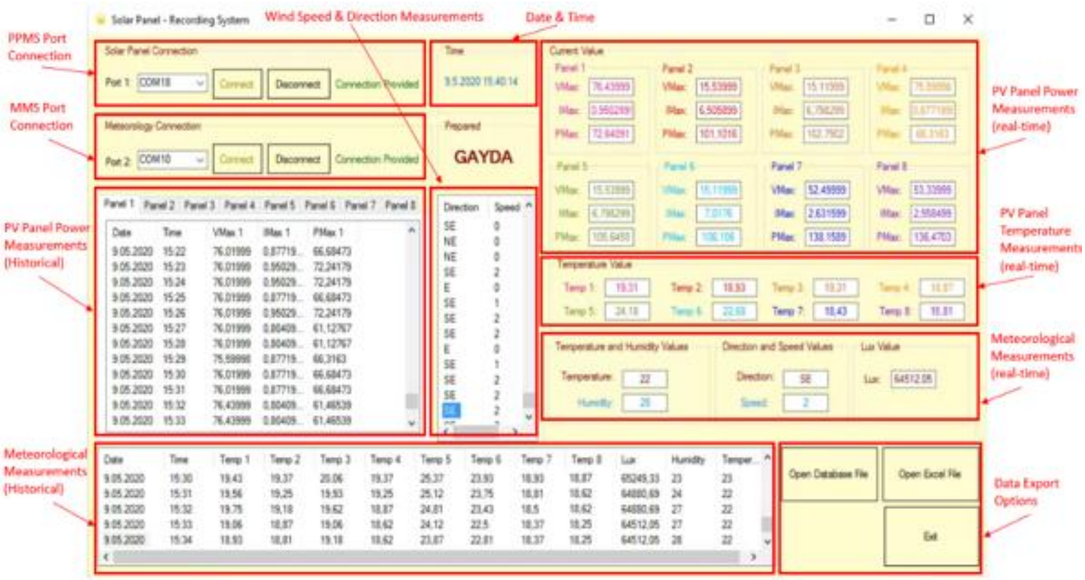

Figure 3.39 View of data monitoring interface in DAS computer

3.1.4 Power Supply of the System

It is essential to design the photovoltaic power supply examining the following details. PV panels to be used in conversion must have sufficient power to feed the requested system. Furthermore, the power output of a PV panel can vary depending on the amount of sunlight falling on it. This variability is shaped by atmospheric factors such as the Sun's movement throughout the day, cloudy skies, rain, snow, and humidity. As the Sun moves across the sky for a day, the panels generate different amounts of power throughout the day. Due to these variations in weather conditions, the power at the PV panel output is not stable, even fluctuation is observed. These fluctuations cannot be directly delivered to a device. If given, it will cause the device not to work due to insufficient power or damages the device due to fluctuation. Therefore, it is necessary to store the generated power in a battery. Before the PV panel output is given to a battery, the voltage and current fluctuations at the panel output must be regulated. A charge controller is used to regulate these fluctuations. All these details were taken into account when designing the PPMAS power station (Figure 3.40).

A flexible configuration with a 1440W battery system was created. It consists of a solar panel, a charge controller, and a 24V-60A battery assembly to operate PPMAS system energy autonomously (Figure 3.41) [77]. The power supply system runs the PPMAS system three days under insufficient sun conditions. 270W Poly-Crystalline PV panel is used according to the power of the batteries (Figure 3.41).

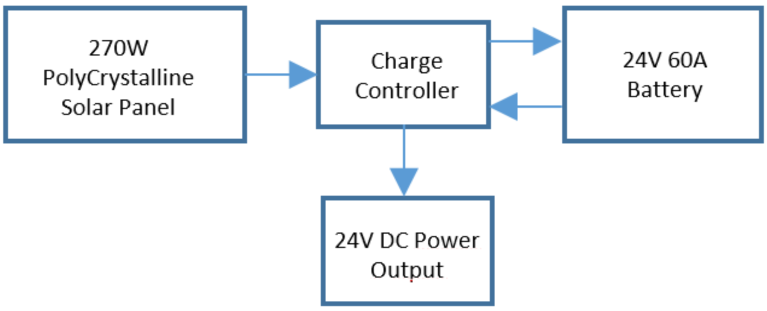

Figure 3.40 System power supply

Figure 3.41 Batteries and charge controller in the power supply

3.1.4.1 DC-DC Converter

In order to regulate the power input of the DAS sub-system computer, MMS sub-system PCBs, and PPMS sub-system PCBs, a DC-DC converter is used with the following specifications (Figure 3.42). The LM2596 power supply is a dc buck converter; it can operate under 3A load. LM2596 power supply; It can give adjustable output.

a)

b)

Figure 3.42 DC-DC converter pcb a) front-side b) back-side

LM2596 Adjustable DC-DC converter has the feature of regulating input voltages between 4V DC - 35V DC, to the range 1.23V DC - 30V DC by adjusting the potentiometer on it. There is an LM2596 regulated integrated circuit on the module. The output current is a maximum of 2A.

CHAPTER 4

EXPERIMENTAL RESULTS & DISCUSSION

In the scope of this experimental study, it is aimed to analyze and compare the power generation performances of PolyCrystalline, MonoCrystalline, CIS, CdTe PV panel pairs, within a specified time, under varying weather conditions in Ankara, Turkey. The generated power and temperatures of PV panels and atmospheric parameters are measured and stored using the developed system PPMAS.

In [89], different locations' inclination angles are examined and discussed, and for Ankara province, it is about 30°. Therefore, in this study, the PV panels' inclination angle is set to 30° and facing to the south to get sunlight better based on the location where the PV panels are installed. Furthermore, measurements obtained by PV panels and meteorological sensors have been collected at a one-second interval for six months between the first of December 2019 and 30 May 2020. The measured values, which are I_{mp}, V_{mp}, P_{max} in DC for each PV panel and wind speed and direction, ambient temperature, humidity, ambient light, and PV panel temperatures, have been stored to analyze the performance of PV panels as well as understanding reliability of the designed PPMAS system.

4.1 Verification of Designed PPMAS System

The designed sub-systems, which are MMS and PPMS in the PPMAS system, are tested and calibrated in a laboratory environment to improve the measurement accuracy. Vantage pro2 wireless meteorology station, Tt-Technic RXN305D2 power supply, Cem DT-1301 lux meter, Tektronix MSO 2024B oscilloscope, and Fluke-289 multimeter are selected for calibrating MMS and PPMS since they are widely used and perform measurements accurately.

4.1.1 Calibration of MMS

It is significantly essential to calibrate the MMS sub-system to get the atmospheric measurements accurately. In order to achieve this, a vantage pro2 wireless meteorology station is used to calibrate MMS sensor measurements. Vantage pro2 wireless meteorology station with ambient temperature, humidity, wind speed, and direction sensors, is installed next to the MMS sub-system. The MMS sub-system is calibrated according to the measurements obtained using the Vantage pro2 meteorology station. Thus, atmospheric values are accurately measured after calibrating the MMS sub-system.

Moreover, the Max44009 sensor is used in the MMS to estimate solar radiation, where it is installed to get the sun's illuminance. Note that the sensor and PV panels' angle is the same, and the sensor is calibrated using Cem DT-1301 Lux meter. The measurement unit is in Lux. The measured value is multiplied by 0.00833, to convert Lux to W/m2, [90].

4.1.2 Calibration of PPMS

Another important sub-system in the PPMAS system is the PPMS sub-system, which is needed to be calibrated to measure the generated power of PV panels accurately. Tektronix MSO 2024B oscilloscope, Fluke-289 multimeter, and Tt-Technic RXN305D2 power supply with 0-30V 0-5A are used to calibrate the PPMS sub-system. As a result, the calibrated PPMS sub-system can measure the generated power of PV panels accurately.

4.2 PV Panels

In this study, new and old PV panel technologies have been used, and the characteristics of these PV panels are tabulated in Table 4.2. Thus, in this experiment, eight PV panels are used: new and old MonoCrystalline with 140W, new and old CIS with 125W, new and old PolyCrystalline with 150W, and new and old CdTe with 60W. A solar power station is used to supply the power requirement of the experimental system. The power station consists of one 270W PolyCrystalline PV panel, two 12V/60A batteries, as shown in Figure 3.41. Thus, the PPMAS works properly under insufficient sunlight (i.e., cloudy day) upto 3-days.

4.3 Climate Data in Ankara Province

The climate data between 1927 and 2019 in Ankara province, Turkey, is presented in Table 4.1. According to the climate data, the highest average temperature is obtained in July and August with 23.3 °C. Moreover, the greatest average maximum and the least minimum temperatures between 1927 and 2019 are estimated at 30.4 °C in August and with 0.1 °C in January. The longest and shortest average sunshine durations are 11.3 hours in July and 2.5 hours in December. Furthermore, the highest amount of average monthly rainfall is observed at 44.9 mm. in December.

Table 4.1 Climate data for Ankara province (Turkey) between the years of 1927 and 2019 [91].

	Jan	Feb	Mar	Apr	May	Jun	Jul	Aug	Sep	Oct	Nov	Dec	Yearly
Ave. Temp.(°C)	0.1	1.6	5.7	11.2	16.0	19.9	23.3	23.3	18.8	13.1	7.2	2.4	11.9
Ave. Max. Temp.(°C)	4.1	6.4	11.4	17.3	22.3	26.6	30.2	30.4	25.9	19.9	13.0	6.4	17.8
Ave. Min. Temp.(°C)	-3.2	-2.3	0.6	5.3	9.6	12.9	15.8	15.9	11.7	7.0	2.5	-0.8	6.3
Ave. Sunshine Duration (hour)	2.6	3.8	5.1	6.6	8.5	10.0	11.3	10.7	9.2	6.7	4.5	2.5	81.5
Ave. Rainy Days	12.3	11.2	10.7	11.2	12.3	8.7	3.6	2.7	4.0	6.9	8.2	11.7	103.5
Ave. Total Monthly Rainfall (mm.)	40.2	35.1	39.1	42.5	51.5	34.4	14.3	12.7	18.0	27.7	31.5	44.9	391.9

4.4 Solar Radiation

Solar Radiation is a significantly essential parameter that is used to calculate the efficiencies of the PV panels. Figure 4.1 shows the weekly average results of solar radiation. This data is obtained using the MMS sensor box in the designed PPMAS system for six months in Ankara, Turkey. In Figure 4.1, the first-week average result is obtained between the 1st of December 2019 and 7th of December 2019, and week 26 represents the date of the 30th of May 2020. According to the results, the least and highest average solar radiation results are estimated with 1968 Wm2 in week 4 and

9459 Wm2 in week 24, respectively. As a result, these estimations demonstrate that the lowest solar radiation is obtained in December 2019, and the highest solar radiation is obtained in May 2020. There can be different reasons to get various weekly solar radiation results such as weather conditions, angle of sunlight, location of Ankara, etc. [92].

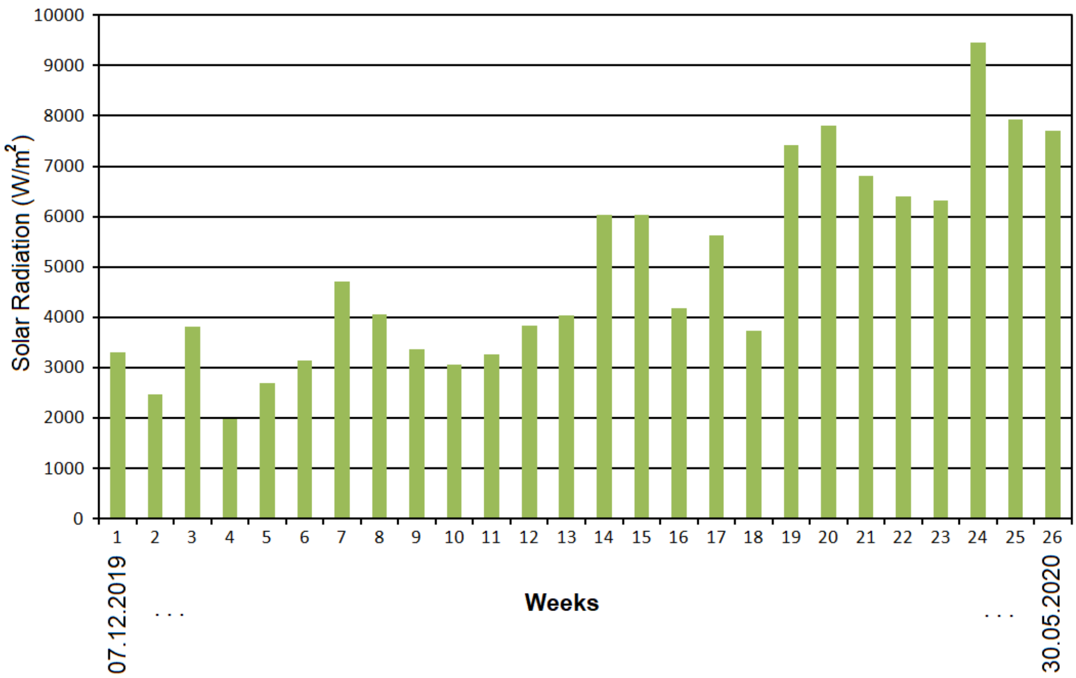

Figure 4.1 Weekly average results of solar radiation between December 2019 - May 2020 in Ankara

4.5 Effect of Atmospheric Variations on PV Panel Temperatures

Figure 4.2 depicts average weekly atmospheric temperature, wind speed, and PV panel temperatures for six months between December 2019 and May 2020. These results show that PV panel temperature depends on the ambient temperature. For instance, in week 15, the average weekly temperature is 13.05 °C, and the average of PV panel temperatures is increased by 1.25 °C, which becomes 14.30 °C, and in week 4, the average weekly temperature is 4.50 °C and the average of PV panel temperatures is 5.73 °C. Moreover, based on the six months measurement, the estimated average temperature is 7.88 °C, and the average of PV panel temperatures is 9.06 °C. According to the results in Figure 4.2, the least and highest average temperatures are measured with -1.78 °C in week 8 and with 21.60 °C in week 24, respectively.

Moreover, these results clarify that May is the month with the highest daily average temperature. However, January is the lowest daily average temperature. Furthermore, wind speed is low and nearly constant all the months between December and May in Ankara. The average wind speed of these six months is 2.93 m/s, which indicates that Ankara is not a windy city [93].

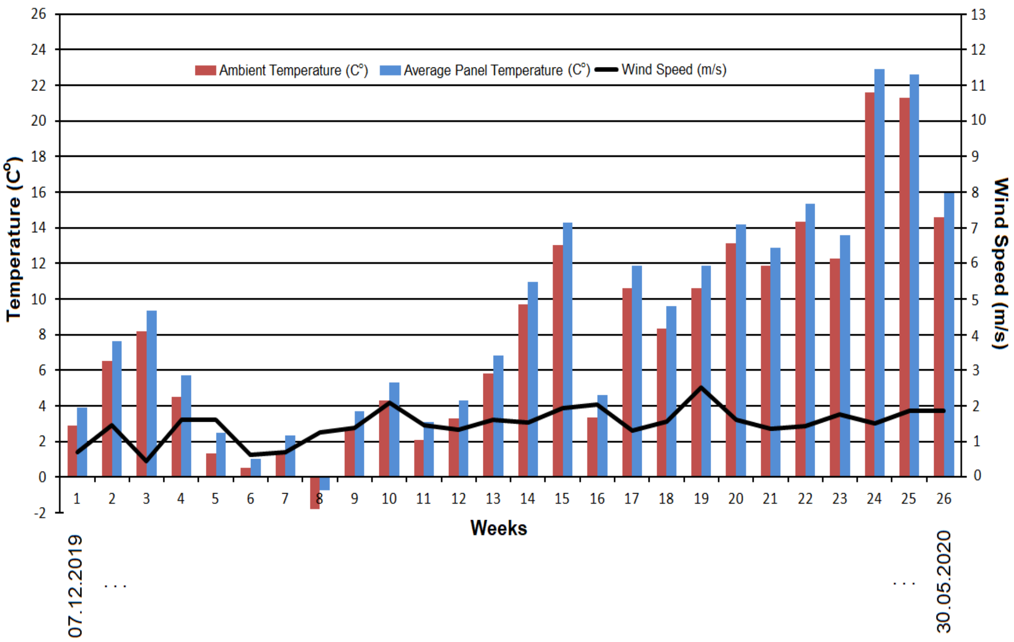

Figure 4.2 Weekly average ambient temperature, panel temperature, and wind speed between December 2019 and May 2020 in Ankara

Table 4.2. Characteristics of new and old pv panel technologies used in the study

PV Panel Type	P_{nom} (Nominal Power)	V_{oc} (Open Circuit Voltage)	I_{sc} (Short Circuit Current)	V_{mpp} (Voltage at MPP)	I_{mpp} (Current at MPP)
MonoCrystalline (Mono-new)	140Wp (±3%)	21,5V	8,33A	18,0V	7,78A
MonoCrystalline (Mono-old)	140Wp (±3%)	21,5V	8,33A	18,0V	7,78A
PolyCrystalline (Poly-new)	150Wp (±3%)	22,4V	8,46A	18,2V	7,95A
PolyCrystalline (Poly-old)	150Wp (±3%)	22,4V	8,46A	18,2V	7,95A
CIS (CIS-new)	125Wp (±4%)	59,3V	3,22A	44,0V	2,84A
CIS (CIS-old)	125Wp (±4%)	59,3V	3,22A	44,0V	2,84A
CdTe (CdTe-new)	60Wp (±5%)	89,7V	1,23A	62,2V	0,99A
CdTe (CdTe-old)	60Wp (±5%)	89,7V	1,23A	62,2V	0,99A

4.6 Daily Investigation of PPMAS

Measurement data were taken from the database of the DAS sub-system computer. With this data, different graphic combinations can be created to perform various performance analyzes. In this section, some graphs are performed to analyze the data stored in the DAS sub-system. These graphs include daily measurements and analysis.

Figure 4.3 shows a one-day solar illuminance graph obtained by the ambient light sensor with respect to time. The illumination of the sun is measured by the Max44009 sensor in the MMS sub-system. The sensor measures in terms of lux unit. According to the graph, the sun rises about 07:40 and sets about 18:10. The maximum illuminance is 31887,36 Lux and observed at 13:05 on 12 January (2020). Note that various fluctuations are seen in the chart. The blocking of sunlight can cause such fluctuations by the cloud or the sun's interruption due to various atmospheric reasons such as rainy weather.

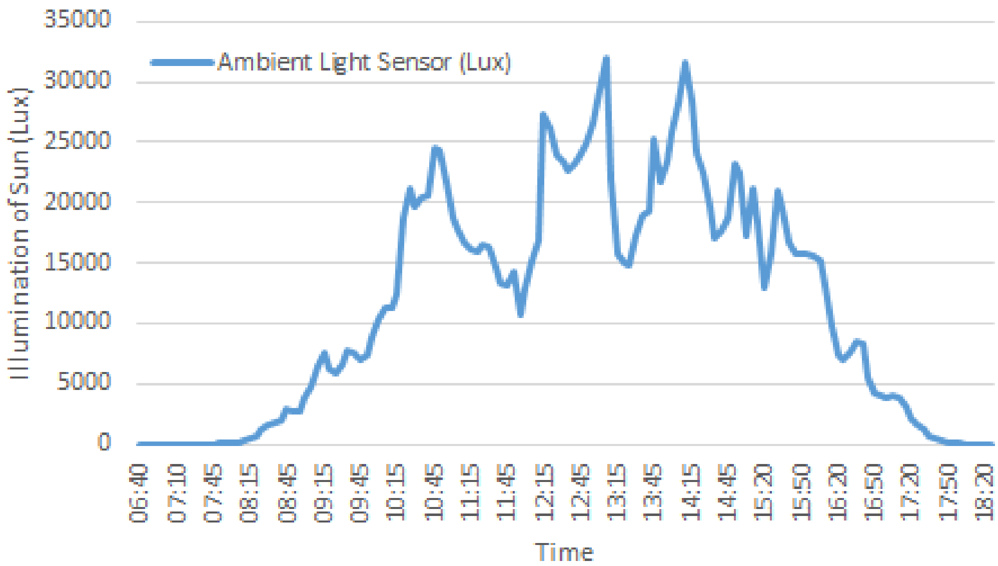

Figure 4.3 Illimunation of the Sun in 12.01.2020

The single-day generated voltage, current, and power measurement of PV panels are performed in Figure 4.4, 4.5, 4.6, and 4.7. Graphics are grouped to analyze the daily performance of new and old PV panel technologies. One-day measurements start with the sunrise at 06:40 in the morning and end with the sunset at 18:35. Instantaneous voltage (V_{mp}), current (I_{mp}), and power (P_{max}) measurements of new and old PV panel technologies in the specified time range are shown in the graphics. In Figure 4.4, Mono-new and Mono old, in Figure 4.5, Poly-new and Poly-old, in Figure 4.6, CIS-new and CIS-old, in Figure 4.7, CdTe-new and CdTe-old PV panel technologies are analyzed.

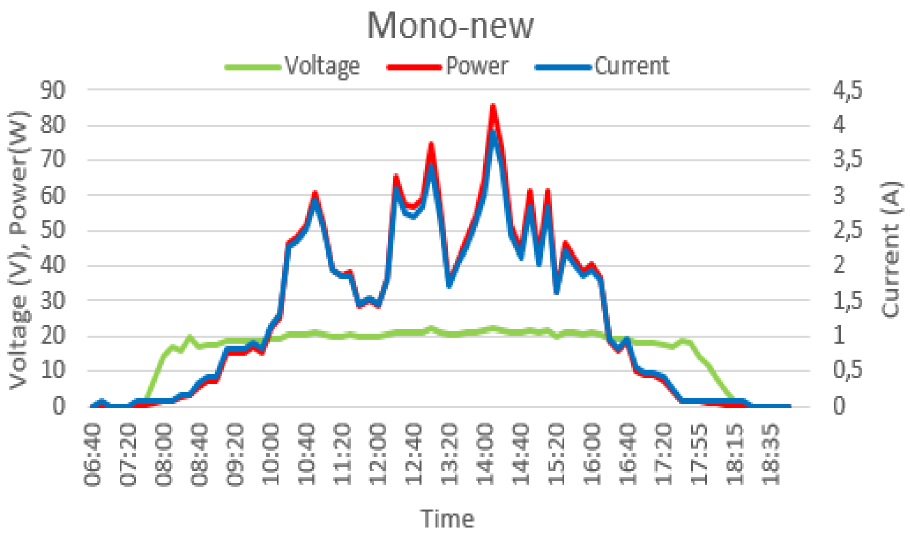

a)

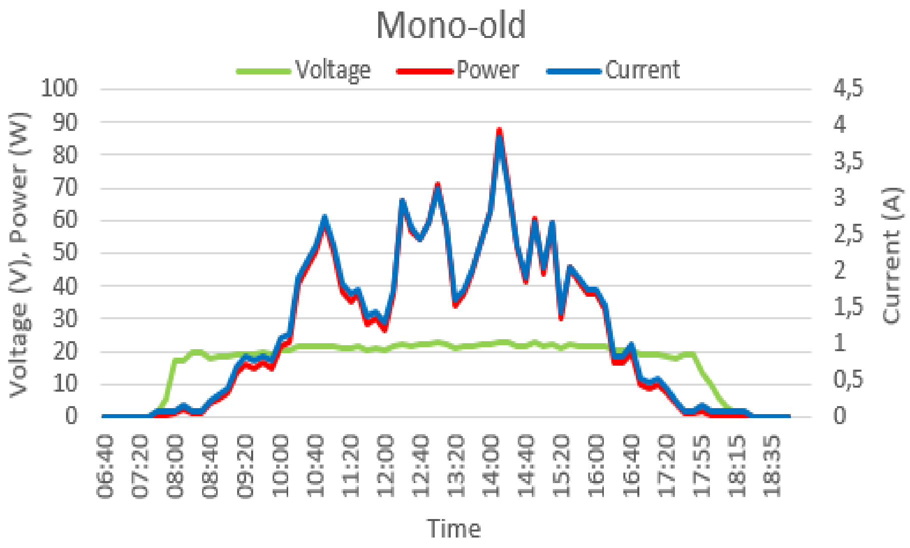

b)

Figure 4.4 Single day pv measurements a) mono-new b) mono-old [94]

In Figure 4.4 a) and b), it is seen that movement in voltage values of Mono-new and Mono-old PV panels between 20V and 21V after sunrise. Mono-new and Mono-old current measurement values reach 3,9A and 3,8A instantly, between 14:00 and 14:40

hours. The instantaneous maximum power values are 87W and 89W, respectively, observed in Mono-new and Mono-old panels at the same time interval.

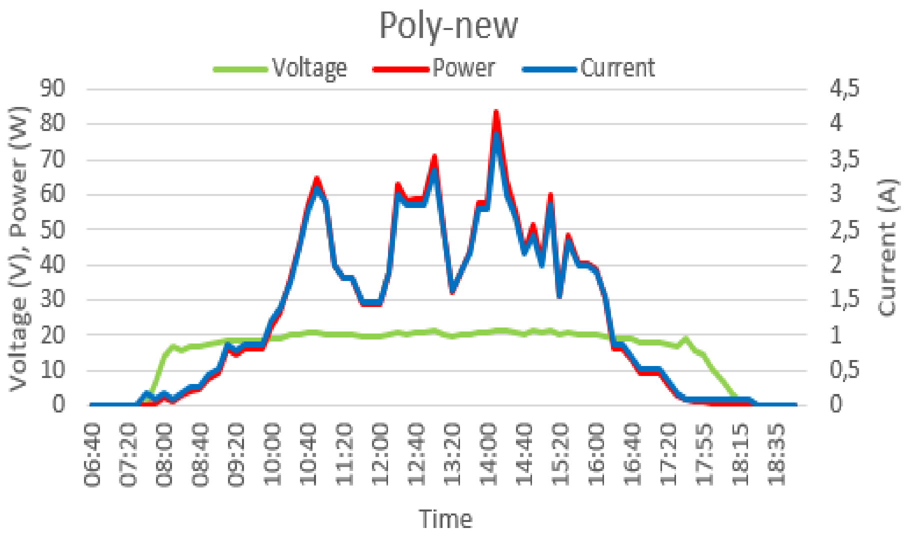

a)

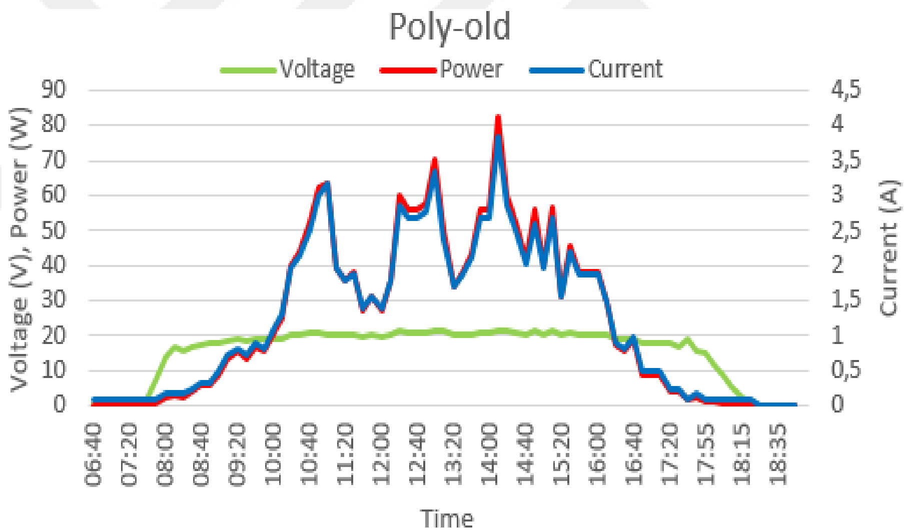

b)

Figure 4.5 Single day pv measurements a) poly-new b) poly-old [94]

In Figure 4.5 a) and b), it is observed that the voltage values of Poly-new and Poly-old panels move between 20V and 21V after sunrise. Poly-new and Poly-old current measurement values reach 3,85A and 3,8A instantly, between 14:00 and 14:40 hours. The instantaneous maximum power values are 84W and 83W, respectively, observed in Poly-new and Poly-old panels at the same time interval.

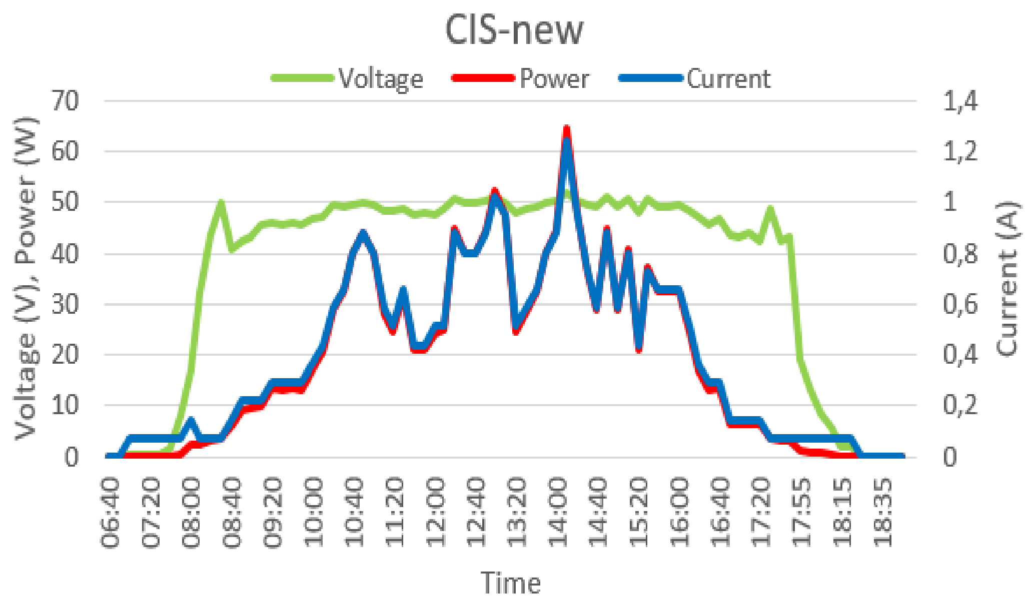

a)

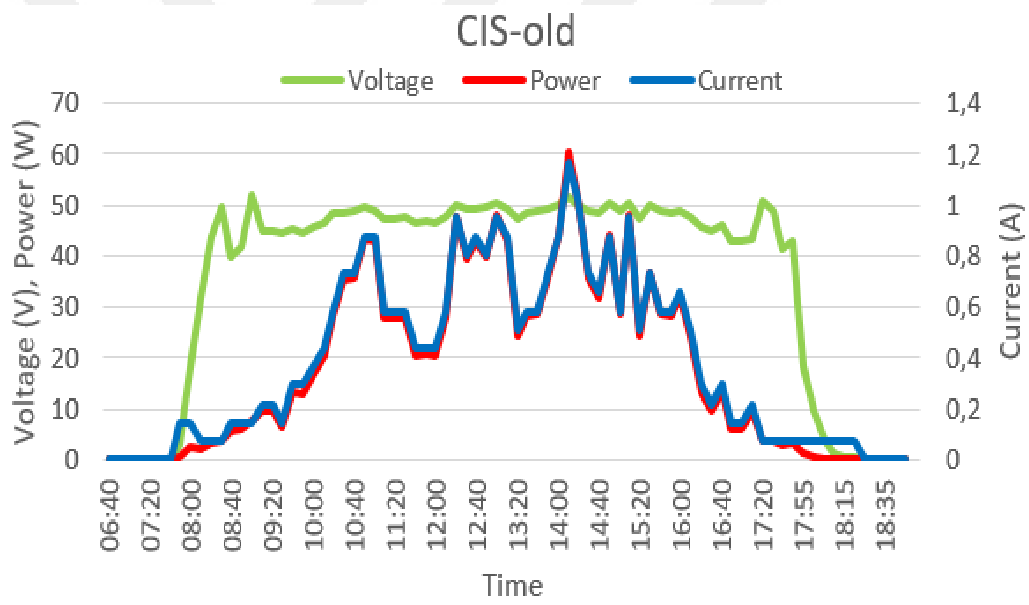

b)

Figure 4.6 Single day pv measurements a) CIS-new b) CIS-old [94]

In Figure 4.6 a) and b), it is observed that the voltage values of CIS-new and CIS-old panels fluctuate between 45V and 51V with the sunrise. CIS-new and CIS-old current measurement values reach 1,25A and 1,19A instantly, between 14:00 and 14:40 hours. The instantaneous maximum power values are 65,5W and 60,5W, respectively, observed in CIS-new and CIS-old panels at the same time interval.

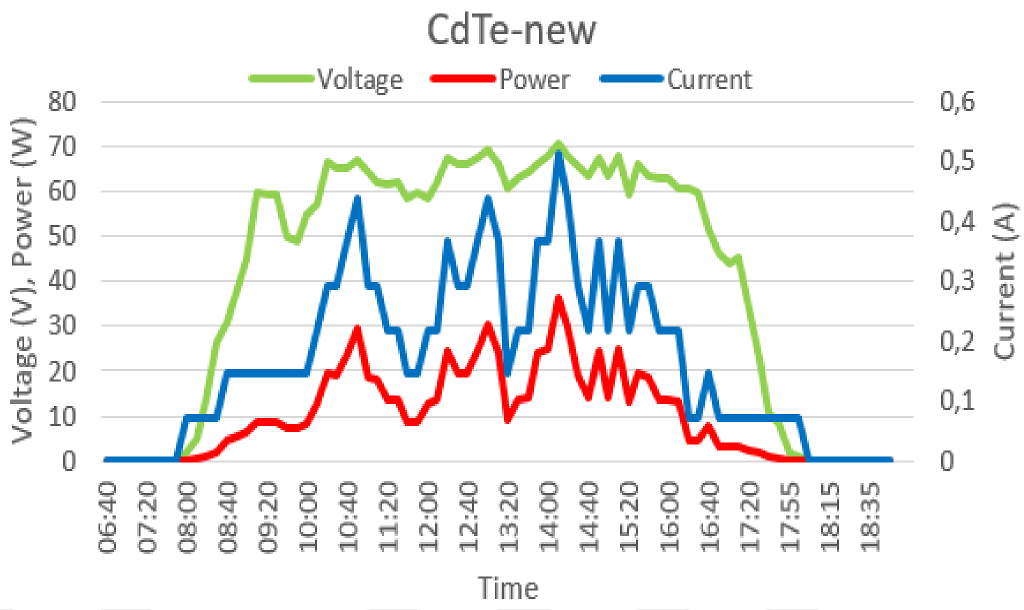

a)

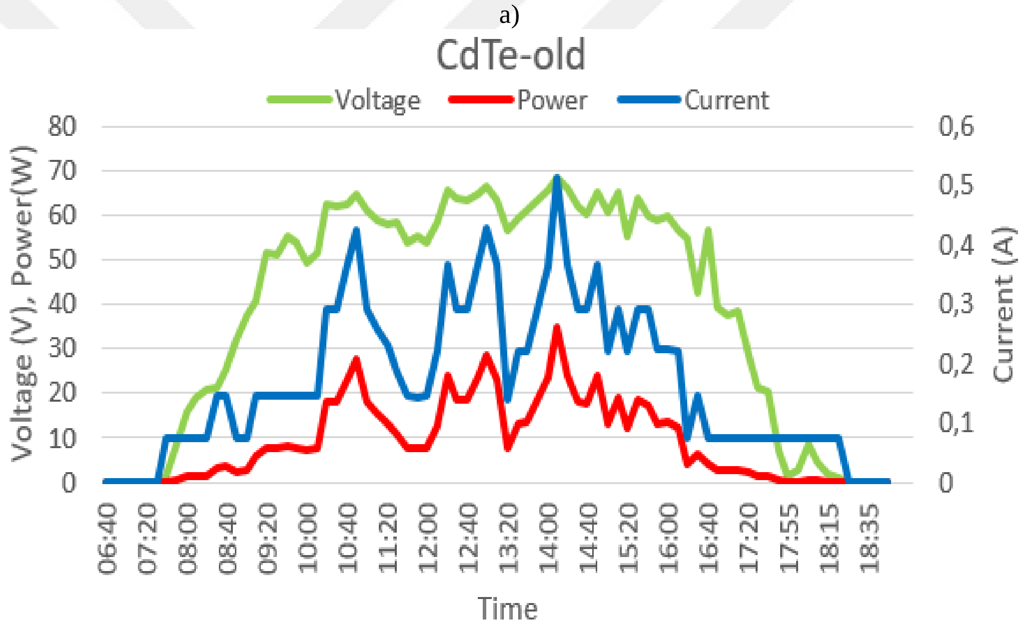

b)

Figure 4.7 Single day pv measurements a) CdTe-new b) CdTe-old [94]

In Figure 4.7 a) and b), it is observed that the voltage values of CdTe-new and CdTe-old panels fluctuate between 50V and 70V after sunrise. CdTe-new and CdTe-old current measurement values reach 0,52A instantly for both of them, between 14:00 and 14:40 hours. The instantaneous maximum power values are 37W and 35,5W, respectively, observed in CdTe-new and CdTe-old panels at the same time interval.

Figure 4.8 a) and b) show the instant power generation graph of four new and old PV panels regarding solar radiation on 12.01.2020. Based on the results, all PV panels generate the highest power between 14:00 and 14:40 hours. Besides these results, it can be seen from the graphs that new PV panels generate slightly higher power than the old PV panels on 12.01.2020.

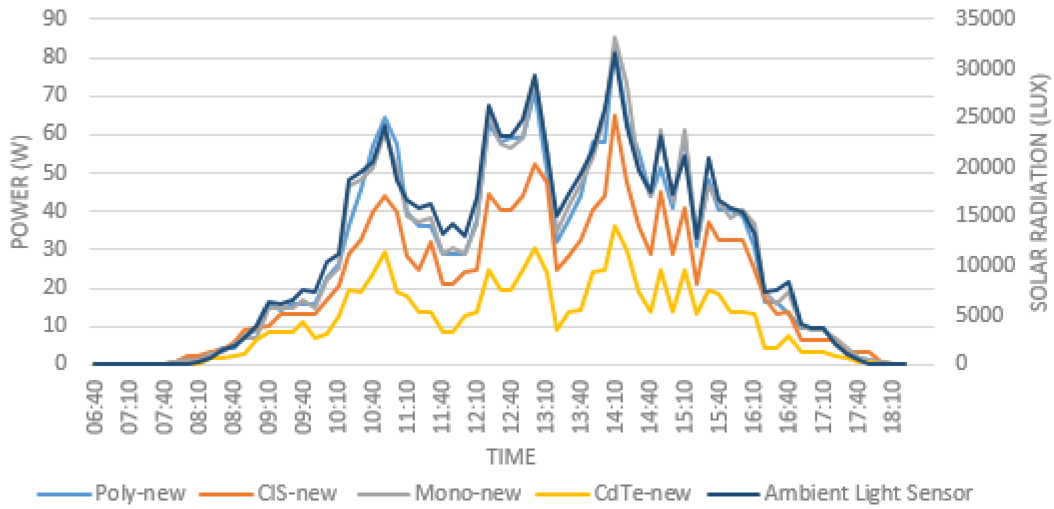

a)

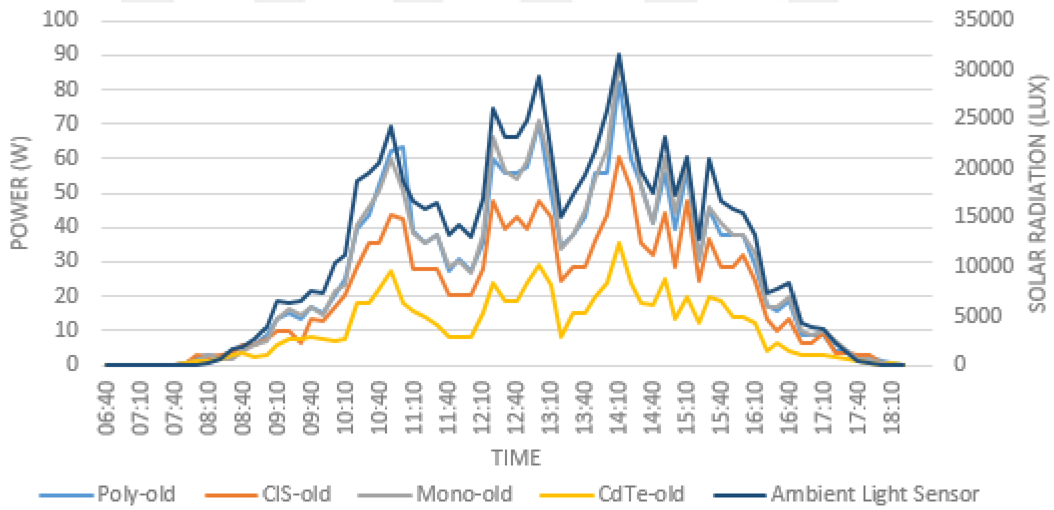

b)

Figure 4.8 Instant power generation of pv panels a) new pv panels with solar radiation b) old pv panels with solar radiation

Figure 4.9 presents the total power generation of solar panels for a single day (12.01.2020). The lowest power generation is observed in CdTe-new and CdTe-old PV panels. The highest power generation is seen in Mono-new Mono-old, Poly-new, and Poly old PV panels, where daily power generations are very close to each other. CIS-new and CIS-old PV panels are the third-highest power generated PV panels on 12.01.2020.

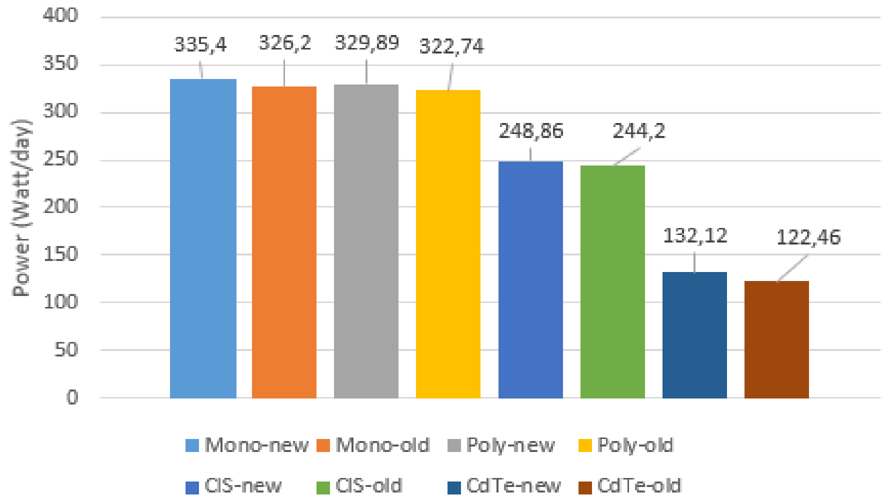

Figure 4.9 Single day generated total powers of pv panels [94]

Another graphics derived from MMS temperature & humidity measurements for one day (Figure 4.10). In the graph, it is observed that humidity and air temperature make opposite movements. When the PV panels generate the highest power between 14:00 and 14:40 hours, the air temperature is the highest, and the humidity is the lowest.

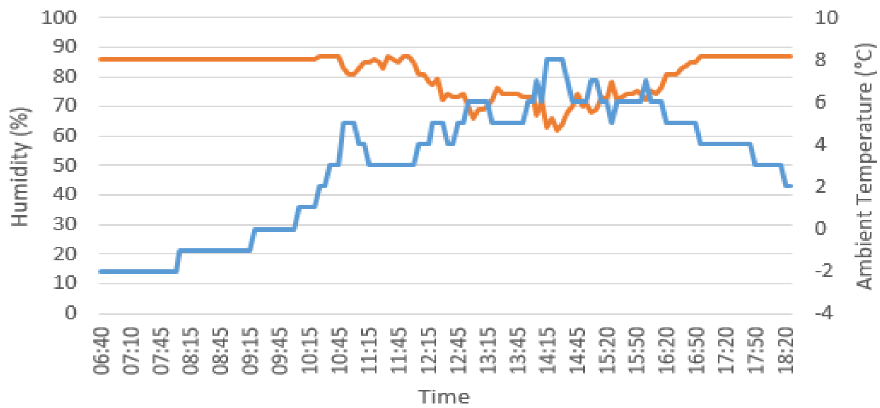

Figure 4.10 Ambient temperature and humidity measurements on 12.01.2020

4.7 Performance Assessment of Different PV Panels for Power Generation

Four different PV panel technologies, PolyCrystalline-based, MonoCrystalline-based, CIS-based, and CdTe-based, have been used for performance assessment. Besides this, each PV technology has one new and one old PV panel. Thus, the performance of new PV panels and old PV panels is evaluated. Each PV panel's generated power is measured within a specified time under Ankara's same outdoor conditions. The measured powers of eight PV panels are stored in the designed PPMAS system.

Figure 4.11 illustrates the weekly average power generated by new and old PV panels between December 2019 and May 2020. Based on these results, all PV panels generate maximum power between 9.05.2020 and 16.05.2020 and the lowest power between 21.02.2020 and 28.02.2020. These results show that the new PV panel technologies provide better power generation performance than the old PV panel technologies in all the weeks. For instance, between 14.12.2019 - 21.12.2019, mono-new, and mono-old generate a daily average of 327 Wh and 316 Wh, respectively, and CIS-new generates a daily average of 15 Wh more than CIS-old.

In terms of power generation performance, mono-new provides a 3.10% better performance than mono-old, poly-new provides 3.34% better performance than poly-old, CIS-new provides 5.53% better performance than CIS-old, and CdTe-new provides 6.97% better performance than CdTe–old. These results indicate that the CdTe PV panel is degraded more than the other PV panel technologies. There can be many factors that may affect PV panels' performance, and these factors are discussed in [78].

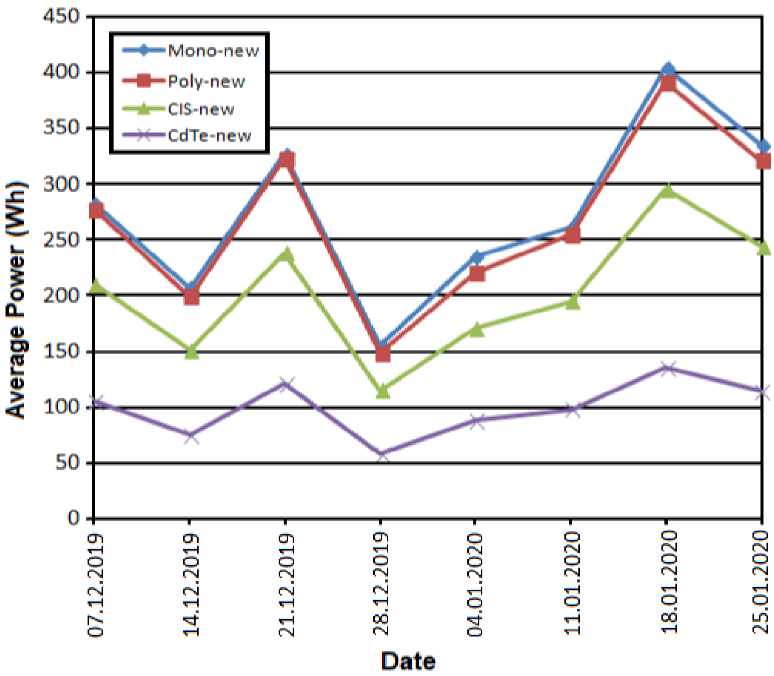
Mono-new
Poly-new
CIS-new
CdTe-new
Average Power (Wh)
450
400
350
300
250
200
150
100
50
0
07.12.2019
14.12.2019
21.12.2019
28.12.2019
04.01.2020
11.01.2020
18.01.2020
25.01.2020
Date

a)

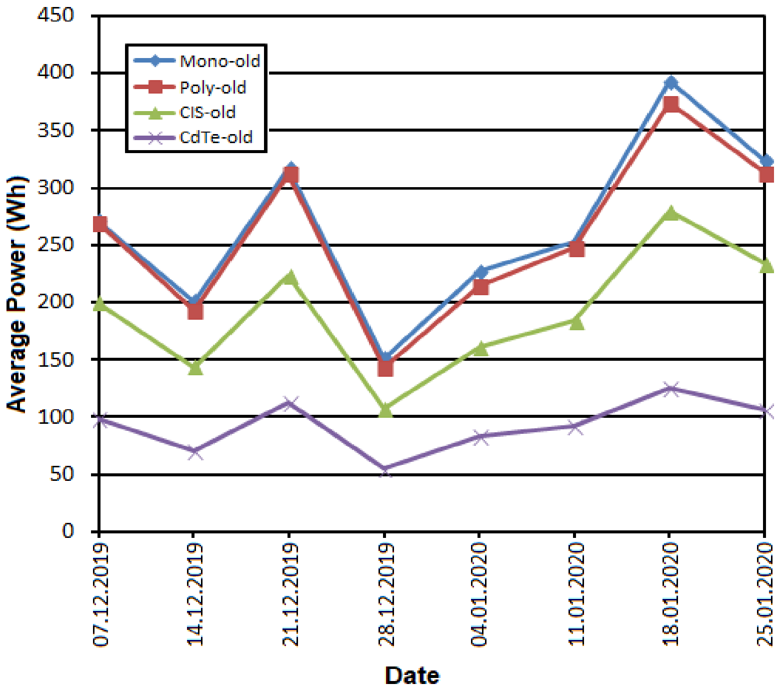
Mono-old
Poly-old
CIS-old
CdTe-old
Average Power (Wh)
450
400
350
300
250
200
150
100
50
0
07.12.2019
14.12.2019
21.12.2019
28.12.2019
04.01.2020
11.01.2020
18.01.2020
25.01.2020
Date

b)

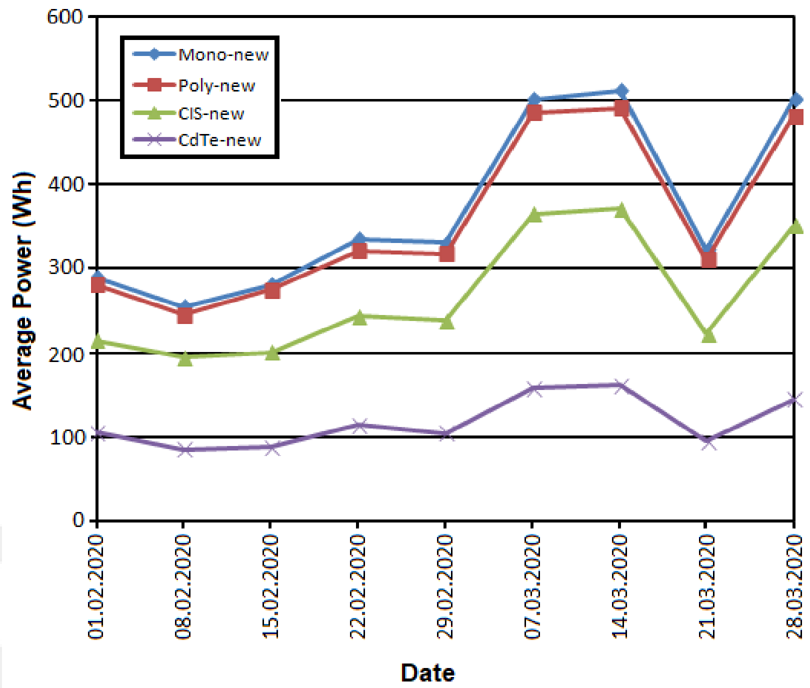
600
500
400
300
200
100
0
Mono-new
Poly-new
CIS-new
CdTe-new
Average Power (Wh)
01.02.2020
08.02.2020
15.02.2020
22.02.2020
29.02.2020
07.03.2020
14.03.2020
21.03.2020
28.03.2020
Date

c)

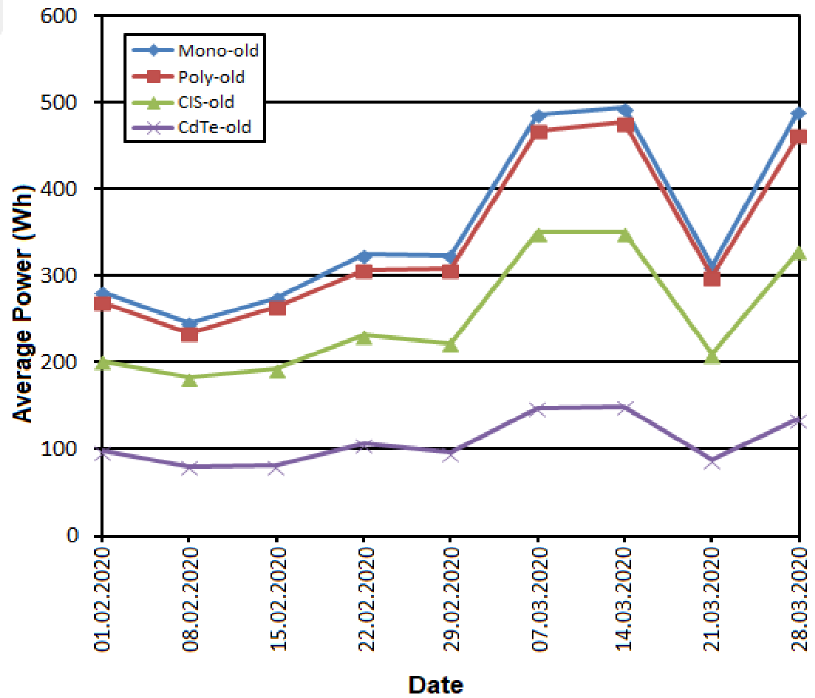
600
500
400
300
200
100
0
Mono-old
Poly-old
CIS-old
CdTe-old
Average Power (Wh)
01.02.2020
08.02.2020
15.02.2020
22.02.2020
29.02.2020
07.03.2020
14.03.2020
21.03.2020
28.03.2020
Date

d)

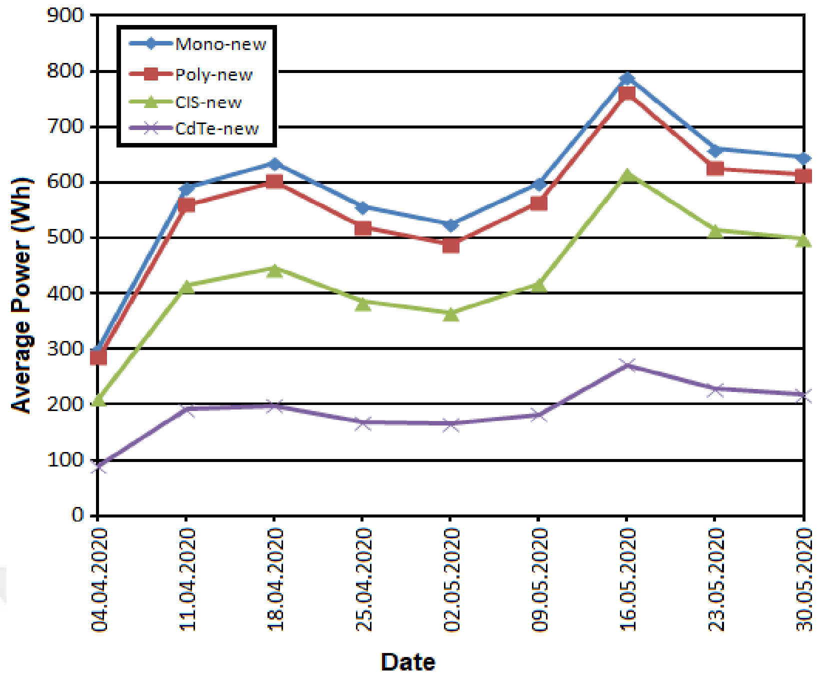

e)

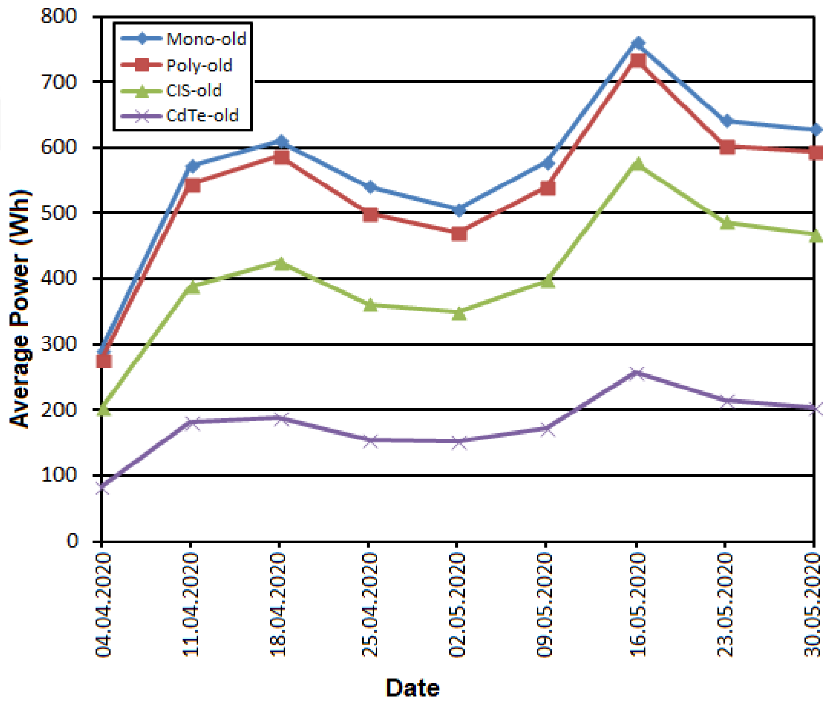

f)

Figure 4.11 Weekly average power generated by new and old pv panels, (a), (b) December and January, (c), (d) February and March, (e), (f), April and May.

Figure 4.12 (a) and (b) depict monthly panel efficiencies of new and old PV panels, respectively. Note that, monthly efficiencies of PV panels are calculated according to the formula given in Equation (10).

The results in Figure 4.12 (a) show that the new MonoCrystalline PV panel (Mono-new) has the highest efficiency values in all the months between December 2019 and May 2020 and the new PolyCrystalline PV panel (Poly-new) has slightly less efficiency than Mono-new in all the months. The Mono-new PV panel's maximum efficiency value is estimated in February with 8.73%, and the lowest efficiency value of this panel is estimated in March with 8.21%. In December 2019, the monthly efficiency value of Mono-new is 8.48% since the efficiency value of Poly-new is 8.28%, which is 0.20% is lower than Mono-new. Average 6-months of efficiencies of new PV panels are 8.46%, 8.11%, 5.65% and 3.88% for Mono-new, Poly-new, new CIS PV panel (CIS–new) and new CdTe PV panel (CdTe–new), respectively. According to the results, CIS-new is the third-best PV panel, and the CdTe-new is the worst PV panel in terms of monthly panel efficiency estimation in all the months.

Figure 4.12 (b) depicts the monthly panel efficiency of old PV panels between December 2019 and May 2020. According to the results, old MonoCrystalline (Mono-old) and old PolyCrystalline (Poly-old) PV panels have the best panel efficiencies in all the months as comparing to the other old PV panel technologies. Besides of this, old CIS (CIS-old) and old CdTe PV panels (CdTe-old) have the less panel efficiencies in all the months. Moreover, Mono-old, Poly-old, and CIS-old PV panels have the highest efficiencies in February, whereas the CdTe-old PV panel has the maximum efficiency in December. March is the month that all old PV panels have the lowest efficiencies. Average 6-months efficiencies of old PV panels are 8.22%, 7.85%, 5.35%, and 3.63% for Mono-old, Poly-old, CIS-old, and CdTe–old, respectively. Amongst all old PV panels, the Mono-old PV panel has the best efficiency estimations in all the months. Furthermore, the average 6-months efficiency of the Mono-old PV panel is greater than the average 6-months efficiency of Poly-new, CIS-new, and CdTe-new PV panels.

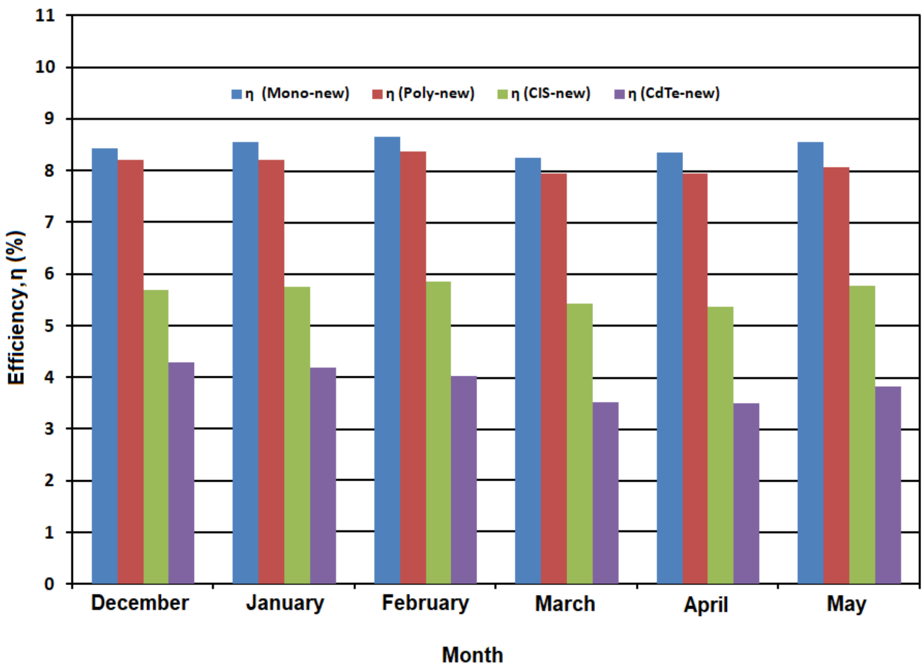

a)

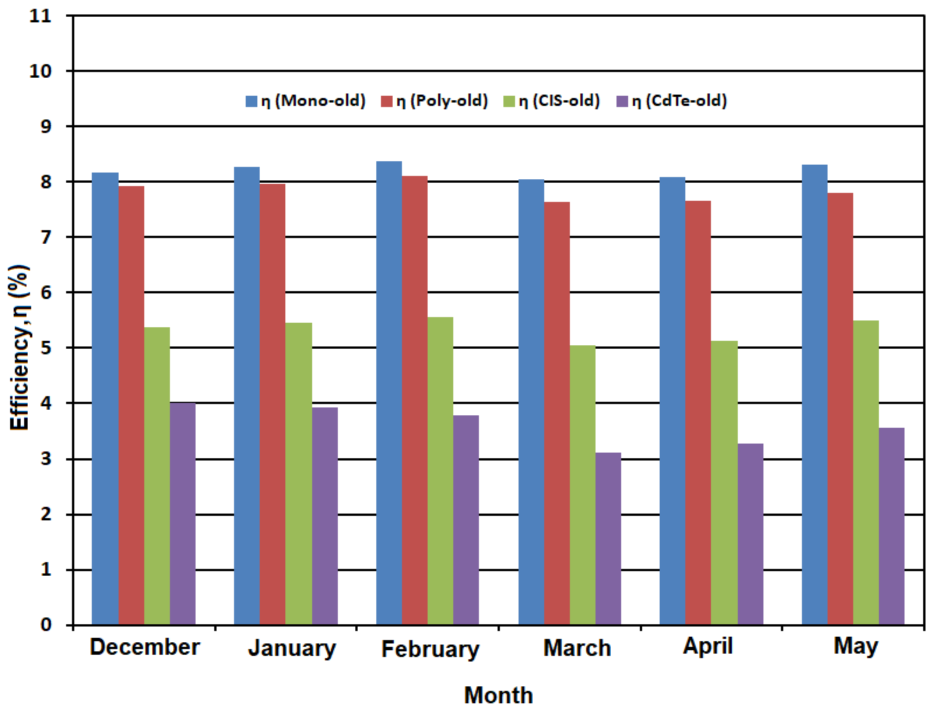

b)

Figure 4.12 Monthly panel efficiency of (a) four new pv panels, (b) four old pv panels.

Consequently, the results in Figure 4.12 (a) and (b) indicate that Mono-new and Mono-old PV panels are the best panel technologies amongst all the new and old PV panels in terms of monthly panel efficiency, respectively. Even though the Mono-old PV panel has some degradation in time, it has better average 6-months efficiency than some new PV panels.

Table 4.3 illustrates the monthly average of humidity between December 2019 and May 2020 in Ankara. According to the results, the highest humidity is measured in December with 83.6%, and the lowest humidity is measured in May with 55.1% in Ankara. Humidity affects electricity generating performance of PV panels. For instance, very small water drops on PV panels can reflect the sunlight away from PV panels, and this reduces producing power because less sunlight hits the surface of PV panels. According to Table 4.3, the least efficiencies of old and new PV panels are obtained in March when the humidity is high. On the other hand, the highest efficiencies of new and old PV panels are achieved in February when the humidity is low. Note that even though humidity is an important factor that affects the performance of PV panels, there are other important factors that affect the performance of PV panels, such as temperature, wind, solar radiation, etc.

TABLE 4.3 Monthly average of humidity between December 2019 and May 2020 in Ankara.

Month	Humidity in Percentage (%)
December	83.6%
January	76.2%
February	72.9%
March	73.5%
April	61.4%
May	55.1%

4.8 Statistical Analysis of Data

4.8.1 Performance Analysis of PV Panels and Photovoltaic Panel Measurement System using Non-Parametric Tests

The purpose of using the non-parametric tests is to understand and analyze the performance, stability, and reliability of the PV panels. The main advantage of using the non-parametric tests is that they can handle probabilistic and non-probabilistic measurements obtained from the PV panels without any limitation.

This section presents and examines different test results obtained using various non-parametric test measurement approaches. Three different non-parametric tests: Friedman, Friedman Aligned, and Quade are applied to the efficiency values of eight PV panels to achieve the test results, as shown in Figure 4.12 (a) and (b). The aim of applying Friedman, Friedman Aligned, and Quade non-parametric tests are to understand statistically whether there is any difference or similarity between the PV panels used over the given set of data. Note that these tests compute the ranks of the PV panels' performance, i.e., the best performing PV panel receives the rank of 1, the second-best rank 2, etc.

The mathematical background and further details of the non-parametric methods can be obtained in [95 – 98]. More statistical experimental results are based on Iman–Davenport, Bonferroni–Dunn, Holm, Hochberg, Holland, Rom, Finner, Li, Shaffer, and Bergmann–Hommel tests as well as adjusted p-value has been computed using the publicly available JAVA software [95 – 98].

Table 4.4 Average rankings of eight pv panels using the non-parametric statistical procedure, statistics and p-values

PV Panel Type	Friedman	Friedman Aligned	Quade
CdTe-new	4.314	19.203	4.262
Mono-old	4.399	22.996	4.768
CIS-new	3.242	8.408	3.036
Poly-old	5.592	13.205	5.855
Poly-new	2.492	5.546	2.079
Mono-new	1.714	3.206	1.121
CdTe-old	7.185	45.687	7.663
CIS-old	7.057	42.375	7.211

Table 4.4 shows the average ranking results estimated using the Friedman, the Friedman Aligned, and the Quade non-parametric tests. According to the results, the Mono-new PV panel is the best performing panel, with an average rank of 1.714, 3.206, and 1.121 for the Friedman, Fried-man Aligned, and Quade tests, respectively. Moreover, the p-values have been calculated using the statistics of each of the tests applied (23.163, 5.148, and 15.613). Furthermore, the Iman Davenport statistic and p-value are computed 12.538×10^{-7}, 0.4021, and 7.128×10^{-9}, respectively. Moreover, the Poly-new performs very close to the Mono-new with the second-ranking place comparing to the others. The CdTe-old gives the worst performance with the last ranking place with the average rank of 7.185, 45.687, and 7.663 for the Friedman, Fried-man Aligned, and Quade tests, respectively.

In the next statistical analysis, multiple comparison post hoc procedures (eight) are applied to evaluate the control of Mono-new with the rest of the PV panels. Computing p-values illustrate the results for each comparison. Tables 4.5, 4.6, and 4.7 depict the p-value results using the rankings computed by the Friedman, Friedman Aligned, and Quade tests, respectively [95–98]. These results verify the significant improvement in the Mono-new PV panel's usage over the other PV panels for all the post-hoc procedures considered. Moreover, Li’s statistical technique reaches the lowest p-values in the comparisons. Therefore, it is the most certain one amongst the others to reach the clearest conclusion.

Table 4.5 Adjusted *p*-values for Friedman (Mono-new is the control pv panel).

PV Panel	Unadjusted	Bonferroni	Holm / Hochberg/ Hommel	Holland	Rom	Finner	Li
CdTe-old	6.143×10^{-78}	4.300×10^{-77}	4.300×10^{-77}	0.0	4.088×10^{-77}	0.0	6.191×10^{-78}
CIS-old	2.094×10^{-74}	1.466×10^{-73}	1.256×10^{-73}	0.0	1.194×10^{-73}	0.0	2.111×10^{-74}
Poly-old	4.643×10^{-40}	3.250×10^{-39}	2.321×10^{-39}	0.0	2.207×10^{-39}	0.0	4.680×10^{-40}
Mono-old	4.580×10^{-20}	3.206×10^{-19}	1.832×10^{-19}	0.0	1.747×10^{-19}	0.0	4.616×10^{-20}
CdTe-new	6.644×10^{-19}	4.651×10^{-18}	1.993×10^{-18}	0.0	1.993×10^{-18}	0.0	6.697×10^{-19}
CIS-new	1.778×10^{-7}	1.245×10^{-6}	3.557×10^{-7}	3.557×10^{-7}	3.557×10^{-7}	2.075×10^{-7}	1.793×10^{-7}
Poly-new	0.0078	0.0548	0.0078	0.0078	0.0078	0.0078	0.0078

Table 4.6 Adjusted *p*-values for Friedman Aligned (Mono-new is the control pv panel).

PV Panel	Unadjusted	Bonferroni	Holm/ Hochberg/ Hommel	Holl-and	Rom	Finner	Li
CIS-old	$9.571x10^{-47}$	$6.699x10^{-46}$	$6.699x10^{-46}$	0.0	$6.369x10^{-46}$	0.0	$9.571x10^{-47}$
Poly-old	$1.039x10^{-45}$	$7.275x10^{-45}$	$6.236x10^{-45}$	0.0	$5.929x10^{-45}$	0.0	$1.039x10^{-45}$
CdTe-old	$1.634x10^{-45}$	$1.144x10^{-44}$	$8.172x10^{-45}$	0.0	$7.772x10^{-45}$	0.0	$1.634x10^{-45}$
CIS-new	$9.032x10^{-45}$	$6.322x10^{-44}$	$3.612x10^{-44}$	0.0	$3.407x10^{-44}$	0.0	$9.032x10^{-45}$
CdTe-new	$1.135x10^{-44}$	$7.951x10^{-44}$	$3.612x10^{-44}$	0.0	$3.407x10^{-44}$	0.0	$1.135x10^{-44}$
Mono-old	$2.970x10^{-44}$	$2.079x10^{-43}$	$5.940x10^{-44}$	0.0	$5.940x10^{-44}$	0.0	$2.970x10^{-44}$
Poly-new	$1.625x10^{-35}$	$1.137x10^{-34}$	$1.625x10^{-35}$	0.0	$1.625x10^{-35}$	0.0	$1.625x10^{-35}$

Table 4.7 Adjusted *p*-values for Quade (Mono-new is the control pv panel).

PV Panel	Unadjusted	Bonferroni	Holm/ Hochberg/ Hommel	Holland	Rom	Finner	Li
CdTe-old	$3.656x10^{-25}$	$2.559x10^{-24}$	$2.559x10^{-24}$	0.0	$2.433x10^{-24}$	0.0	$4.198x10^{-25}$
CIS-old	$5.061x10^{-22}$	$3.542x10^{-21}$	$3.036x10^{-21}$	0.0	$2.887x10^{-21}$	0.0	$5.811x10^{-22}$
Poly-old	$6.416x10^{-14}$	$4.491x10^{-13}$	$3.208x10^{-13}$	$3.208 x10^{-13}$	$3.051x10^{-13}$	$1.497x10^{-13}$	$7.367x10^{-14}$
Mono-old	$7.611x10^{-9}$	$5.328x10^{-8}$	$3.044x10^{-8}$	$3.044x10^{-8}$	$2.903x10^{-8}$	$1.332x10^{-8}$	$8.739x10^{-9}$
CdTe-new	$6.522x10^{-7}$	$4.565x10^{-6}$	$1.956x10^{-6}$	$1.956x10^{-6}$	$1.956x10^{-6}$	$9.130 x10^{-7}$	$7.488x10^{-7}$
CIS-new	0.0024	0.0162	0.0048	0.0048	0.0048	0.0028	0.0027
Poly-new	0.1290	0.9034	0.1290	0.1290	0.1290	0.1290	0.1290

Table 4.8 shows ten different hypotheses using four different statistical techniques: Nemenyi, Holm, Shaffer, and Bergmann, to achieve p-values. According to the p-values, the first four hypotheses by all the post hoc procedures are rejected because the levels of significance (α) is $\alpha = 0.05$. For example, let us compare hypotheses 4, which is Mono-old vs Poly-old. The p-values estimated by Nemenyi, Holm, Shaffer, and Bergmann procedures [99 – 102] are less than $\alpha = 0.05$, so we reject hypotheses 4 for the Mono-old vs Poly-old. A similar procedure is used for all the hypotheses, so the first four hypotheses are rejected. On the other hand, the other six hypotheses are not rejected because the computed p-values by Nemenyi, Holm, Shaffer, and Bergmann

procedures are bigger than 0.05. As a result, the hypotheses demonstrate the improvement of Mono-new over CdTe-old, CIS-old, and Poly-new and that of Poly-new panel over Poly-old. If α is 0.1, then the first six hypotheses are rejected since the computed p-values of all the post hoc procedures for the first six hypotheses are less than 0.1. However, the rest of the hypotheses, which is hypotheses 7, 8, 9, and 10, are not rejected. By selecting α as 0.01, we can evaluate more hypotheses. These hypotheses for α = 0.01 verify that Mono-new performs better than CdTe-old, CIS-old, and Poly-new, and Poly-new performs better than Poly-old, and CIS-new performs better than Mono-old and CdTe-new.

Table 4.8 Adjusted *p*-values for tests for multiple comparisons among all pv panels.

Index	Hypotheses	Nemenyi [100]	Holm [99]	Shaffer [101]	Bergmann [102]
1	Mono-new vs CdTe-old	4.981×10^{-6}	1.778×10^{-6}	1.778×10^{-6}	1.245×10^{-6}
2	Mono-new vs CIS-old	1.592×10^{-5}	5.120×10^{-6}	5.120×10^{-6}	2.844×10^{-6}
3	Poly-new vs Mono-new	3.524×10^{-4}	1.007×10^{-4}	1.007×10^{-4}	6.293×10^{-5}
4	Poly-new vs Poly-old	0.0012	3.229×10^{-4}	3.229×10^{-4}	1.845×10^{-4}
5	Mono-old vs CIS-new	0.0521	0.0634	0.0642	0.0586
6	CdTe-new vs CIS-new	0.0703	0.0862	0.0965	0.7574
7	Poly-new vs Mono-new	0.2192	0.3131	0.3131	0.2342
8	CIS-new vs Poly-new	0.2916	0.3131	0.3131	0.3120
9	CdTe-old vs CIS-old	18.495	1.3210	1.3210	1.3210
10	CdTe-new vs Mono-old	21.551	1.3210	1.3210	1.3210

4.9 Global Relevance of the Research Results

Table 4.9 presents the efficiency results of different PV panels in different cities and countries. For instance, in [103], performances of four different PV panels which are Mono, Poly, CIGS, and CdTe, are analyzed in Nicosia, Cyprus, based on the data collected annually, and the results show that Mono PV panel provides the best performance comparing to the other PV panels. The Mono PV panel's performance has been analyzed in other countries such as Brunei, Morocco, India, and Turkey. However, the efficiency results have been obtained based on different time durations.

According to the results, it is clear that the Mono PV panel provides the best performance with 11.20% in Cyprus and India, and the efficiency of the Mono PV panel is the least with 5.40% in Brunei. Moreover, Poly's highest and lowest efficiencies are 14.50% and 7.60% in Poland and Italy, respectively. Note that Cyprus, India, and Poland's efficiency results are estimated based on the collected data annually. Therefore, Mono and Poly PV panels' efficiencies are higher than Mono and Poly PV panels' efficiencies in Ankara. The main reason for getting lower efficiency of Mono in Ankara is that the data was collected in winter and spring periods, and the efficiencies of Mono and Poly PV panels are with 8.46% and 8.11% for Ankara Province, Turkey. It is important to emphasize that the PV panels' efficiencies will be much higher when the summer data is considered. Furthermore, in other researches, only new PV panels were used for performance comparison. In our study, new and old PV panels have been used for performance assessment and analyses.

Table 4.9 Global relevance of the research results.

PV Technology	Efficiency	Location	Evaluation Period	Reference
Mono Poly CIGS CdTe	11.20% 11.00% 9.20% 7.20%	Nicosia / CYPRUS	Annual	[103]
Poly	8.30%	Katar-Kalan / India	Annual	[104]
Mono	5.40%	Brunei	6-months	[105]
Mono Poly	10.27% 9.56%	Agadir / Morocco	Annual	[106]
Poly	11.80%	Singapore	18-months	[107]
Poly	7,60%	Calabria, Italy	2-months	[108]
Poly CIGS CdTe	14.50% 11.00% 8.70%	Poland	Annual	[109]
Mono Poly CIS	11.20% 11.90% 10.80%	Hamirpur Himachal Pradesh / India	Annual	[110]
Mono Poly CIS CdTe	8.46% 8.11% 5.65% 3.88%	Ankara / Turkey	6 months	Current Study

CHAPTER 5

CONCLUSIONS AND FUTURE WORK

The thesis presents two different studies which are 1) a designed Photovoltaic Panel Measurement and Analysis System (PPMAS) and 2) detailed performance analysis and comparison of four new and four old PV panels which are based on PolyCrystalline, MonoCrystalline, CIS, and CdTe. The designed PPMAS system consists of three different sub-systems. The sub-systems are calibrated to accurately obtain the atmospheric measurements and power generation of PV panels.

The designed PPMS sub-system was built with a circuit architecture applied for the first time in the literature, in which I-V characteristics of eight PV panels are created with a MOSFET electronic load on the circuit board. In that respect, a new circuit design method for the I-V characterization of PV panels was presented to the literature.

It is possible to obtain the characteristics of a PV panel using the MOSFET electronic load. Applied voltage to gate-source pins is decreased or increased gradually, to use a MOSFET as a variable resistor. Here, the MOSFET must be driven quickly, not to stay under DC load for a long time. If the MOSFET is under DC load for more than the time specified in its SOA (Safe Operating Area) graph, it may be damaged or overheat and cause a failure in measurements. For this reason, precise driver circuit design is essential. The necessary driver circuit design has been successfully realized to quickly adjust the MOSFET's resistance value under DC load conditions.

UART based data acquisition system has been successfully provided in designed PPMAS system. UART serial communication between Data Acquisition Sub-system (DAS) and measurement sub-systems, including Photovoltaic Panel Measurement Sub-system (PPMS) and Meteorology Measurement Sub-system (MMS), has been managed without interruption for ten months. Measurement data from all sensors are transmitted to the respective fields in the DAS sub-system's software interface in real-time, respectively. UART serial communication plays an essential role in the smooth and error-free transfer of data to the DAS sub-system.

The Designed MMS sub-system collects measurements from sensors through several communication protocols. The designed circuit board within the MMS sub-system; successfully measures wind speed, direction, ambient temperature, humidity, ambient light, and eight-panel temperatures. Unlike conventional and costly measurement systems examined in the literature, low-cost measurement sensors have been integrated into the MMS sub-system.

The developed DAS sub-system software interface and database can display and record successfully. Instant data can be observed through the interface. DAS has a data storage capacity of approximately 50 years. The DAS sub-system can be accessed remotely with the Wifi feature, and measurements can be remotely monitored and backed up.

When the studies in the literature are observed, the designed PPMAS system is unique in that it is adaptable to the industry, low cost, expandable, portable, self-powered, remote access, and unique circuit designs that can analyze eight PV panels at the same time.

The designed PPMAS system with PV panels is installed in Yildirim Beyazit University Campus, Ankara, Turkey, and performed for six months between December 2019 and May 2020. According to the results, the PPMAS system performs well to obtain measurements: ambient light, ambient temperature, humidity, wind direction, wind speed and panel temperatures, and power generation of PV panels.

Comparing the generated power performance of PV panels, mono-new provides a 3.10% higher performance than mono-old, poly-new provides a 3.34% higher performance than poly-old, CIS-new provides a 5.53% higher performance than CIS-old, and CdTe-new provides a 6.97% higher performance than CdTe–old. These results indicate that the Mono PV panel is degraded less than the other PV panel technologies, and the CdTe PV panel is degraded more than the other PV panel technologies.

According to the results, February is the best month for Mono, Poly, and CIS to have the best efficiency measurements, whereas CdTe has the best measurement in

December. Besides this, CdTe-based PV panel technology has less efficiency measurements in all the months.

Average 6-months efficiencies of new PV panels are 8.46 %, 8.11%, 5.65%, and 3.88% for Mono-new, Poly-new, CIS–new, and CdTe–new, respectively. Average 6-months efficiencies of old PV panels are 8.22%, 7.85%, 5.35%, and 3.63% for Mono-old, Poly-old, CIS-old, and CdTe–old, respectively. According to PV panel efficiency evaluations, Mono-new and Mono-old PV panels have the highest efficiency in the 6-month average. Also, Poly-new and Poly-old PV panel efficiencies are very close to that of Mono-new and Mono-old PV panels. CdTe-new and CdTe-old PV panel efficiencies are the lowest at 6-month average. The third high efficiency has been observed in CIS-new and CIS-old PV panels.

Test results obtained from the experimental system are statistically examined and discussed to analyze PV panels' performance in monthly panel efficiencies. According to the results, the Mono-new PV panel is the best performing PV panel. Furthermore, the Poly-new PV panel performs very close to the Mono-new PV panel with comparing to the others. The CdTe-old gives the worst performance with the last place, applying Friedman, Fried-man Aligned, and Quade tests, respectively.

The thesis aims to realize the multi-input PV panel measurement and analysis system and measure the power generation and efficiency of different PV panel technologies under outdoor conditions. Necessary studies such as data communication and PCB designs have been carried out to perform measurements and analyses. It has been proven that the developed system has successfully completed measurements. Also, software and hardware have been developed for data storage. The stored data, the powers and efficiencies generated by the PV panels were compared.

Regarding future works, the current version of the designed PPMAS can measure the generated power of up to eight PV panels; this system will be modified to measure the generated power of more than eight PV panel technologies. Moreover, the performance of different PV panel technologies in different locations of Turkey will be assessed and analyzed to understand the efficiencies of PV panels in various places in Turkey. In this work, we discussed the performance of PV panel technologies produced by Mono-crystalline, Poly-crystalline, CIS, and CdTe. Other PV panel technologies such as Amorphous Silicon (a-Si) and Gallium Arsenide (GaAs)-based PV panels will also be used for performance assessment. The current PPMAS system can work three days under insufficient sun configurations with its battery system's help. As future work, the battery capacity will be increased; thus, the system can work up to seven days under insufficient sun conditions.

REFERENCES

[1] IEA (2019), "Renewables 2019", IEA, Paris https://www.iea.org/reports/renewables-2019 Accessed 16 Mar 2020.

[2] C. J. Traverse, R. Pandey, M. C. Barr, R. R. Lunt, "Emergence of highly transparent photovoltaics for distributed applications", Nature Energy, vol. 2, no. 11, pp. 849-860, 2017.

[3] G. G. Kim, J. H. Choi, S. Y. Park, B. G. Bhang, W. J. Nam, H. L. Cha,... & H. K. Ahn, "Prediction model for PV performance with correlation analysis of environmental variables", IEEE Journal of Photovoltaics, vol. 9 no. 3, pp. 832-841, 2019.

[4] A. M. Ghazali, A. M. A. Rahman, "The performance of three different solar panels for solar electricity applying solar tracking device under the Malaysian climate condition", Energy and Environment Research, vol. 2, no. 1, 235, 2012.

[5] S. Glunz, M. Bivour, C. Messmer, F. Feldmann, R. Müller, C. Reichel, ... & M. Hermle. "Passivating and carrier-selective contacts-Basic requirements and implementation", In 2017 IEEE 44th Photovoltaic Specialist Conference (PVSC), pp. 2064-2069, 2017.

[6] A. Bosio, S. Pasini, N. Romeo, "The History of Photovoltaics with Emphasis on CdTe Solar Cells and Modules", Coatings, vol. 10, pp. 344-355, 2020.

[7] I. E. Tinedert, F. Pezzimenti, M. L. Megherbi, A. Saadoune. "Design and simulation of a high efficiency CdS/CdTe solar cell", Optik, vol. 208, pp. 1-12, 2020.

[8] C. Y. Ou, S. Som, C. H. Lu, "Incorporation of copper–indium back-end layers in the solution-based Cu (In, Ga) Se2 films: enhancement of photovoltaic performance of fabricated solar cells", Materials Research Express, vol. 7, no. 2, pp. 5-18, 2020.

[9] A. G. Olabi, “Renewable energy and energy storage systems”, Energy, vol. 136, pp. 1-6, 2017.

[10] M. F. Nayan, S. M. S. Ullah and S. N. Saif, “Comparative analysis of PV module efficiency for different types of silicon materials considering the effects of environmental parameters”, 3rd International Conference on Electrical Engineering and Information Communication Technology (ICEEICT), Dhaka, pp. 1-6, 2016.

[11] A. Müller, M. Ghosh, R. Sonnenschein, P. Woditsch, “Silicon for photovoltaic applications”, Materials Science and Engineering: B, vol. 134, no. 2-3, pp. 257-262, 2006.

[12] C. E. C. Nogueira, J. Bedin, R. K. Niedzialkoski, S. N. M. de Souza, J. C. M. das Neves, “Performance of monocrystalline and polycrystalline solar panels in a water pumping system in Brazil”, Renewable and Sustainable Energy Reviews, vol. 51, pp. 1610-1616, 2015.

[13] M. Demirtaş, B. Tamyürek, E. Kurt, I. Çetinbaş, M. K. Öztürk, “Effects of Aging and Environmental Factors on Performance of CdTe and CIS Thin-Film Photovoltaic Modules”, Journal of Electronic Materials, vol. 48, no. 11, pp. 6890-6900, 2019.

[14] D. M. Bierman, A. Lenert, W. R. Chan, B. Bhatia, I. Celanović, M. Soljačić, & E. N. Wang, “Enhanced photovoltaic energy conversion using thermally based spectral shaping”, Nature Energy, 1(6), pp. 1-7, 2016.

[15] E. R. Cholleti, Md Akhtar khan, “Bio-Synthetic Affordable Nano Solar cell”, Materials Today: Proceedings, 4(8), pp.7694-7703, 2017.

[16] D. Lincot, “The new paradigm of photovoltaics: From powering satellites to powering humanity”, Comptes Rendus Physique, 18(7-8), 381-390, 2017.

[17] R. K. Nema, S. Nema, & G. Agnihotri, “Computer simulation based study of photovoltaic cells/modules and their experimental verification”, International Journal of Recent Trends in Engineering, 1(3), 151-156, 2009.

[18] T. P. Sahu, T. V. Dixit, & R. Kumar, “Simulation and analysis of perturb and observe MPPT algorithm for PV array using ĊUK converter”, Advance in Electronic and Electric Engineering, 4(2), 213-224, 2014.

[19] M. A. B. Siddique, S. R. Karim, S. I. Sharif, & M. T. Hoque, “Modeling of Single Diode Solar Photovoltaic Module using Matlab”, International Journal of Computer Applications, November, 178(3), 39-45, 2017.

[20] S. Silvestre, “Strategies for fault detection and diagnosis of pv systems”, In Advances in Renewable Energies and Power Technologies, pp. 231-255, 2018.

[21] H. Park, Y. J. Kim, & H. Kim, “PV cell model by single-diode electrical equivalent circuit”, Journal of Electrical Engineering & Technology, 11(5), 1323-1331, 2016.

[22] A. Bouraiou, M. Hamouda, A. Chaker, M. Sadok, M. Mostefaoui, & S. Lachtar, “Modeling and simulation of photovoltaic module and array based on one and two diode model using Matlab/Simulink”, Energy Procedia, 74, 864-877, 2015.

[23] H. Qu, & X. Li, “Temperature dependency of the fill factor in PV modules between 6 and 40° C”, Journal of Mechanical Science and Technology, 33(4), 1981-1986, 2019.

[24] T. Khatib, W. Elmenreich, & A. Mohamed, “Simplified iv characteristic tester for photovoltaic modules using a dc-dc boost converter”, Sustainability, 9(4), 657, 2017.

[25] C. E. C. Nogueira, J. Bedin, R. K. Niedzialkoski, S. N. M. de Souza, & J. C. M. das Neves, “Performance of monocrystalline and polycrystalline solar panels in a water pumping system in Brazil”, Renewable and Sustainable Energy Reviews, 51, 1610-1616, 2015.

[26] S. Qazi, "Fundamentals of standalone photovoltaic systems”, Standalone Photovoltaic (PV) Systems for Disaster Relief and Remote Areas, 31-82, 2017.

[27] L. Arnberg, M. Di Sabatino, & E. J. Øvrelid, "State-of-the-art growth of silicon for PV applications", Journal of crystal growth, 360, 56-60, 2012.

[28] C. P. Liu, M. W. Chang, & C. L. Chuang, "Effect of rapid thermal oxidation on structure and photoelectronic properties of silicon oxide in monocrystalline silicon solar cells", Current Applied Physics, 14(5), 653-658, 2014.

[29] A. Polman, M. Knight, E. C. Garnett, B. Ehrler, & W. C. Sinke, "Photovoltaic materials: Present efficiencies and future challenges", Science, 352(6283), 2016.

[30] D. D. B. Mesquita, J. L. D. S. Silva, H. S. Moreira, M. Kitayama, & M. G. Villalva, "A review and analysis of technologies applied in PV modules", In 2019 IEEE PES Innovative Smart Grid Technologies Conference-Latin America (ISGT Latin America) pp. 1-6, 2019.

[31] P. G. V. Sampaio, & M. O. A. González, "Photovoltaic solar energy: Conceptual framework", Renewable and Sustainable Energy Reviews, 74, 590-601, 2017.

[32] S. Varlamov, B. Eggleston, J. Dore, R. Evans, D. Ong, O. Kunz, ... & M. Green, "Diode laser processed crystalline silicon thin-film solar cells", In Laser-based Micro-and Nanopackaging and Assembly VII (Vol. 8608, p. 86080Q). International Society for Optics and Photonics, 2013.

[33] R. H. Plante, Solar Energy, "Photovoltaics, and Domestic Hot Water: A Technical and Economic Guide for Project Planners, Builders, and Property Owners", Academic Press, 2014.

[34] I. O. Oladeji, L. Chow, C. S. Ferekides, V. Viswanathan, & Z. Zhao, "Metal/CdTe/CdS/Cd1− xZnxS/TCO/glass: A new CdTe thin film solar cell structure", Solar energy materials and solar cells, 61(2), 203-211, 2000.

[35] M. Dey, M. Dey, M. A. Matin, & N. Amin, "High efficient and stable ultra-thin CdTe solar cell with a potential copper telluride BSF", In 2016 9th International Conference on Electrical and Computer Engineering (ICECE), pp. 590-593, 2016.

[36] M. Moradi, R. Teimouri, M. Saadat, & M. Zahedifar, “Buffer layer replacement: a method for increasing the conversion efficiency of CIGS thin film solar cells”, Optik, 136, 222-227, 2017.

[37] R. (Ed.). Street, “Technology and applications of amorphous silicon”, Springer Science & Business Media, Vol. 37, 1999.

[38] A. Ghahremani, & A. E. Fathy, “High efficiency thin-film amorphous silicon solar cells”, Energy Science & Engineering, 4(5), 334-343, 2016.

[39] Y. Xu, J. Yuan, S. Zhou, M. Seifrid, L. Ying, B. Li,... & W. Ma, “Ambient Processable and Stable All-Polymer Organic Solar Cells”, Advanced Functional Materials, 29(8), 1806747, 2019.

[40] A. Facchetti, “Polymer donor–polymer acceptor (all-polymer) solar cells”, Materials Today, 16(4), 123-132.

[41] A. Taşçıoğlu, O. Taşkın, A. Vardar, “A power case study for monocrystalline and polycrystalline solar panels in Bursa City, Turkey”, International Journal of Photoenergy, 2016.

[42] E. Elibol, O. T. Özmen, N. Tutkun, O. Köysal, “Outdoor performance analysis of different PV panel types”, Renewable and Sustainable Energy Reviews, vol. 67, pp. 651-661, 2017.

[43] S. Seme, K. Sredenšek, B. Štumberger, M. Hadžiselimović, “Analysis of the performance of photovoltaic systems in Slovenia”, Solar Energy, vol. 180, pp. 550-558, 2019.

[44] M. S. Adaramola, E.E.T. Vågnes, “Preliminary assessment of a small-scale rooftop PV-grid tied in Norwegian climatic conditions”, Energy Conversion and Management, vol. 90, pp. 458-465, 2015.

[45] L. M. Ayompe, A. Duffy, S. J. McCormack, M. Conlon “Measured performance of a 1.72 kW rooftop grid connected photovoltaic system in Ireland” Energy Conversion and Management, vol. 52, no. 2, pp. 816-825, 2011.

[46] M. Adar, Y. Najih, M. Gouskir, A. Chebak, M. Mabrouki, A. Bennouna, “Three PV plants performance analysis using the principal component analysis method”, Energy, vol. 207, 2020.

[47] L. Carmo de Lima, L. A. Ferreira, H. B. L. Morais, “Performance analysis of a grid connected photovoltaic system in northeastern Brazil” Energy Sustain. Dev., vol. 37, pp. 79-85, 2017.

[48] Z. A. Eluma, A. S. Momodu. “Climate change mitigation and renewable energy for sustainable development in Nigeria: a discourse approach”, Renew. Sustain. Energy Rev., vol. 76, pp. 72-80, 2017.

[49] A. Hamzeh, S. Hamed, Z. Al-Omari, A. Sandouk, G. Aldahim, “First year performance of a PV plant in Jordan compared to PV plants in the region” Int. J. Renew. Energy Res., vol. 5, pp. 983-990, 2015.

[50] H. Maammeur, A. Hamidat, L. Loukarfi, M. Missoum, K. Abdeladim, T. Nacer, “Performance investigation of grid-connected PV systems for family farms: case study of North-West of Algeria“, Renew. Sustain. Energy Rev., vol. 78, pp. 1208-1220, 2017.

[51] I. Marinić-Kragić, S. Nižetić, F. Grubišić-Čabo, A. M. Papadopoulos, “Analysis of flow separation effect in the case of the free-standing photovoltaic panel exposed to various operating conditions”, Journal of Cleaner Production, vol. 174, pp. 53-64, 2018.

[52] H. Rezk, I. Tyukhov, M. Al-Dhaifallah, A. Tikhonov, “Performance of data acquisition system for monitoring PV system parameters”, Measurement, vol. 104, pp. 204-211, 2017.

[53] J. Machacek, Z. Prochazka, J. Drapela, “System for measuring and collecting data from solar-cell systems”, In 2007 9th International Conference on Electrical Power Quality and Utilisation (pp. 1-4). IEEE, 2007.

[54] A. El Hammoumi, S. Motahhir, A. Chalh, A. El Ghzizal, A. Derouich, “Low-cost virtual instrumentation of PV panel characteristics using Excel and Arduino

in comparison with traditional instrumentation", Renewables: Wind, Water, and Solar, vol. 5, no. 1, 2018.

[55] M. A. Muñoz-García, O. Marin, M. C. Alonso-García, F. Chenlo, "Characterization of thin film PV modules under standard test conditions: Results of indoor and outdoor measurements and the effects of sunlight exposure", Solar Energy, vol. 86, no. 10, pp. 3049-3056, 2012.

[56] D. Polverini, M. Field, E. Dunlop, W. Zaaiman, "Polycrystalline silicon PV modules performance and degradation over 20 years", Progress in Photovoltaics: Research and Applications, vol. 21, no. 5, 1004-1015, 2013.

[57] S. Kıvrak, T. Özer, "Solar Panels Characteristic Determining Circuit Design and Implementation", International Journal of Latest Technology in Engineering, Management & Applied Science (IJLTEMAS), vol. 7, no. 11, pp. 1-4, 2018.

[58] E. M. D. S. Brito, A. D. S. Antônio, A. F. Cupertino, & H. A. Pereira, "Characterization of solar panel using capacitive load" In 2014 11th IEEE/IAS International Conference on Industry Applications pp. 1-7, 2014.

[59] E. E. Van Dyk, A. R. Gxasheka, & E. L. Meyer, "Monitoring current–voltage characteristics and energy output of silicon photovoltaic modules", Renewable Energy, 30(3), 399-411, 2005.

[60] J. M. Enrique, E. Duran, M. Sidrach-de-Cardona, J. M. Andujar, M. A. Bohorquez, & J. Carretero, "A new approach to obtain IV and PV curves of photovoltaic modules by using DC-DC converters", In Conference Record of the Thirty-first IEEE Photovoltaic Specialists Conference, 2005. pp. 1769-1772, 2005.

[61] F. Mhaboobkhan, M. Fathimaparveen, K. Gokila, & P. Logapriya, "Implementation of high speed data transfer serialized 128/130bit encoding algorithm using 90nm technology", In 2019 5th International Conference on Advanced Computing & Communication Systems (ICACCS) pp. 732-736, 2019.

[62] J. Dudak, P. Tanuska, G. Gaspar, & P. Fabo, “ARM-Based Universal 1-Wire Module Solution”, Journal of Sensors, 2018.

[63] V. Pamadi, & B. G. Nickerson, “Getting Started With 1-Wire Bus Devices”, 2015.

[64] J. Machacek and J. Drapela, "Control of serial port (RS-232) communication in LabVIEW," 2008 International Conference - Modern Technique and Technologies, Tomsk, pp. 36-40, 2008.

[65] S. Saha, M. A. Rahman and A. Thakur, "Design and implementation of a BIST embedded high speed RS-422 utilized UART over FPGA," 2013 Fourth International Conference on Computing, Communications and Networking Technologies (ICCCNT), Tiruchengode, pp. 1-5, 2013.

[66] W. Andrysiewicz, D. Kościelnik and M. Miśkowicz, "I2C hardware master serial interface for asynchronous ADCs," 2015 IEEE International Symposium on Systems Engineering (ISSE), Rome, pp. 77-81, 2015.

[67] M. Versen and S. Kipfelsberger, "Introduction to microcomputer technology with the MSP430 Launch Pad in remote labs," 2014 IEEE Global Engineering Education Conference (EDUCON), Istanbul, pp. 202-205, 2014.

[68] S. J. Marinkovic and E. M. Popovici, "Nano-Power Wireless Wake-Up Receiver With Serial Peripheral Interface," in IEEE Journal on Selected Areas in Communications, vol. 29, no. 8, pp. 1641-1647, September 2011.

[69] T. Praveen Blessington, B. Bhanu Murthy, G. V. Ganesh and T. S. R. Prasad, "Optimal implementation of UART-SPI Interface in SoC," 2012 International Conference on Devices, Circuits and Systems (ICDCS), Coimbatore, pp. 673-677, 2012.

[70] H. T. Lim, D. Herrscher, M. J. Waltl, & F. Chaari, “Performance analysis of the IEEE 802.1 ethernet audio/video bridging standard”. In SimuTools pp. 27-36, 2012.

[71] H. Hassan, R. A. Bakar and A. T. F. Mokhtar, "Face recognition based on auto-switching magnetic door lock system using microcontroller," 2012 International Conference on System Engineering and Technology (ICSET), Bandung, pp. 1-6, 2012.

[72] V. Puri and A. Nayyar, "Real time smart home automation based on PIC microcontroller, Bluetooth and Android technology," 2016 3rd International Conference on Computing for Sustainable Global Development (INDIACom), New Delhi, pp. 1478-1484, 2016.

[73] B. Sarp, T. Karalar, H. Kusetogullari, "Real Time Smart Door System for Home Security", International Journal of Scientific Research in Information Systems and Engineering (IJSRISE), pp. 121-123, 2015.

[74] T. Celik, & H. Kusetogullari, "Solar-powered automated road surveillance system for speed violation detection", IEEE Transactions on Industrial Electronics, 57(9), pp. 3216-3227, 2009.

[75] H. Kusetoğullari, & T. Celik, "A road surveillance system powered by solar energy and wireless transmission", 2011.

[76] A. Demirbaş, "Global renewable energy resources", Energy sources, 28(8), pp. 779-792, 2006.

[77] M. Karabulut, H. Kusetogullari, & S. Kivrak, "Outdoor Performance Assessment of New and Old Photovoltaic Panel Technologies Using a Designed Multi-Photovoltaic Panel Power Measurement System", International Journal of Photoenergy, 2020.

[78] M. Kumar, A. Kumar, "Performance assessment and degradation analysis of solar photovoltaic technologies: A review", Renewable and Sustainable Energy Reviews, vol. 78, pp. 554-587, 2017.

[79] Microchip, PIC18F2420/2520/4420/4520 Data Sheet, 28/40/44-Pin Enhanced Flash Microcontrollers with 10-Bit A/D and nanoWatt Technology, 2008.

[80] T. B. Onofre, E. E. P. da Silveira, W. W. A. Silva, A. L. N. Martins, & G. L. Reis, “Implementation of a laboratory-based low cost AC Chopper Soft-Starter”, In 2016 17th International Conference on Harmonics and Quality of Power (ICHQP) pp. 885-889, 2016.

[81] E. Durán, J. Galán, J. M. Andújar, M. Sidrach-de-Cardona. ”A new method to obtain IV characteristics curves of photovoltaic modules based on SEPIC and cuk converters”, EPE Journal, vol. 18, pp. 5-15, 2008.

[82] S. Sarikh, M. Raoufi, A. Bennouna, A. Benlarabi, B. Ikken. Design of an IV “Characteristic Tracer for Photovoltaic Systems”, In 2017 International Renewable and Sustainable Energy Conference (IRSEC), pp. 1-5, 2017.

[83] IXYS, X2-Class HiPerFETTM Power MOSFET IXFH60N65X2, N-Channel Enhancement Mode Avalanche Rated Fast Intrinsic Diode, 2016.

[84] Y. Du, C. J. Fell, B. Duck, D. Chen, K. Liffman, Y. Zhang, Y., ... & Y. Zhu, “Evaluation of photovoltaic panel temperature in realistic scenarios”, Energy Conversion and Management, vol. 108, pp. 60-67, 2016.

[85] K. A. Moharram, M. S. Abd-Elhady, H. A Kandil, H. El-Sherif, “Enhancing the performance of photovoltaic panels by water cooling”, Ain Shams Engineering Journal, vol. 4, no. 4, pp. 869-877, 2013.

[86] Microchip, PIC16F882/883/884/886/887 Data Sheet, 28/40/44-Pin, Enhanced Flash-Based 8-Bit CMOS Microcontrollers with nanoWatt Technology, 2009.

[87] Aosong Electronics Co.,Ltd, Digital-output relative humidity & temperature sensor/module DHT22 (DHT22 also named as AM2302), Capacitive-type humidity and temperature module/sensor.

[88] Maxim Integrated, DS18B20 Programmable Resolution 1-Wire Digital Thermometer, 2019.

[89] M. Z. Jacobson,V. Jadhav, “World estimates of PV optimal tilt angles and ratios of sunlight incident upon tilted and tracked PV panels relative to horizontal panels”, Solar Energy, vol. 169, pp. 55-66, 2018.

[90] P. Michael, “A Conversion Guide: Solar Irradiance and Lux Illuminance”, IEEE Dataport, 2019.

[91] Tarim ve Orman Bakanligi Meteoroloji Genel Müdürlüğü, Resmi İstatistikler, 2020. [Online]. Available: https://www.mgm.gov.tr/veridegerlendirme/il-ve-ilceler-istatistik.aspx. [Accessed: 05- Aug- 2020].

[92] A. Çağlar, C. Yamalı, D. K. Baker, B. Kaftanoğlu, “Measurement of solar radiation in Ankara, Turkey”, Journal of Thermal Science and Technology, vol. 33, no. 2, 135-142, 2013.

[93] Mehmet Karabulut, Sinan Kivrak, "Fotovoltaik Panel Analizi İçin Geliştirilen Meteorolojik Ölçüm Sistemi Ile Ankara İlinde Yapilan Ölçümlerin Değerlendirilmesi” 5nd International Conference on Material Science and Technology in Cappadocia (IMSTEC’20), (Accepted), 2020.

[94] Mehmet Karabulut, Sinan Kivrak, "Çok Girişli Güç Ölçüm Sistemi İle Fotovoltaik Panel Teknolojilerinin Ankara İklim Şartlarinda Performans Değerlendirmesi” 5nd International Conference on Material Science and Technology in Cappadocia (IMSTEC’20), (Accepted), 2020.

[95] D. J. Sheskin “Handbook of Parametric and Nonparametric Statistical Procedures” (4th ed.), Chapman & Hall/CRC, 2006.

[96] W. H. Kruskal, W. A. Wallis, “Use of ranks in one-criterion variance analysis”, Journal of the American statistical Association, vol. 47, no. 260, pp. 583-621, 1952.

[97] D. Quade, “Using weighted rankings in the analysis of complete blocks with additive block effects”, Journal of the American Statistical Association, vol. 74, no. 367, pp. 680-683, 1979.

[98] W. Daniel, “Applied Nonparametric Statistics” (2nd ed.), Duxbury Thomson Learning, 2000.

[99] S. Holm. “A simple sequentially rejective multiple test procedure”, Scandinavian journal of statistics, 65-70, 1979.

[100] P.B. Nemenyi. “Distribution-free multiple comparisons”, Princeton University, 1963 (master's thesis).

[101] J. P Shaffer, “Modified sequentially rejective multiple test procedures”, Journal of the American Statistical Association, vol. 81, no. 395, pp. 826-831, 1986.

[102] G. Bergmann, G. HommelI “Improvements of general multiple test procedures for redundant systems of hypotheses”.

[103] G. Makrides, B. Zinsser, G. E. Georghiou, M. Schubert, J. H. Werner, “Outdoor efficiency of different photovoltaic systems installed in Cyprus and Germany”, In 2008 33rd IEEE Photovoltaic Specialists Conference, pp. 1-6, 2008.

[104] V. Sharma, S. S. Chandel. ”Performance analysis of a 190 kWp grid interactive solar photovoltaic power plant in India”, Energy, vol. 55, pp. 476-485, 2013.

[105] A. Q. Malik, S. J. B. H. Damit. ”Outdoor testing of single crystal silicon solar cells”, Renewable Energy, vol. 28, no. 9, pp. 1433-1445, 2003.

[106] A. Tihane, M. Boulaid, A. Elfanaoui, M. Nya, A. Ihlal. “Performance analysis of mono and poly-crystalline silicon photovoltaic modules under Agadir climatic conditions in Morocco”, Materials Today: Proceedings, vol. 24, pp. 85-90, 2020.

[107] S. Wittkopf, S. Valliappan, L. Liu, K. S. Ang, S. C. J. Cheng. ”Analytical performance monitoring of a 142.5 kWp grid-connected rooftop BIPV system in Singapore”, Renewable Energy, vol. 47, pp. 9-20, 2012.

[108] M. Cucumo, A. De Rosa, V. Ferraro, D. Kaliakatsos, V. Marinelli. ”Performance analysis of a 3 kW grid-connected photovoltaic plant”, Renewable Energy, vol. 31, pp. 1129-1138, 2006.

[109] S. Gulkowski, A. Zdyb, P. Dragan. ”Experimental efficiency analysis of a photovoltaic system with different module technologies under temperate climate conditions”, Applied Sciences, vol. 9, no. 1, pp. 141-151, 2019.

[110] N. Kumar, P. Yadav, S. S. Chandel. ”Comparative analysis of four different solar photovoltaic technologies”, In 2015 International Conference on Energy Economics and Environment (ICEEE), pp. 1-6, 2015.